An Experimental Facility for Studying Heat Transfer in Supercritical Fluids

by

Kai Jiang

Thesis submitted to the Faculty of Graduate and Postdoctoral Studies
in partial fulfillment of the requirements for the degree of

MASTER OF APPLIED SCIENCE

in Mechanical Engineering

Ottawa-Carleton Institute for Mechanical and Aerospace Engineering
University of Ottawa
Ottawa, Canada

Abstract

A state-of-art research facility has been built at the University of Ottawa, which is suitable for thermalhydraulic experiments in support of the development of the Canadian Supercritical-Water-Cooled Reactor (SCWR). The facility is a recirculating flow loop, using carbon dioxide as a medium and having three different test sections, two tubes with inner diameters of 8 and 22 mm, respectively, and a three-rod bundle. The loop can operate within ranges of pressure, temperature, heat flux and mass flux, which are of interest to the current SCWR design. The present thesis includes a comprehensive description of the facility. It also documents the procedure and results of its commissioning, as well as some preliminary measurements that have been collected so far. It is intended to provide an insight to the design of the facility and its functionality and to serve as a reference for future research activities. A number of tests performed by previous researchers in other facilities were replicated and nearly identical results were obtained. It was demonstrated that the design of the facility is sound and its performance is adequate within the intended ranges of operation conditions. It is expected that the results obtained in this facility will make a significant contribution to the understanding of supercritical heat transfer and pressure losses in the SCWR context.

Acknowledgements

I am deeply grateful to Dr. Stavros Tavoularis for his invaluable guidance and generous support during the entire course of my graduate study. His extraordinary academic knowledge, meticulous nature and dedication to his students ensure the quality of my research and this thesis.

I would like to thank my colleagues in the University of Ottawa supercritical research group, Dr. Dé Groeneveld and Hussam Zahlan, for helping to expand my understanding of the subject matter. I extend my gratitude to the staff at the university mechanical and civil machine shop, John Perrins, James MacDermid, Stanley Weedmark, Michael Burns and Leo Denner, as well as contractor Dave Petry for their indispensable technical support.

The financial support granted by Natural Resources Canada (NRCan), Natural Sciences and Engineering Research Council of Canada (NSERC) and Atomic Energy Canada Limited (AECL), along with the donation of a rod bundle for my experiments by AECL are greatly appreciated.

Last but not least, I wish to dedicate this thesis to my parents, Wendong and Zhengwei, without whom none of my achievements would have been possible.

Table of Contents

Nomenclature

A	area, m^2
c_p	specific heat, J/(kg·K)
D	diameter, m
E	Internal energy, W
g	gravitational acceleration, m/s^2
G	mass flux, $kg/(m^2 \cdot s)$
h	distance, m; convection heat transfer coefficient, $W/(m^2 \cdot K)$
H	height, m; specific enthalpy, kJ/kg
I	electric current, A
k	thermal conductivity, W/(m·K)
L	length, m;
m	mass, kg
$\dot{m}$	mass flow rate, kg/s
N	number of samples
P	pressure, Pa, psia, psig; wetted perimeter, m
ΔP	pressure drop, Pa
P_R	percentage of deviation, %
Pr	Prandtl number
q	heat flux, W/m^2, kW/m^2
Q	total heat power, W, kW

r	radius, m
R	electric resistance, Ω
Ra	Rayleigh number
Ra*	modified Rayleigh number
t	thickness, m; time, s
T	temperature, K, °C
u	velocity, m/s
U	uncertainty
V	volume, m^3
w	width, m
x	variable
Z	axial location, m

Greek Letters

α	thermal diffusivity, m^2/s; temperature coefficient of resistance, K^{-1}
β	volumetric thermal expansion coefficient, K^{-1}
Δ	differential
θ	zenith angle, °
μ	dynamic viscosity, kg/(m·s), arithmetic mean
ν	kinematic viscosity, m^2/s
ρ	density, kg/m^3; electrical resistivity, Ω·m
σ	Stefan-Boltzmann constant, standard deviation

Subscripts

avg	average

ac	acceleration
b	bulk fluid
B	buoyancy
c	critical
cv	control volume
cond	conductive
conv	convective
D	diameter
exp	experimental
f	flow
fr	friction
F	fluid
g	gravitational
h	heated
hy	hydraulic
i	inner, index
in	inlet
max	maximum value
min	minimum value
net	total
o	outer
out	outlet
p	constant pressure
pc	pseudocritical
r	radial

rms	root mean square
s	surface
v	volumetric
w	wall
θ	azimuthal
λ	spectral
∞	unheated flow
0	reference, initial value

Superscripts

*	dimensionless quantity

Overbar

$\bar{}$	time average

Abbreviations

AECL	Atomic Energy of Canada Limited
CHF	Critical heat flux
CO_2	Carbon dioxide
CRL	Chalk River Laboratories
DP	Differential pressure, differential pressure transmitter
HTD	Heat transfer deterioration
ID	Inner diameter
N_2	Nitrogen
OD	Outer diameter

SC	Supercritical
SCHT	Supercritical heat transfer
SCUOL	Supercritical University of Ottawa Loop
SCWR	Supercritical-Water-Cooled Reactor
SS	Stainless steel
TS	Test section

List of Tables

List of Figures

Chapter 1 Introduction

1.1 Development of a Supercritical-Water-Cooled Reactor

The Supercritical-Water-Cooled Reactor (SCWR, Figure 1.1) is one of the six advanced, fourth generation nuclear reactor concepts proposed by the Generation IV International Forum (GIF), a consortium of thirteen member countries that lays the groundwork for the fourth generation of nuclear energy systems[1]. Operating with water at pressures higher than the thermodynamic critical pressure, SCWRs are expected to have superior thermodynamic efficiency. Once constructed, they will be able to produce safe and clean energy at reduced cost compared with the current generation of nuclear reactors.

Since its inception in January 2000, GIF has been overseeing a large amount of research and development (R&D) activities conducted in its member countries. These activities pertain to many aspects essential to developing a practical nuclear energy system,

[1] https://www.gen-4.org/gif/jcms/c_9360/scwr, retrieved June 25, 2014.

such as fuels and materials design, core physics, balance of plant and safety analysis. GIF aims to complete R&D of the SCWR by 2020 and to deploy it commercially around 2030[2].

The Canadian National Program on Generation IV Technologies represents Canada's effort in fulfilling its responsibilities as a GIF member state. Its involvement in SCWR development includes two distinct facets of a core design concept (Figure 1.2): 1) Thermalhydraulics and Safety; 2) Materials and Chemistry. Supported by this program, the supercritical heat transfer research group at the University of Ottawa focuses on a range of thermalhydraulics topics, including heat transfer, turbulence and the construction of a look-up table. The Super-Critical University of Ottawa Loop (SCUOL), a dedicated, state-of-art experimental facility, has been designed and constructed by the group. The majority of the data used for the present thesis was collected at this facility. Results and discussions can be found in later chapters.

1.2 Heat Transfer in Supercritical Fluids

A supercritical (SC) fluid is any fluid at a pressure higher than its critical pressure. Although distinct liquid and gas phases do not exist at SC pressures, SC fluids exhibit features of both liquid and gas. For instance, SC fluids can diffuse and completely fill up a container like a gas, while also being able to dissolve other substances like a liquid.

[2]A Technology Roadmap for Generation IV Nuclear Energy Systems, https://www.gen-4.org/gif/upload/docs/application/pdf/2013-09/genivroadmap2002.pdf, retrieved June 25, 2014.

Because of the single-phase nature of supercritical fluids, using them as coolant in a nuclear reactor can eliminate some of the potential safety issues that are inherent to reactors operating at subcritical pressures. For example, "boiling crisis" would not occur in a SCWR since SC coolant does not boil. However, as shown in Figure 1.3, the thermophysical properties of a SC fluid vary drastically when the temperature is near the psudocritical temperature, defined as the temperature at which the specific heat is maximal. This in turn can cause unusual heat transfer behaviour under certain circumstances. So far three different heat transfer modes have been observed in previous works:

- Normal heat transfer, in which case the heat transfer coefficient (HTC, an indication of the efficiency of heat transfer) can be easily predicted by established correlations.

- Deteriorated heat transfer (DHT), with values of the HTC that are relatively low within a part of a test section; it usually occurs in tubes at high heat fluxes and low mass fluxes and is thought to be due to buoyancy forces and/or flow acceleration (Fewster and Jackson, 2004). This mode can be suppressed or even eliminated by the presence of turbulence-enhancing devices.

- Enhanced heat transfer, with relatively high values of the HTC within some part of a test section.

Figure 1.4 shows one of the previous experiments in which all three modes were observed. The prediction of the occurrences of these modes is crucial to the successful realization of a complex yet safe heat and mass transport system suitable for the SCWR.

1.3 Motivation and objectives

Understanding heat transfer characteristics near and above critical conditions is crucial to the successful design of the SCWR. Many studies, both numerical and experimental, have been conducted on bare tubes and simple geometries like annuli. However experimental works on complex geometries such as rod bundles are scarce. In recent years the interest of understanding how spacers and obstacles affect supercritical heat transfer is also on the rise. One of the priorities of the SCHT project at the University of Ottawa is to generate such data and to extend current knowledge of heat transfer in the latest SCWR fuel bundle design (Figure 1.5).

The main objectives of this thesis are to describe the research facility in detail, to explain its underlying design principle and to document the procedures of the preliminary heat transfer coefficient measurements conducted in three test sections: a 8-mm tube, a 22-mm tube and a 3-rod bundle. The results of these tests will be compared with previously published results for assessing the design, construction and performance of the experimental setup. The thesis can also be used as reference for continuing research activities using the facility.

1.4 Thesis outline

This thesis is organized into seven chapters. Chapter 1 provides a brief description of the SCWR concept and some basic information regarding heat transfer in supercritical fluids. It also includes a section summarizing out the motivation and objectives of this work. An

outline of the thesis is provided at the end of this chapter. Chapter 2 contains an extensive literature review of previous experimental work done on test sections of various geometries under supercritical conditions. Important parameters used by different researchers are highlighted. The chapter also includes some recent numerical studies on the same subject for the purpose of comparison. Chapter 3 describes the Super-Critical University of Ottawa Loop, on which the experiments were performed. Detailed information of the bare tube test sections, the 3-rod bundle test section and accompanying instrumentation are presented. In the fourth chapter, measurement procedures are documented. Calculations carried out for data analyses are explained here as well. Commissioning and preliminary test results are presented in chapter 5. Comparison to published results from the literature is presented. Chapter 6 introduces the publications I authored or contributed to that are relevant to the present study. In the concluding seventh chapter, all the findings of this study are summarised. Appendix A contains supplemental illustrations, whereas Appendix B consists of copies of three papers presented in conferences, which were co-authored by the author of this thesis. It is noted that figures are placed at the end of the corresponding chapter.

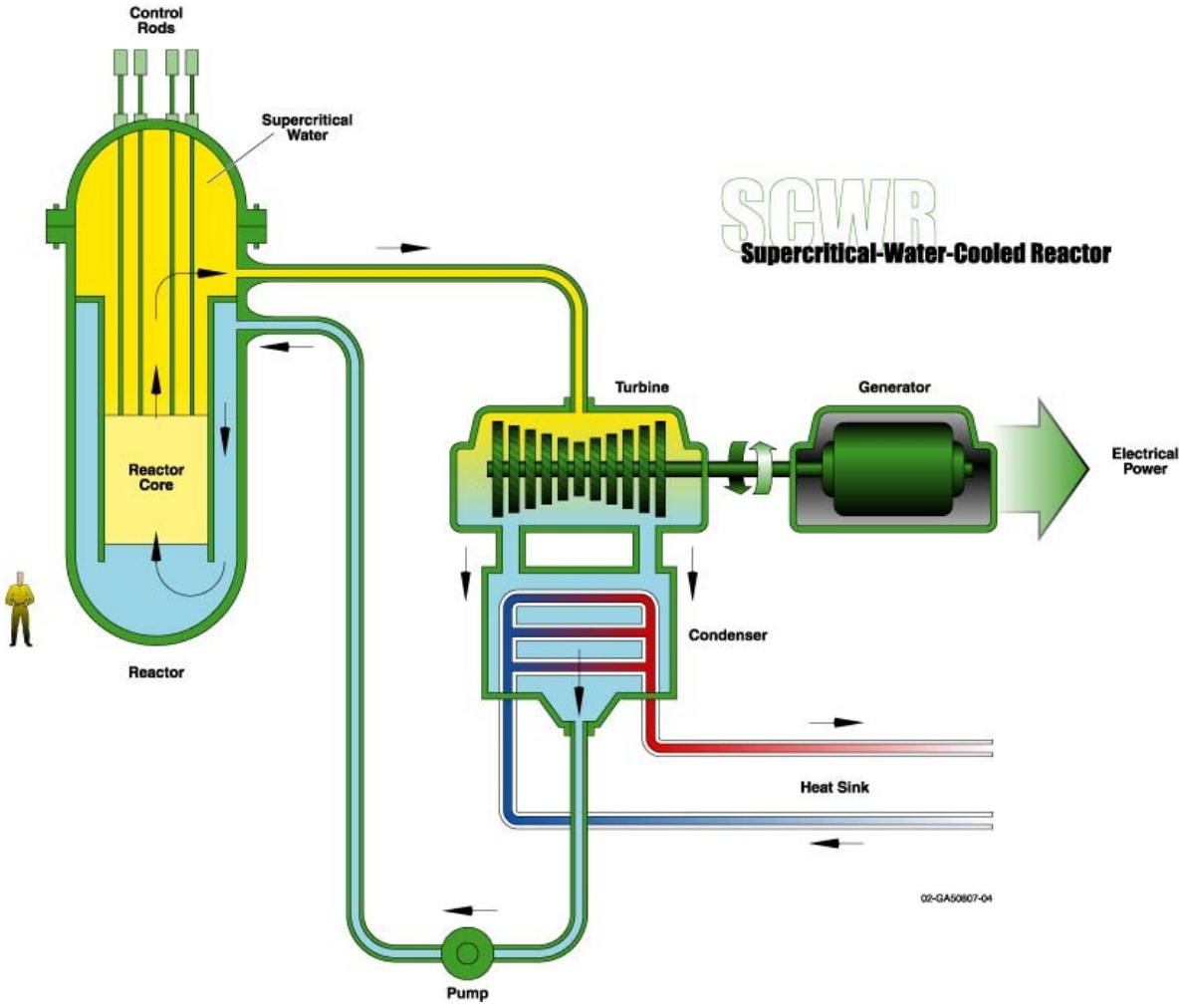

Figure 1.1 – The GIF SCWR design concept. (GIF website).

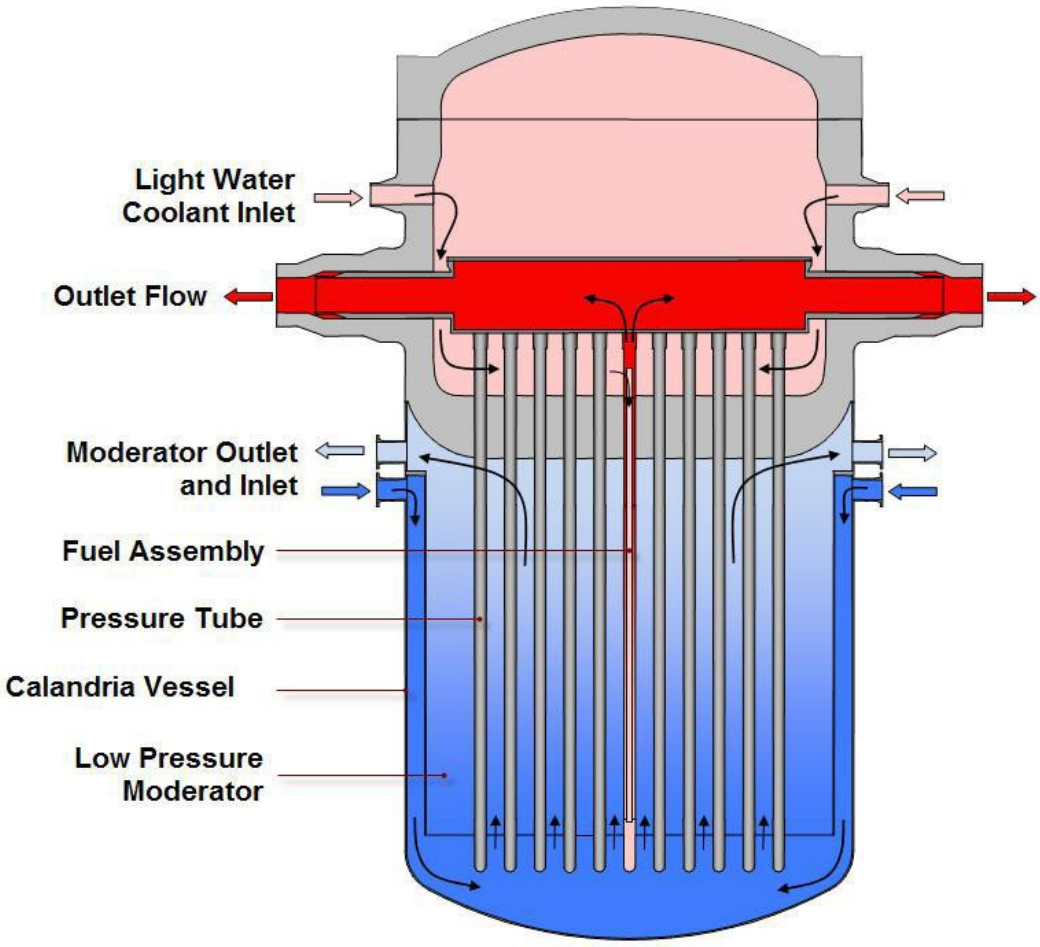

Figure 1.2 – The Canadian SCWR core design concept (Yetisir et al., 2013).

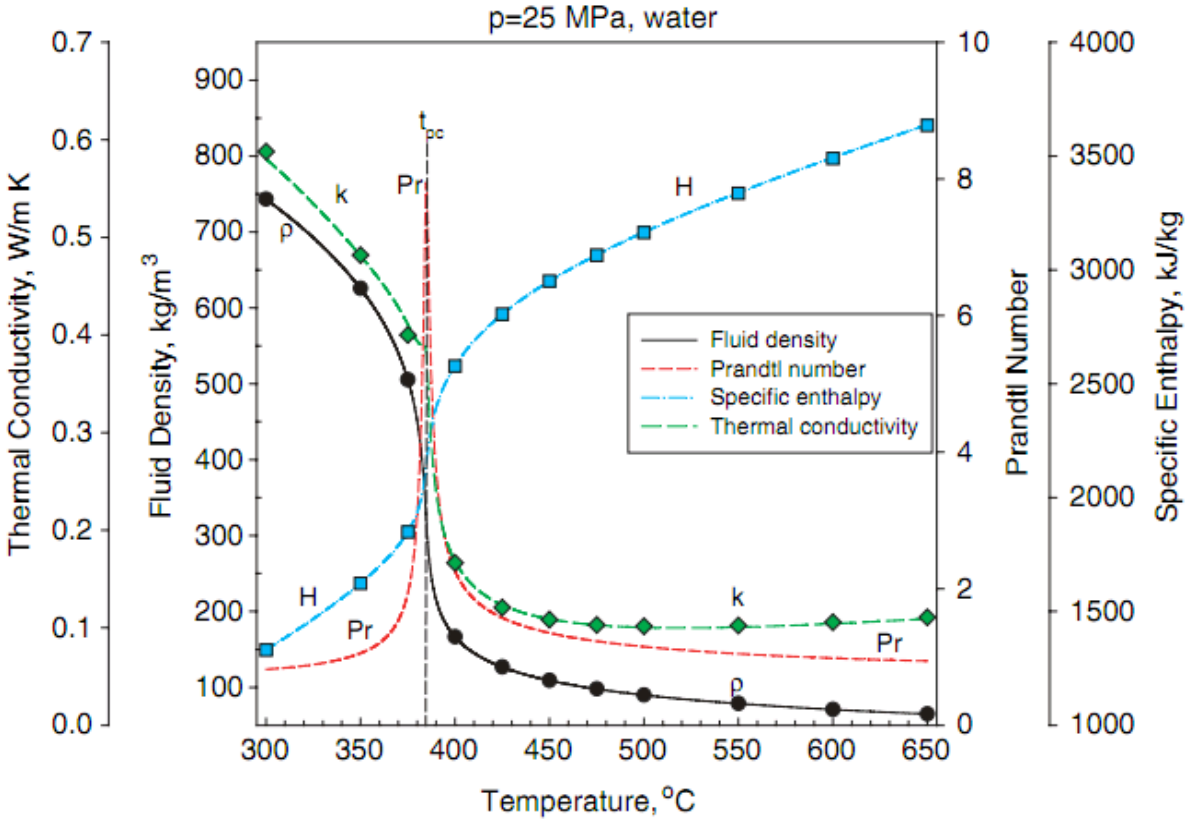

Figure 1.3 – Property changes of water at 25 MPa (Pioro et al., 2007).

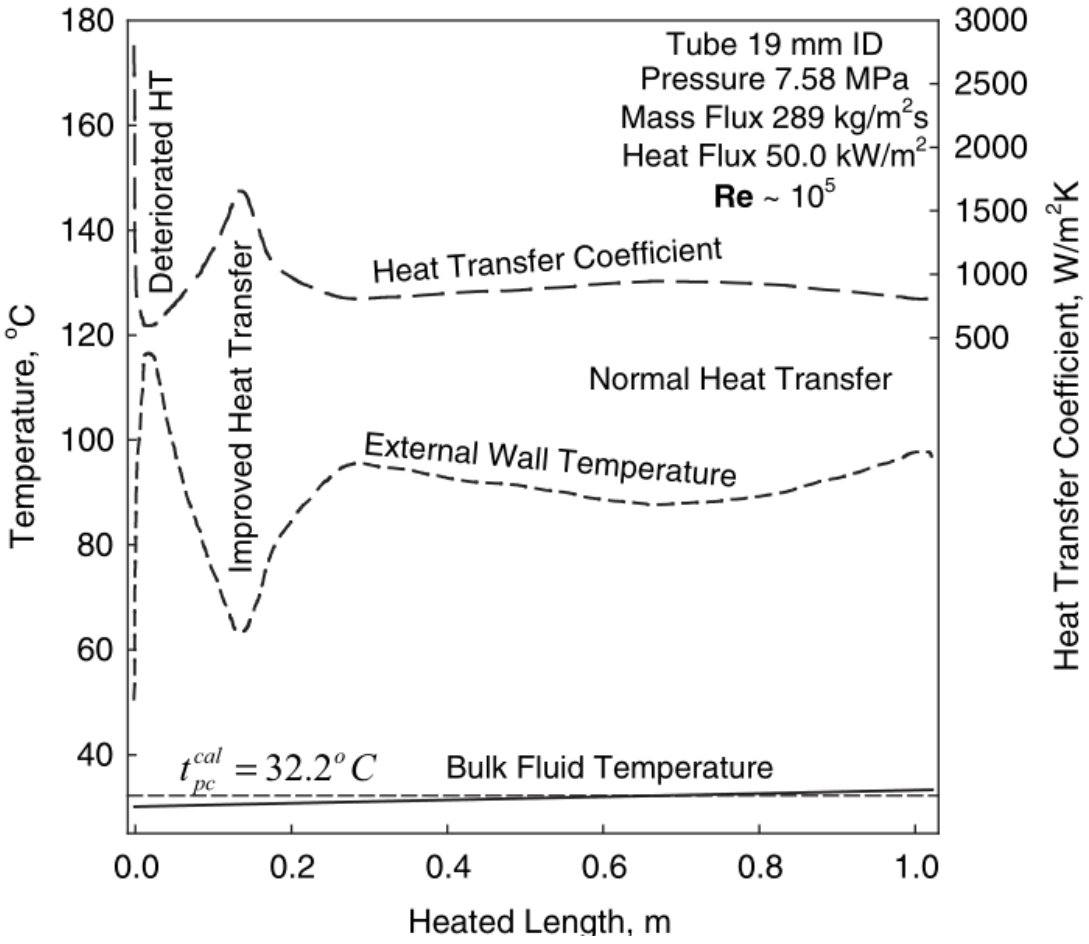

Figure 1.4 – Three different heat transfer modes in supercritical carbon dioxide (Fewster, 1976).

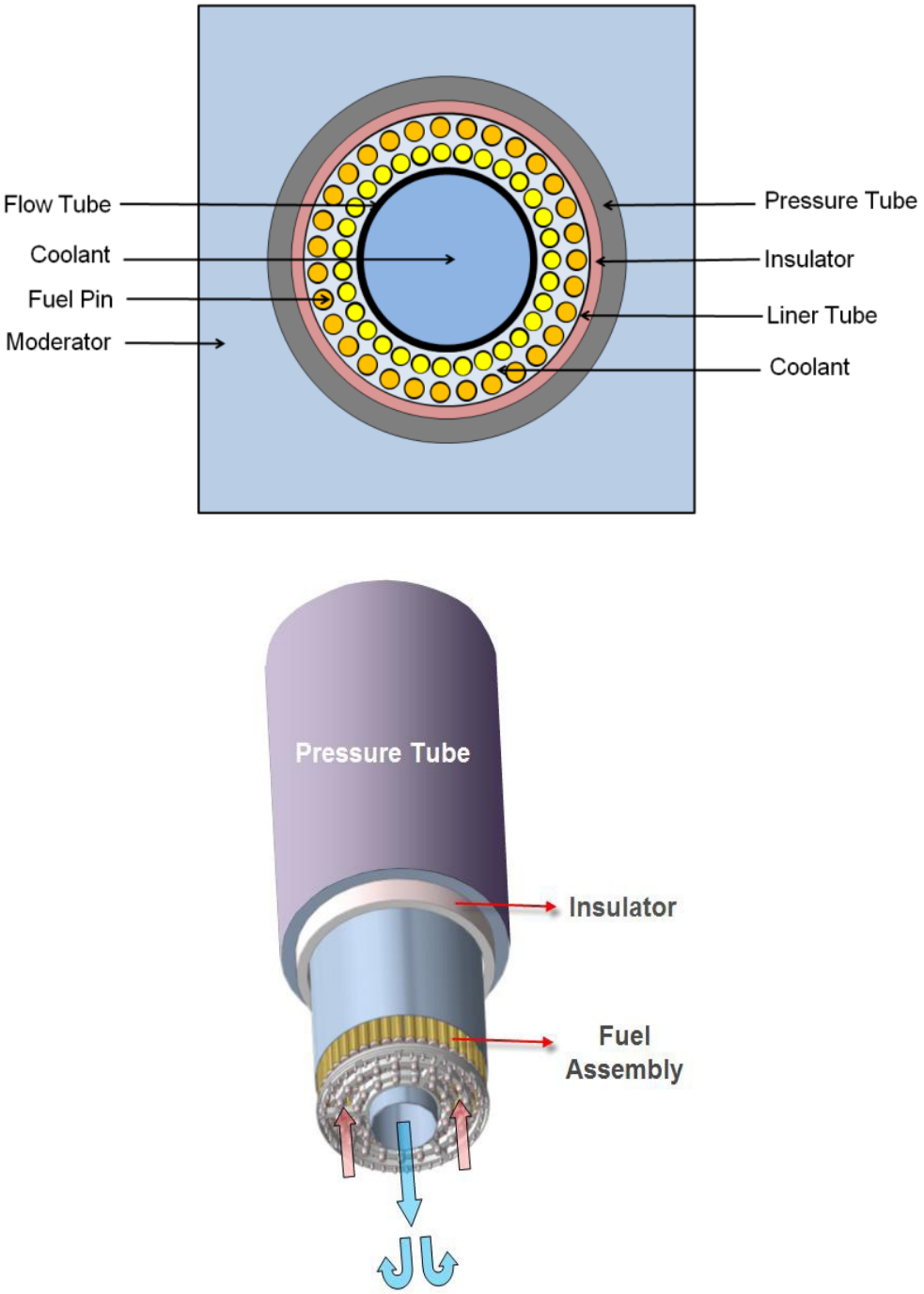

Figure 1.5 – A fuel bundle design for the Canadian SCWR concept (Yetisir et al., 2013).

Chapter 2 Literature Review

2.1 General comments

Experimental works of heat transfer in supercritical fluids were first conducted in the 1950s (Pioro and Duffey, 2003). Instead of experimenting with supercritical water, many researchers chose to use other modeling fluids (surrogate fluids) to reduce cost and safety requirements. Helium, carbon dioxide and organic refrigerants (such as Freon) are some of the most frequently used modeling fluids. This chapter will focus on reviewing previous literature pertaining to research activities conducted with carbon dioxide, in view of the fact that SCOUL uses CO_2 as its working fluid. The rationale of using CO_2 is further explained in section 3.1.1.

2.2 Past or existing research facilities similar to SCUOL

The Supercritical Pressure Heat Transfer Investigation for NeXt Generation, or SPHINX, is a research facility built by KAERI (Korea Atomic Energy Research Institute) for conducting heat transfer experiments using supercritical CO_2 (Kim et al., 2007).Its design pressure is 12.0 MPa. Two gear pumps were installed for circulating the CO_2. An

accumulator was placed downstream of the pumps in order to control the loop pressure and reduce pressure fluctuation. An electric preheater was installed to regulate the fluid temperature at the inlet of the TS. A Coriolis flow meter was used to measure the mass flow rate. Mass flow regulation was achieved through a combination of adjusting the bypass valve and the pump speed. A compact spiral-type cooler was used to cool the CO_2 leaving the TS. A pressure safety relieve valve was installed to prevent over-pressurization of the main loop. By 2007, three different test sections had been installed in SPHINX: a tube of 4.4 mm ID, a tube of 9.0 mm ID, as well as a concentric annular channelwith an outer housing tube of 10 mm ID, an inner heated tube of 8 mm ID and a heated length of 1.8 m. All three TS were installed vertically. K-type thermocouples were installed along the TS for measuring heated wall temperature profiles which were used to calculate the heat transfer coefficient. Instrumentation permitted measurements of pressures and fluid temperatures at various loop locations, pressure drop across the TS, mass flux and heat flux supplied to the TS.

Fewster and Jackson (2004) studied supercritical heat transfer at their facility with CO_2 at 7.58 MPa. The loop was designed to provide test sections with either upward or downward flow. A canned centrifugal pump circulated CO_2 in the loop. A preheater and a precooler were placed in parallel just upstream of the TS for regulating fluid inlet temperature. CO_2 was cooled by a shell and tube cooler upon leaving the TS. Mass flow rate was measured with a sharp-edged orifice plate flow meter. The facility had two test sections: an SS316 tube with 5 mm ID and an SS321 tube with 8 mm ID. The heated lengths for both test sections were 150 diameters (750 mm and 1200 mm, respectively).

Measured variables included loop pressure, wall temperature distribution along the TS, inlet and outlet fluid temperatures, heating power and mass flow rate.

2.3 Previous experimental investigations of supercritical heat transfer using carbon dioxide

Pioro and Duffey (2003) have provided a comprehensive review of heat transfer and hydraulic resistance experiments using CO_2 at supercritical pressures conducted up to 2003. The experiments were categorized by the type of heat transfer (free or forced convection) and type of test sections (vertical tubes, horizontal tubes or other geometries). Important parameters for each work, such as experiment pressure, bulk fluid temperature, heat flux, mass flux and Reynolds number were clearly presented in tables. A few typical test results were selected and shown in plots. Significant findings in the articles, such as the occurrences of different heat transfer regimes and the effect of additional test section features (tube roughness, internal ribs, inserts, spacers, wire-wraps and so on), were also highlighted.

Fester and Jackson (2004) documented experiments conducted in two bare tube sections of 5 and 8 mm ID at the pressure of 7.58 MPa. For the 5 mm TS, tests with mass flow rates from 0.0845 kg/s to 0.0058 kg/s in a descending order were performed. Wall temperature profiles for downward and upward flows under same the conditions were plotted side by side to reveal the influence of buoyancy on heat transfer. It was reported that when the flow rate was reduced to 0.029 kg/s some difference between downward

and upward temperature profiles started to appear, which was attributed to buoyancy effects. As the mass flow rate was further reduced to 0.0129 kg/s, with the heat flux fixed at 68 kW/m^2, onset of strong localized heat transfer deterioration was observed. The development of HTD with an increase of heat flux at this flow rate was also illustrated. For the 8 mm test section, buoyancy effects developed more readily and appeared even at the highest flow rate. When the mass flow rate was reduced to 0.045 kg/s, the influence of buoyancy was apparent along the entire heated length. Further reducing the flow rate to 0.02 kg/s caused very localized HDT in the upward flow. The location where peak wall temperature occurred could be adjusted by varying the inlet fluid temperature.

Kim et al. (2005) presented experimental heat transfer characteristics of turbulent supercritical CO_2 flows in vertical tubes with circular, triangular, and square cross-sections. The test pressure was held at 8 MPa with inlet bulk temperatures ranging from 15 to 32 °C, imposed heat flux from 3 to 180 kW/m^2 and mass flux from 209 to 1230 kg/m^{2}s. The corresponding Reynolds numbers were in the range from 3×10^4 to 1.4×10^5. Each test section had an entrance length of 600 mm, a heated length of 1200 mm and a hydraulic diameter of about 8 mm. Wall temperature distributions along the heated length were measured using thermocouples. The distributions measured in different test sections but under the same test conditions were compared to examine the effect of the cross-sectional shape. The heat transfer deterioration conditions for the three TCs were determined in terms of heat flux and mass flux at a given inlet bulk temperature. An improved heat transfer correlation that accommodates the effects of property variation and buoyancy was proposed as well.

Song et al. (2007) refer to some experimental investigations of supercritical heat transfer in CO_2 conducted at KAERI's SPHINX facility. Two Inconel 625 tubes with ID of 4.4 mm and 9.0 mm were used as test sections. Test pressure for both TS was 8.12 MPa and the heated lengths were 2100 mm and 2650 mm, respectively. Six combinations of different mass fluxes (400 or 1200 kg/m^{2}s), heat fluxes (30 or 50 kW/m^2) and TS diameters were tested. Each combination consisted of a few experiments with different inlet fluid temperatures. Wall temperature and heat transfer coefficient profiles along the TSs were plotted. Heat transfer enhancement was observed in some tests and attributed to the formation of pseudo-boiling region, whose enthalpy is significantly higher and permits higher heat flux to be transmitted. Heat transfer deterioration started to appear in the 4.4 mm TS when the heat flux was increased to 50 kW/m^2 at the mass flux of 400 kg/m^{2}s. However, for the 9.0 mm TS, HTD appeared for both 30 and 50 Kw/m^2. Comparisons of wall temperature and heat transfer coefficients in the two TS under the same conditions were made and it was indicated that the efficiency of heat transfer is consistently lower as tube diameter increases. They also believed that some of the results confirmed that integral scaling is preserved even for the case with HTD when the criterion of the same q/G and L/D is maintained. It was also suggested that HTD is a specific heat transfer mode and not a transient.

Bae et al. (2011) experimented using upwardly flowing CO_2 in a heater rod of 6.32 mm ID with an internal helical wire of 1.3 mm OD. The pressure range was from 7.75 to 8.12 MPa, the mass flux range was from 400 to 1200 kg/m^{2}s and the heat flux range was from 30 to 90 kW/m^2. The heat transfer coefficient was almost double the value obtained in previous experiments with a plain tube of the same size near the

pseudocritical temperature. The effects of the wire-wrap spacer diminished as bulk fluid temperature moved away from the pseudo-critical temperature.

Chapter 3 Experimental Facility and Instrumentation

3.1 Experimental facility

3.1.1 Background

The Super-Critical University of Ottawa Loop (SCUOL) has been constructed for conducting heat transfer and fluid dynamics studies under sub-, near- and super-critical conditions.

Carbon dioxide was chosen as the working fluid because of its chemical inertness and its lower critical pressure and critical temperature compared to those of water (see Table 3.1). Therefore, by comparison to an experimental facility that uses supercritical water, SCUOL has less strict safety requirements and lower construction and operating costs. In addition, the normalized physical properties of water and carbon dioxide overlap when they are plotted vs. normalized pressures and temperatures. Such behaviour suggests that the data produced with carbon dioxide can be used for an application to water-based designs with some modification (Kim et al., 2006).

Table 3.1 – Critical conditions for water and CO_2

Property	**Value**	
	Water	**CO_2**
Critical pressure [MPa]	22.1	7.4
Critical temperature [°C]	374.1	31.0
Critical density [°C]	315	468

The facility is enclosed within two adjacent rooms, having concrete walls, as depicted in Figure 3.1. The main lab on the left side, measuring approximately3 m (W) ×6 m (D) × 5.5 m (H) in size, contains the primary CO_2 flow circuit, the power supply, the instrumentation and most of the support infrastructure, such as chilled water lines and electrical wiring. An overhead crane was installed for moving heavy equipment and supplies. The freezer chamber (Figure 3.2) on the right side houses a separate refrigeration system that can be used to cool the primary CO_2 loop to temperatures unachievable using university-supplied chilled water. Its working is explained in subsection 3.1.6.

A 3D CAD model of the entire facility has been built using the SolidWorks software package. It has become an integral part of the project as it proved to be a powerful tool for the design and construction processes. In a number of occasions it was also used to obtain important dimensional information that would be otherwise difficult to visualize and

measure using conventional means. Most of the facility overviews, 2D and 3D drawings presented in the thesis were generated from this model.

3.1.2 Primary flow circuit and CO_2 supply

The primary flow circuit (Figure 3.3) of SCUOL is an approximately 2 m tall, closed flow loop designed for a maximum system pressure of 15 MPa (2175 psia) and a nominal operating pressure of 10 MPa (1450 psia). Figure 3.4 is a schematic diagram showing the locations of the loop's main components, which will be introduced in the following sections.

The majority of the loop piping consists of stainless steel 316 (SS316) seamless tubing (Swagelok, Solon, Ohio, USA). Five different sizes are used: 25.4mm (1″) outer diameter (OD) with 2.1mm (0.083″) wall thickness, 12.7 mm (0.5″) OD with 0.89 mm (0.035″) wall thickness, 9.5 mm (3/8″) OD with 0.89 mm (0.035″) wall thickness and 3.2 mm (1/8″) OD with 0.71 mm (0.028″) wall thickness. They are nominally rated for working pressures of 21.4 MPa (3100 psia), 16.5 MPa (2400 psia), 17.9 MPa (2600 psia), 27.6 MPa (4000 psia) and 58.6 MPa (8500 psia), respectively. A large variety of fittings (Figure A.1) are used to connect the piping. These include crosses, tees, unions, reducers and adapters. All tube fittings and the majority of the valves used in the loop were also manufactured by Swagelok and were of high build quality and pressure ratings. The rest of the valves were manufactured by PMP Precision Valve Co. Ltd. of St. Laurent, Quebec, Canada and was degreased and cleaned. The reason for degreasing and cleaning is explained in subsection 3.1.10.

CO_2 with a purity of 99.998% (Grad 4.8) is fed into the loop from one of the high pressure cylinders (Linde Canada, Mississauga, Ontario, Canada). A pressure regulator

(TESCOM Model 44-1812-24, Emerson Process Management, a division of Emerson Electric Company, Ferguson, Missouri, USA) is installed at the outlet of the cylinder to control the filling pressure while charging the loop.

3.1.3 Pumps

The CO_2 flow in the loop is circulated by two gear pump-motor assemblies (Figure A.2figure A.2), connected in parallel. Having positive displacement, gear pumps were chosen for their smooth pulseless flow delivery, which is desirable for the present study. Each assembly consists of a gear pump produced by Micro pump (Model GL-H23.JFS.E-M2N1CH15, Figure A.3), driven by a 1-horsepower electric motor (56C WEG) through a rare-earth magnetic coupling. The use of this contactless coupling eliminates the possibility of fluid leak and contamination from lubricant inside the driving motor. The pump body, gears and O-rings seals are made of 316 stainless steel, PEEK™ and PTFE (Teflon®), respectively, which are all compatible with supercritical CO_2. The pump cup has a customized construction that can withstand a maximum system pressure of 10.3 MPa (1500 psia). The motors are driven by an inverter (Leeson® MICRO Series, Figure A.4). With the motors wired in a 2-pole configuration, each pump is nominally capable of delivering a maximum flow rate of 0.0177 m^3/min.

3.1.4 Accumulators

Loop pressure is stabilized by a group of five bellow-type accumulators (Figure A.5), pressurized with compressed nitrogen. These accumulators (Hydropad® Model 322000, Flexicraft Industries, Chicago, Illinois, USA) have a completely welded construction with all SS wetted parts. Compressed N_2 is housed in a rugged metal shell with a nominal capacity of0.00052 m^3 (32 in^3). CO_2 is separated by a metal bellow with a maximum fluid

displacement of 0.00031 m^3 (19.0 in^3). This design ensures a maintenance-free service and allows the use of corrosive liquids and high temperatures, which could not be accommodated by other units. By adjusting the pressure of the compressed N_2, the pressure of the CO_2can be maintained at 0.34-0.69 MPa (50-100 psi) below the N_2 pressure. The accumulators are mounted on a frame made of aluminium, which is fixed on a scale (HW-200-KV-WP, A&D Company Ltd., Tokyo, Japan). The weight of CO_2 inside the accumulators can be measured by comparison of the reading of the scale to its value when the accumulators are empty of CO_2.

3.1.5 Heat exchangers

After being heated up in the test sections, the CO_2needs to be cooled back to the desired inlet temperature so that a state-state circulation within the loop can be maintained. Two double-helical-coil tube-and-shell type heat exchangers (Model FXF-6223U, Sentry Equipment Corp, Oconomowoc, Wisconsin, USA, Figure A.6) were purchased and installed in 2009. They have a stainless steel construction and are rated for 2 MPa at 343 °C on the shell side and 17.6 MPa at 537 °C on the tube side. In January 2013, it was determined that two additional heat exchangers were required to achieve the cooling capacity specified by the desire heat flux value and to reduce flow resistance in the CO_2 circuit. By that time the FXF-6223U model had been discontinued by the manufacturer and succeeded by model FXR-6222U, which has the identical thermal characteristics and mounting dimensions. Two units of the latter model were purchased from the same supplier and connected in the loop.

The four heat exchangers are connected in parallel in order to minimize flow resistance. Two separate cooling systems can be connected to each or all of the heat exchangers, depending on needs: 1) chilled water supplied by the University of Ottawa

which is maintained at around 9 °C in summer and around 14 °C in winter; 2) a refrigeration system housed in the adjacent freezer chamber (see details in subsection 3.1.6) for reaching lower cooling temperatures using an ethylene-glycol based coolant(Dowthem® 4000, Dow Chemical Company, Midland, Michigan, USA). The particular blend purchased for the facility contains 50% water by weight and has a freezing point of -33.8 °C and a boiling point of 107.2 °C.

3.1.6 Freezer chamber

The freezer chamber (Figure 3.2) is virtually an oversized walk-in refrigerator constructed by Carmichael Engineering Ltd. of Ottawa, ON, Canada. The chamber can be cooled using two separate refrigeration units. The smaller unit is used to cool the chamber to temperatures above 5 °C, while the larger one is used when temperatures below 5 °C are required. Two canned motor pumps (Dynapump® Model JSB-2HP-1S, Chempump, a division of Teikoku USA Inc., Houston, Texas, USA) are installed near the chamber. Freezer chamber pump #1 delivers cold coolant to the heat exchangers in the primary circuit to cool the CO_2 fluid and returns warm coolant back into a reservoir inside the chamber. Freezer chamber pump #2 circulates the ethylene-glycol coolant through a radiator within the chamber in order to keep the coolant chilled at a desired temperature.

3.1.7 Preheater

In order to adjust the bulk fluid temperature at the test section inlet, a 21.3 kW preheater (CAST-X 3000 circulation heater, Part Number BX17E6G300U-WTT, Cast Aluminum Solutions, Batavia, Illinois, USA) is placed just upstream of the test section (Figure A.7). It consists of two helical coiled tubes and tubular elements cast into an Aluminium body. Its design of using aluminum body as the heat transfer medium between

the tubular element and the process tubes results in a long heater life and a reduced unit size,by comparison to traditional heaters. The dual-tube construction allows high flow rate and low pressure drop in two parallel passages and maintains accurate temperature control quicker when running one coil to heat and one to cool the fluid. The two seamless 316L stainless steel fluid tubes (19 mm OD X 1.7 mm wall thickness X 3556 mm length) can withstand a maximum working fluid pressure of 17.2 MPa and are heated by two three-phase delta circuits each providing AC current at 208 V and 29.6 A.

3.1.8 Power supply

The main power supply (Figure A.9), assembled by Carleton Electric Ltd. of Ottawa, ON, is rated for a maximum output current of 3000 A at 60 V. It draws power from the university's 380 V, 60 Hz, 3-phase AC power grid and outputs rectified DC current at 360 Hz (Figure A.9). This high frequency ensures that the heating of the test section remains nearly uniform both spatially and temporally. Four parallel heavy-gauge cables are used to distribute the current and reduce power loss due to heating of the cables.

3.1.9 Safety features

Carbon dioxide exists in Earth's atmosphere as a trace gas at a concentration of 0.039% by volume[3]. It is relatively inert and only toxic to animal life at very high concentrations (100 times the atmospheric concentration or greater). However it is an asphyxiant, which means that it can reduce or displace the normal oxygen concentration in breathing air. Inhaling oxygen-depleted air can lead to death by asphyxiation. Therefore, CO_2 must be handled with extreme caution in a confined space. Safety precautions in the

[3] http://en.wikipedia.org/wiki/Carbon_dioxide, retrieved on June 16, 2013

present facility include the use of a high volume air ventilation system and an oxygen depletion sensor. An oxygen level monitor (Oxyguard®, OxyGuard International A/S, Farum, Denmark) has been installed to constantly monitor the oxygen concentration in the atmosphere near the floor of the main lab where CO_2 escaping from the loop can accumulate. An audible alarm is triggered when the oxygen concentration drops below 19.6%.

A strainer (0100-YTC1500SS032, Sure Flow Equipment Inc., Tonawanda, New York, USA) was installed upstream of the pump inlets (Figure A.10). Inside the strainer is a 316 stainless steel perforated screen with a mesh size of 100 μm. The screen prevents debris from entering and damaging the pumps, as well as captures contaminants that can potentially hinder test results. The strainer was constructed from cast 316 stainless steel and was rated for a maximum operating pressure of 10.3 MPa (1500 psi) at 313 °C (596 °F).

A proportional relief valve (Swagelok® SS-R4S8, Figure A.11) is installed in the loop to relieve excessive pressure build-up caused by accidents such as loss of flow, pump failure and rapid heating of the test sections. The relief valve is set to open at a set pressure of 9.65 MPa (1400 psia).

As the last line of defence against loop over-pressurization, a rupture disc holder (25.4 mm PolySD Bolted Type Series, Fike Canada Inc., Burlington, Ontario, Canada, Figure A.12) was installed in the loop. As soon as the loop pressure exceeds the set value of 10.3 MPa (1500 psia), the Poly-SD rapture disc inside the holder will burst and release the pressure.

3.1.10 Material compatibility

During early stages of construction of the facility, some of the materials used were identified as incompatible with supercritical CO_2.

We observed that a number of elastomer seals used in some loop components swelled after exposure to SC CO_2, most likely caused by a phenomenon called Rapid Gas Decompression (also known as Explosive Decompression, ED). Many elastomeric seals contain small voids due to their manufacturing processes. When subject to high pressure, fluids can diffuse into these voids upon contact. If the pressure is reduced, the fluids expand rapidly (sometimes change phase) and create high tensile stresses or strains within the seal. This leads to elongation, swelling or even permanent damage to the seal, if its tensile strength is exceeded. To avoid such damage we replaced elastomeric seals with ones that are made of materials less susceptible to ED, including PTFE (Teflon™) and PEEK™.

Supercritical CO_2 is widely used in industrial extraction processes for its excellent ability as a solvent. Being aware of this fact, we suspected that the grease used to lubricate the in-flow valves might dissolve into SC CO_2 and cause detrimental effects. To mitigate this issue, we had all valves that come into contact with the flow thoroughly degreased and cleaned by Dalpro Technologies Inc. of Hamilton, Ontario, Canada.

3.2 Test section design

3.2.1 Inconel® alloys

The two tubular test sections installed in the loop are an Inconel® 600 tube with 8 mm ID and an Inconel® 625 tube with 22mm ID. Trademarked by Special Metals

Corporation of Huntington, West Virginia, USA, Inconel® is a family of austenitic nickel-chromium-based superalloys that often finds use in extreme environments subjected to high pressures and temperatures. Inconel® alloys retain some of their properties over a wide range of conditions; this reduces measurement uncertainties caused by property changes, thus making Inconel® favourable for the present research. Some of the physical constants of Inconel® 600 and 625 alloys can be found in Table 3.2. Thermal and electrical properties variations of both alloys within the temperature range relevant to the present study are presented in Tables 3.3 and 3.4.

Table 3.2 – Physical constants of Inconel® 600 and Inconel® 625 alloys

Property	**Value**	
	Inconel® 600	**Inconel® 625**
Density [kg/m^3]	8470	8440
Melting range [°C]	1354 - 1413	1290 - 1350
Currie temperature [°C]	-124	-196

Table 3.3 – Thermal property variations of Inconel® 600 alloy

Temperature [°C]	**Mean linear expansion [µm/m·°C]**	**Electrical resistivity [µΩ·m]**	**Thermal conductivity [W/m·°C]**
20	10.4	1.03	14.9
100	13.3	1.04	15.9
200	13.8	1.05	17.3
300	14.2	1.07	19.0

Table 3.4 – Thermal property variations of Inconel® 625 alloy

Temperature [°C]	**Mean linear expansion [m/m·°C]**	**Electrical resistivity [μΩ·m]**	**Thermal conductivity [W/m·°C]**
21	Undocumented	1.29	9.8
38	Undocumented	1.30	10.1
93	12.8	1.32	10.8
204	13.1	1.34	12.5
316	13.3	1.35	14.1

3.2.2 8 mm bare tube test section

The 8mm test section has a diameter that is comparable to the hydraulic diameter of a typical sub-channel in the CANFLEX fuel bundle proposed for the next generation of CANDU reactors. This TS was initially used to conduct commissioning tests of the loop and the instrumentation. Later on it was used to perform extensive tests for expanding the University of Ottawa Trans-critical Heat Transfer Look-up Table.

To construct the 8mm test section (Figure A.13) we started with an Inconel® 600 tube of 3.05-m length, 8 mm ID and 1-mm wall thickness. The tube was purchased from Greenville Tube Company of Janesville, Wisconsin, USA. An ANSI class 1500 slip-on flange was welded on each end of the tube. Welding and pressure test were performed at

Rock Welding Ltd. of Ottawa, Ontario, Canada which is a certified high pressure welding company. The test sections were then bolted to matching flanges in the loop using bolts and nuts that meet ASTM A194 standard for high-pressure service. Gaskets (GYLON® Style HP 3561, Garlock Sealing Technologies, Palmyra, New York, US) were placed in between the connecting flanges to provide pressure sealing and electrical insulation, which prevents electric current from leaking to the rest of the loop. GYLON® is a special PTFE (Teflon™) material with minimized creep and cold flow phenomena usually associated with PTFE products, while retaining other positive attributes of PTFE. In addition, the GYLON® material is reinforced with perforated stainless steel inserts, giving the gasket excellent temperature and pressure ratings (up to 260 °C and 17.2 MPa). Power clamps were machined by the University of Ottawa Civil and Mechanical Engineering machine shop for connecting the electrical cables coming from the power supply to the test sections. The ultra-conductive Alloy 101 copper blocks used in the machining process was purchased from McMaster-Carr Supply Company.

In order to determine heat transfer coefficients between the CO_2 fluid and the heated test section, wall temperature distribution along the test section was measured using thermocouples (TC) attached to the outer wall surface of the test section in a pattern depicted in Figure 4.1. Two holes of 0.38 mm (0.015″) ID were drilled using electric discharge machining process near the beginning and end of the heated part of the test section. Fittings with packing glands (Conax® HEGPK-125-A-XX, Conax Technologies, Buffalo, New York, USA) were mounted at these locations and connected to a differential pressure transmitter for measuring the pressure drop across the heated length. Each packing gland comes with a

single-piece PEEK™ insulator/sealant that provides both high pressure sealing up to 28.9 MPa (4200 psig) and electrical insulation up to 800 V (DC) and 200 A.

3.2.3 22 mm bare tube test section

The 22 mm test section is used to investigate tube diameter effects on heat transfer as well as turbulent phenomena in supercritical fluids. Its current design is similar to that of the 8 mm test section, with the following differences.

- The tube material is Inconel® 625 alloy and has a length of 2.86 m, 22 mm ID and 1.5 mm wall thickness.
- The pressure tap fittings are of a different design.
- The mounting pattern of the TC is different from that of the 8 mm test section (see Figure 4.2). The first thermocouple in the heated length (TC3) is located at 20 mm downstream from the bottom power clamp. The TC closest to the outlet (TC42) is located at 30 mm upstream of the upper power clamp.
- The heated length is 2.0 m.

For future in-flow measurements, a new 22 mm test section is under construction. It is welded to a probe insertion and traversing flange, which will house a Pitot tube, a thermocouple and hot- and cold-wire probes for measuring velocity and temperature profiles across the tube.

3.2.4 3-rod bundle test section

A 3-rod bundle test section (Figure 3.5), originally used by AECL, Chalk River Laboratory, for experiments using subcritical water, was donated to our project. It was intended to be installed in SCUOL for investigations of heat transfer in rod bundle sub-channels as well as the evaluation of the effects of spacers. This test section comprised three rods sealed inside a 25.4 mm (1″) ID stainless steel pressure tube. The rods were arranged in a pattern resulting in a pitch-to-diameter ratio of 1.14, which is equal to that of a current CANDU reactor fuel bundle. Each rod consisted of five sections, 500 mm long each, connected in tandem and separated by endplates. The three sections in the middle were made of Inconel® alloy while the other two sections were made of copper. Due to their relatively high resistivity, only the three middle sections would be heated significantly when connected to the power supply, making the heated length 1.50 m. Bearing pads and spacers were installed along the length of the rods to keep them straight and equally spaced. Within each rod there was a sliding TC, which could be traversed along the rod and rotated for measuring axial and circumferential temperature profiles.

Upon receiving this test section we identified a number of issues:

- The materials used for the seals and the insulating liner were suspected to be incompatible with SC CO_2.
- We estimated the rod thickness using measured electrical resistance and known resistivity of Inconel® alloy and found out that the rods might collapse when subject to a large pressure difference, that was within or close to the intended operating pressure range.

- There was severe leakage that required special techniques to fix, which were not available on-site.

Eventually we came to the conclusion that the bundle was not in an adequate condition to perform experiments with. An agreement was reached with AECL to rebuild the bundle. In January 2013, the rebuilt 3-rod bundle (Figure 3.6) was returned to us and was promptly installed in the loop. The following modifications and improvements were made to this test section.

- The insulating liner and the half filler rods were redesigned and fabricated with TEFLON™ and PEEK materials respectively. The machining of these pieces was contracted to IMCO Co. of Ottawa, Ontario, Canada.

- Each group of connected Inconel® rod segments was replaced with one 1.5 m long rod, made from the stock tubes that were used for the existing bare tube test sections. The copper extension rods connected before and after the Inconel rods were remade to be 452 mm long.

- Inside each of the Inconel heated rods, three sliding TC carriers were embedded and connected in tandem by SS push rods, 480 mm apart. By moving the push rods, the TCs slide and allow wall temperature measurements covering the entire heated length. The carrier nearest to the inlet carries one J-type thermocouple (Omega®), while the other two each carries two TCs, 180 degrees across. Figure 3.7 is a cutaway of the middle section of the bundle showing one of the carriers.

- A TC traversing mechanism (Figure 3.8) was mounted vertically at the top of the test section for more refined TC movement control and temperature measurements. Using a di-electric coupling, the end of each push rod was attached to the traverse platform which moves all push rods (essentially all TC carriers) at the same pace longitudinally. Motors on the platform rotate the carriers and enable independent circumferential temperature profile measurements. When the traverse platform moves to the lowest position possible, the bottom group of TCs are 32 mm from the beginning of the heated length. Details regarding instrumentation of the traverse are explained in Section 3.3.4.

- In accordance with AECL's latest SCWR research interest, instead of rod spacers and bearing pads, the rods were fitted with wire-wrap spacers. The wire-wrap pitch was 200 mm. Each wire wrap was fixed on the rod at the start of each pitch as well as in the middle (at 180 degree turn around the rod), using a strap that was 0.10 mm (0.004") thick and 6.35 mm (0.25") wide, which was spot-welded on the rod at its two ends.

3.2.5 Thermal insulation

In order to reduce measurement error caused by radial heat loss, three layers of thermal insulation were applied to each test section. A Teflon™ tape (Swagelok® MS-STR-8 PTFE tape tread sealant, 12.7 mm wide, rated for 232 °C) was wrapped directly around the test section and covered the TCs. The second layer of insulation was a fibreglass cloth tape wrapped on top of the Teflon™ tape along the entire length of the test section. Purchased

from Fisher Scientific of Hampton, New Hampshire, USA, this tape measured 25 mm in width, 0.8 mm in thickness and was usable up to 538 °C. The outermost layer was a commercial-grade foam rubber pipe insulation purchased from McMaster-Carr Supply Company of Elmhurst, Illinois, USA. This tube-shaped insulation was flexible and could be easily cut to shapes that tightly enveloped the test section and the two inner insulation layers. Experimental results indicated heat balance differences of 0.1-5% which suggested adequate insulation performance.

3.3 Instrumentation

3.3.1 Data acquisition system (DAS)

A dedicated computerized data acquisition system (DAS) was purchased from National Instruments of Austin, Texas, USA for monitoring and controlling facility operations, as well as logging experimental results. The backplane of the DAS was a PXI Express chassis (NI PXIe-1065, Figure A.14). Employing the versatile PXI computer bus standard, this chassis provided high speed access to a wide array of plug-in modules for different input signal types, while offering a Windows®-based user interface similar to that found on conventional PCs. In the following subsections, each type of module used is described following the description of the corresponding measured property.

3.3.2 Test section wall temperature

Wall temperature distributions of the tube test sections were measured using T-type thermocouples (Omega SA1XL-T-SRTC, Figure A.15). These TCs were supported on self-adhesive tape and could be directly fastened on the outer surface of the tubular test sections.

The silicone-based adhesive could withstand temperatures up to 260 °C. The TCs had a time constant lower than 0.15 s and an uncertainty of 0.5 °C. For the 8mm test section, a total of 44 TC signals were collected at 10 Hz by three thermocouple input modules (NI PXIe-4353). Each of these modules could take up to 32 inputs with a resolution of 24 bits and 0.32 °C precision at the maximum sampling rate of 90 Hz. The maximum input voltage range was ±80 mV.

Wall temperature profiles of the 3-rod bundle were obtained with a sliding thermocouple mechanism (see Section 3.2.4).

3.3.3 Bulk fluid temperature

In-flow bulk fluid temperature at various locations of the loop were measured with in-flow ultra-precise RTD sensors (Omega® P-M-1/10-1/8-5-1/2-G-15, Figure A.16).Within the range of 0 to 100 °C, these 4-wire 100-ohm DIN platinum RTDs could achieve class 1/10DIN accuracy of ± (0.3 + 0.005 |T|) °C. Three RTD input modules (NI 9217) were plugged in the DAS to read a total of nine signals at 10 Hz. Each module could measure up to four 100-Ω RTD inputs simultaneously at a maximum scan rate of 100 Hz. When operating in 4-wire mode, these modules could achieve a maximum accuracy of 0.35 °C within the range from -150 to 200 °C.

3.3.4 Position measurement in the rod bundle

Due to the design of the 3-rod bundle test section, position and orientation of the sliding thermocouples needed to be determined to produce accurate wall temperature distributions. For detailed information regarding the design of the sliding TC assembly and the driving traverse mechanism, refer to Section 3.2.4.

Longitudinally all TCs moved at the same pace as the motor platform did, although individual TCs were not necessarily at the same axial position. Since the dimension of each push rod was given, the exact location of each TC could be deduced from the position of the traverse platform. For this purpose, a wire-rope potentiometer (Model LX-PA-25, Uni Measure of Corvallis, Oregon, USA) was installed on the traverse. It had a linearity of ±0.25% over its full moving range of 0.625 m. The voltage output from the potentiometer was collected by a voltage measurement module (NI 9225) and converted into usable position information using an equation programmed in the LabVIEW® interface.

Circumferentially, each TC rotated at the same angular speed with the motor that drives the push rod said TC attached to. A quadrature encoder (AMT10X Series, CUI Inc, Tualatin, Oregon, USA) was mated to the shaft of each of the three driving motors and produces digital square-wave signals as they rotate. These signals were captured by an input board (NI PXI-6289, for motor 1 and 2) and an input module (NI 9411, for motor 3) and converted into angle values.

3.3.5 Absolute pressure measurement

The absolute loop pressure was obtained with a pressure transducer (Omega® PX01C1-3KA5T, Figure A.17) with an accuracy of ±10.3 kPa (1.5 psi). This sensor was directly connected to the lower pressure tap, which was located 50mm below the beginning of the heated part of the test section. The pressure transducer required a direct current excitation of 10 to 40 V in order to generate a voltage output of 0-5 V with an accuracy of ±0.05% over a full measurement range of 0-20.7 MPa (0-3000 psi).The signal was picked up by an analog input module (NI PXI-6289) at 10 Hz and then converted to a pressure value in MPa or psia using an equation programmed in the LabVIEW® interface. The module was

capable of taking 32 analog inputs at a maximum sample rate of 625,000 samples/s. It allowed the user to select from seven different measurement ranges according to the circumstance. When using the range of -5 to 5 V (most applicable to the pressure measurement signal), the measurement accuracy was ±510 μV (±0.01%).

3.3.6 Differential pressure measurement

The pressure drop across the heated length of the test section was obtained with an differential pressure transmitter (Omega® PX771A-300DI, Figure A.18). It required a direct current excitation of 7 to 36 V in order to generate a current output of 4 to 20 mA with an accuracy of ±0.1% within the full measurement range of 0 - 74.72 kPa. The current output was wired to a 249±1%Ω resistor that converted it to a voltage output of 1-5 V, which was measured by an analog input module (NI PXI-6289). The voltage could then be converted to a pressure value in kPa or psi using an equation programmed in the LabVIEW® interface. To calculate the frictional pressure loss from the measured pressure difference, one needs to take into account the elevation difference between the transmitter and the pressure taps as well as the variation of fluid density along the test section and the lines connecting test section to the transmitter.

3.3.7 Flow rate

Accurate true mass flow rate was required for calculating some important parameters such as mass flux and heat balance error. For this purpose we purchased a Coriolis flow meter (Micro Motion® Elite® Model CFM050M320N0A2E2ZZ, Emerson Flow Management, Figure A.19). The transmitter (2400SIA11B2EZZZ) onboard the flow meter generated a current output of 4 to 20 mA with an accuracy of ±0.03% (factory calibrated) within the full measurement range of 0-56.7 kg/min. The current output was wired to a

249±1%Ω resistor that converted it to a voltage output of 1-5 V, which was measured by an analog input module (NI PXI-6289). The voltage value was then automatically converted to a flow rate value in kg/s using an equation programmed in the LabVIEW® interface.

3.3.8 Heating power

Power clamps were connected to a voltage measurement module (NI 9225) for measuring the voltage drop across the heated length of the test section. The sample rate set for the experiments was 2,000 samples/s. The module was capable of measuring three inputs simultaneously at 50,000 samples per input per second with a resolution of 24 bits over ±300 V range and an accuracy of 0.034 V. Current measurement was attempted by measuring the voltage drop across a 50-mΩ shunt built into the power supply. However, large measurement variation and discrepancy from expected value made this reading unusable. The heating power was instead calculated from voltage drop and electrical resistance of the test section, which was estimated using Inconel® resistivity values provided by Special Metals.

3.3.9 LabVIEW® software interface

A graphic user interface (Figure A.20) was developed under the LabVIEW® programming environment. The interface was divided into three sub-panels. The left sub-panel presented important readings, including pressure, mass flow rate, CO_2 bulk temperature and test section pressure drop over a set period of time. The middle sub-panel displayed time averages of all loop operating parameters over 10 and 60 s. The difference between each pair of averages was calculated to reflect the trend of change of the corresponding parameter. The right sub-panel displayed some other important information, including the wall TC profiles (spatial and temporal), heating voltage, power and heat

balance. On this sub-panel there were also control dials for adjusting pump operating frequency and log file name.

3.4 Loop control

The LabVIEW® software interface communicated directly with the power inverter (Figure A.4), which drove the CO_2 circulation pumps. The desired operating frequency of the pumps could be controlled by adjusting the value of Set Frequency on the right panel of the interface. Meanwhile, the actual running frequency returned by the inverter was displayed and recorded. Alternatively, one could adjust the settings using the control panel on the inverter. This would overwrite settings placed in the LabVIEW® software interface, providing a kind of safety measure in case the computer freezes. To turn on or off the pumps, the operator had to use the manual switch located on the wall to the left of the DAS (Figure A.21). This physical switch also overwrote the commands sent from the software interface, eliminating the possibility of losing pump control if the software interface accidentally crashed. The switch was interlinked with the power supply control such that killing pump power by pressing the Emergency Stop button also kills heating. This feature prevents dangerous overheating of the test section in the event of accidental pump shutdown during an experiment.

The heating power supplied to the test sections was regulated by a switch box (Figure A.22) on the wall to the left of the operator station. The box was assembled by Carleton Electric Ltd. of Ottawa, Ontario, Canada. To adjust the heating power level once the power supply was started, the operator would turn the potentiometer (clockwise for increasing

power) and observe the power readings on the LabVIEW® interface until the desired power or heat flux was reached.

A temperature controller box (Figure A.23) was installed on the wall outside of the freezer chamber. It measured the temperature inside the freezer chamber using a thermostat and compared the reading with the set value to determine whether or not to run the refrigerator. We were advised to operate the freezer chamber at least once a month in order to keep the refrigeration units sufficiently lubricated to avoid any damage to the components. An operating log was kept on the box to keep track of the usage of the freezer chamber.

The power fed into the preheater was regulated by a control panel (assembled by Zesta Engineering Ltd., Mississauga, Ontario, Canada, Figure A.24). Power control was achieved with a controller (EZ-ZONE® PM type, Watlow, St. Louis, Missouri, USA) mounted inside the panel. This controller used Watlow standard bus that could directly communicate with the LabVIEW® interface programmed in the DAS. This allowed us to control and monitor the preheating power and temperature in real-time. A flow bypass dedicated to the preheater was installed, giving us the ability to regulate the amount of CO_2 being preheated before entering one of the test sections. As the enthalpy values before and after the preheater as well as the preheating power were all measured in the LabVIEW® interface, the actual flow rate of CO_2 bypassed could be easily estimated.

A power inverter (Delta® VFD-B, Delta Power Solutions, Figure A.25) situated next to the freezer chamber entrance regulated the running frequency of freezer chamber pump #1 which delivered the ethylene-glycol coolant to the primary CO_2 circuit. The frequency could be set at any value within the range of 20-60 Hz depending on the coolant flow rate required.

The desired ethylene-glycol coolant temperature could be set on the controller (Figure A.26) for freezer chamber pump #2. The controller sensed the coolant temperature inside the freezer chamber and would switch on the pump if the coolant became warmer than the set value. The coolant would then be circulated through the radiator in the chamber and be chilled. The controller automatically shut the pump down once the coolant was chilled to the desired temperature.

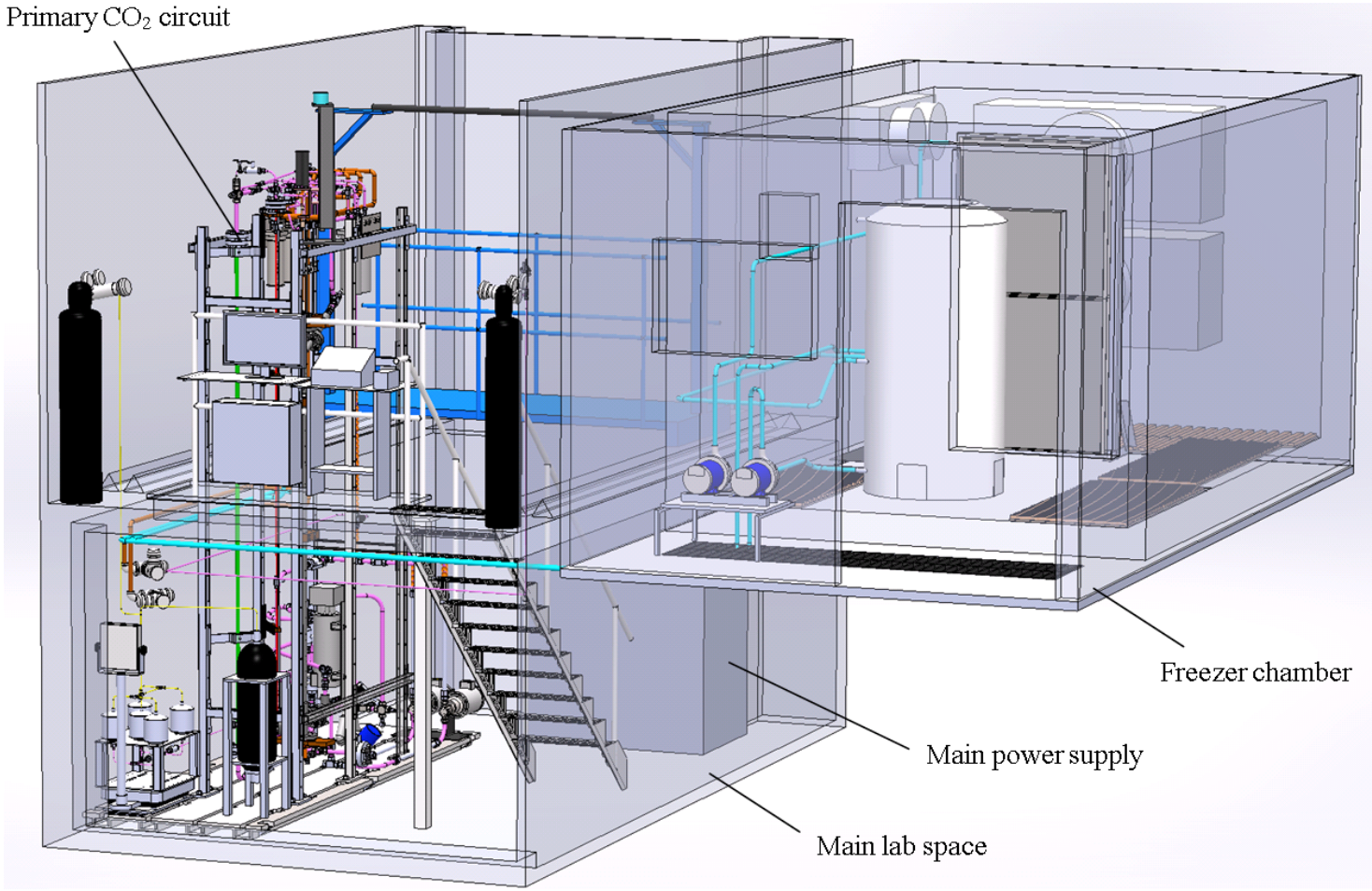

Figure 3.1 – Super-Critical University of Ottawa Loop (SCUOL)

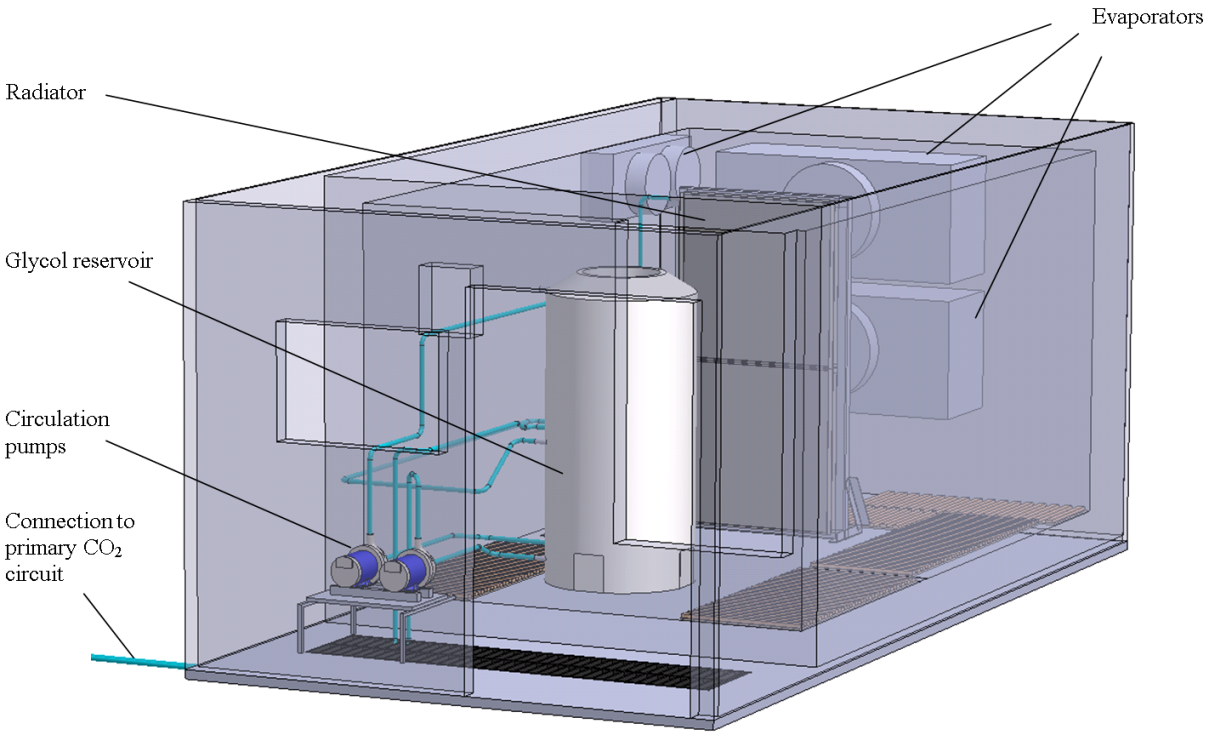

Figure 3.2 – Freezer chamber

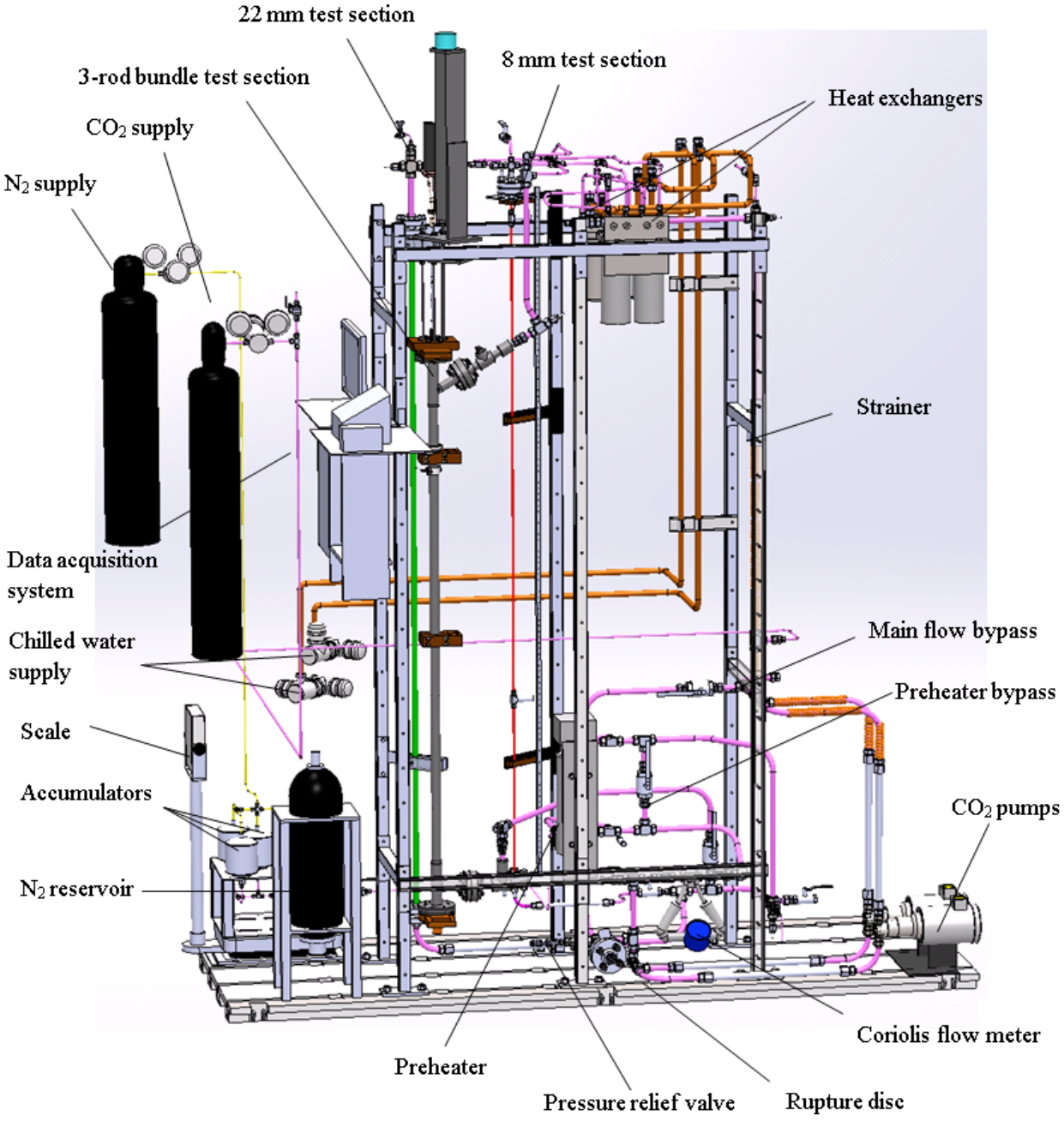

Figure 3.3– Primary CO_2 circuit

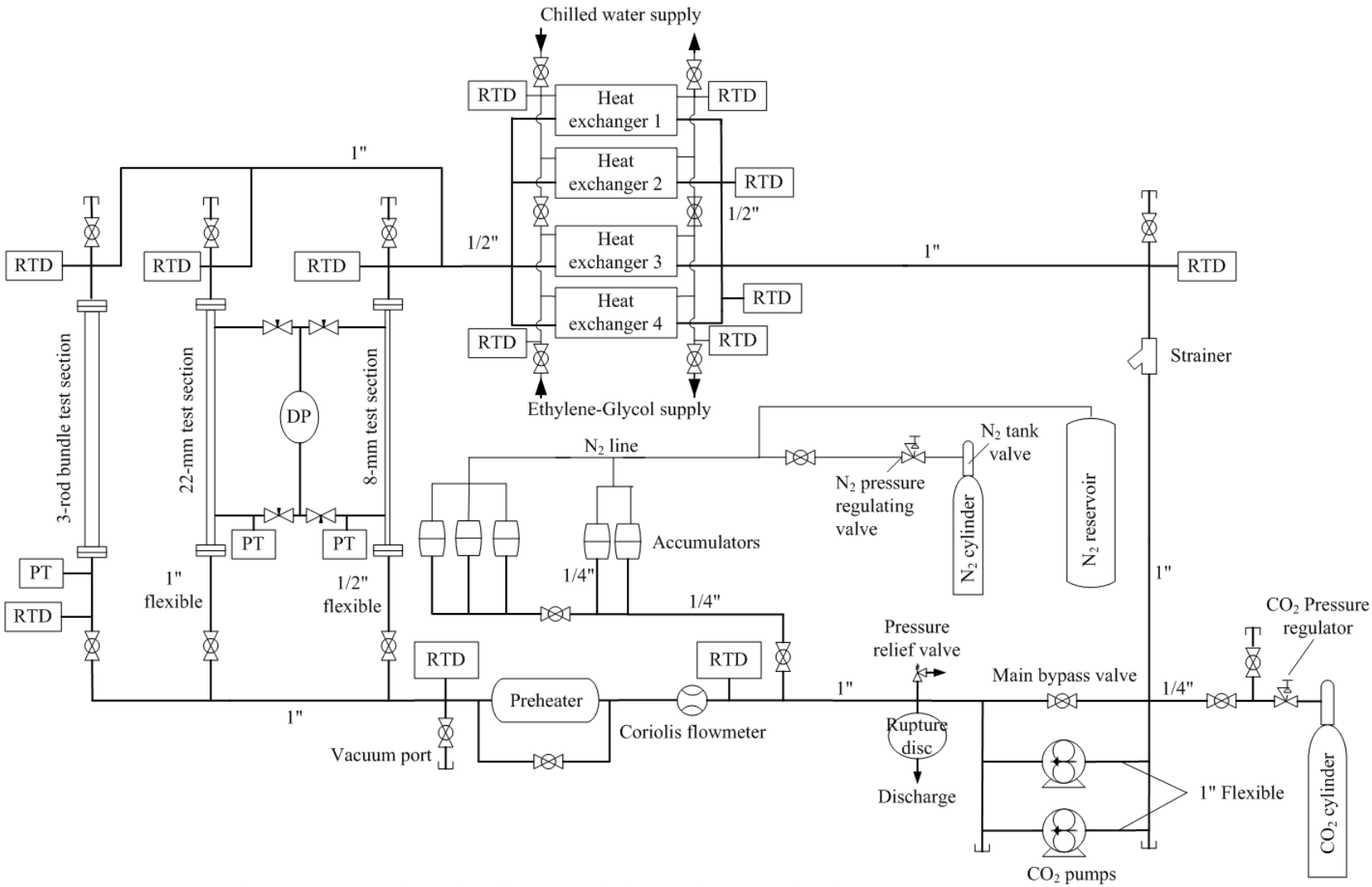

Figure 3.4 – Schematic diagram of the main CO_2 circuit (PT = pressure transducer, DP = differential pressure sensor)

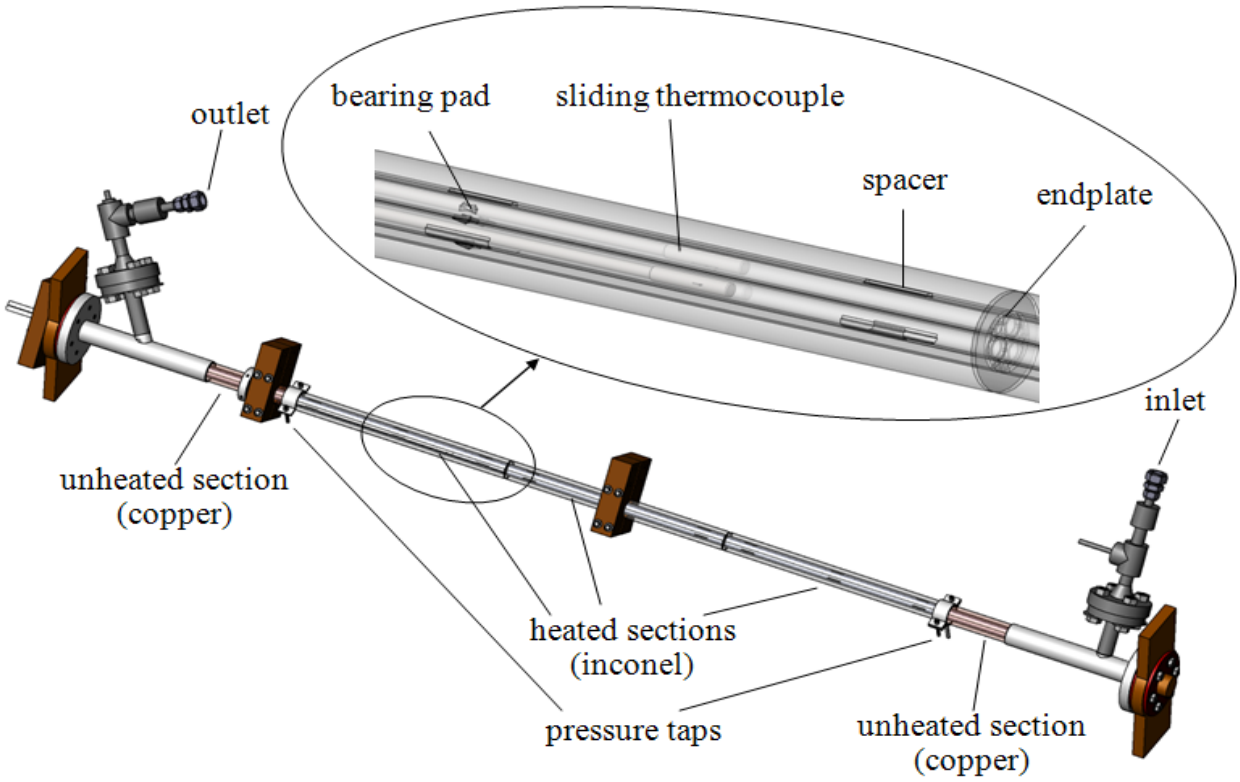

Figure 3.5 – Original 3-rod bundle test section

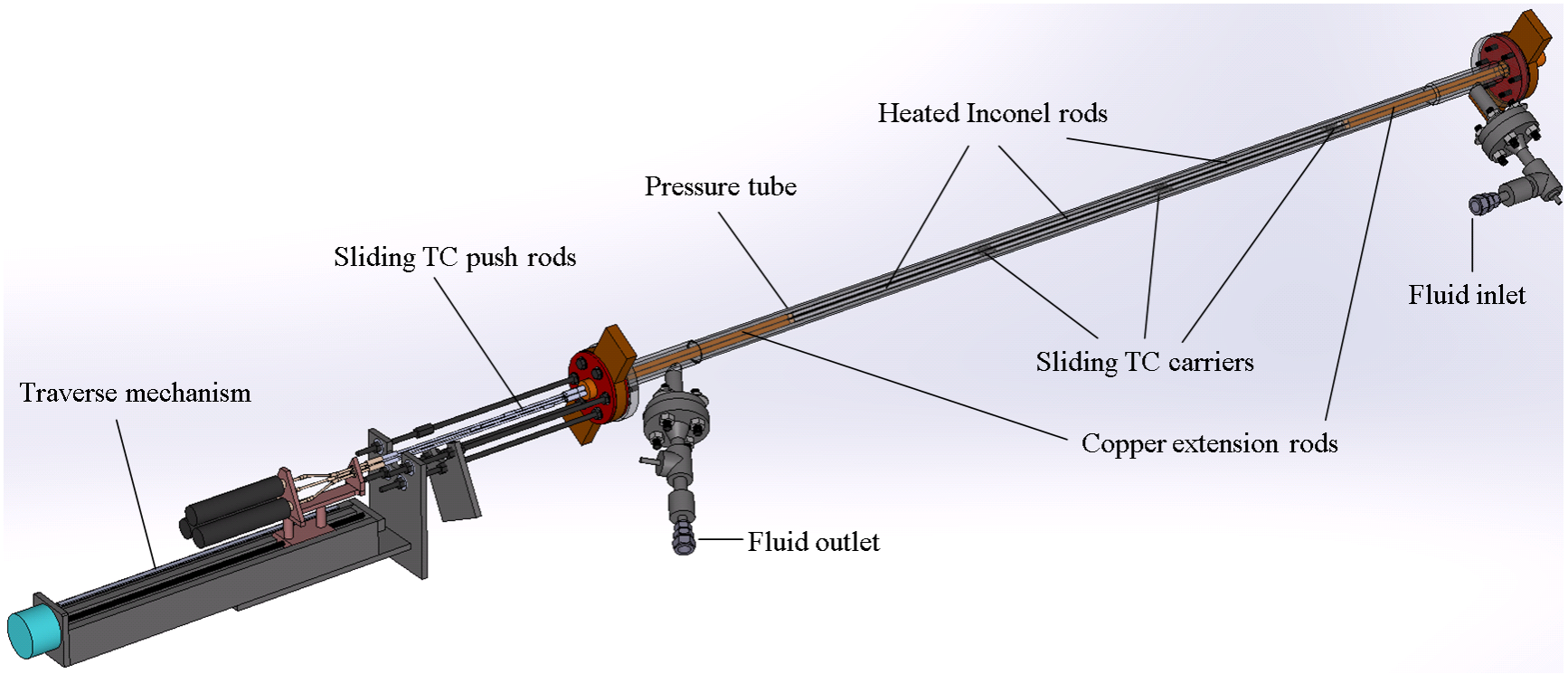

Figure 3.6 – Retrofitted 3-rod bundle test section (Teflon liner omitted for clarity)

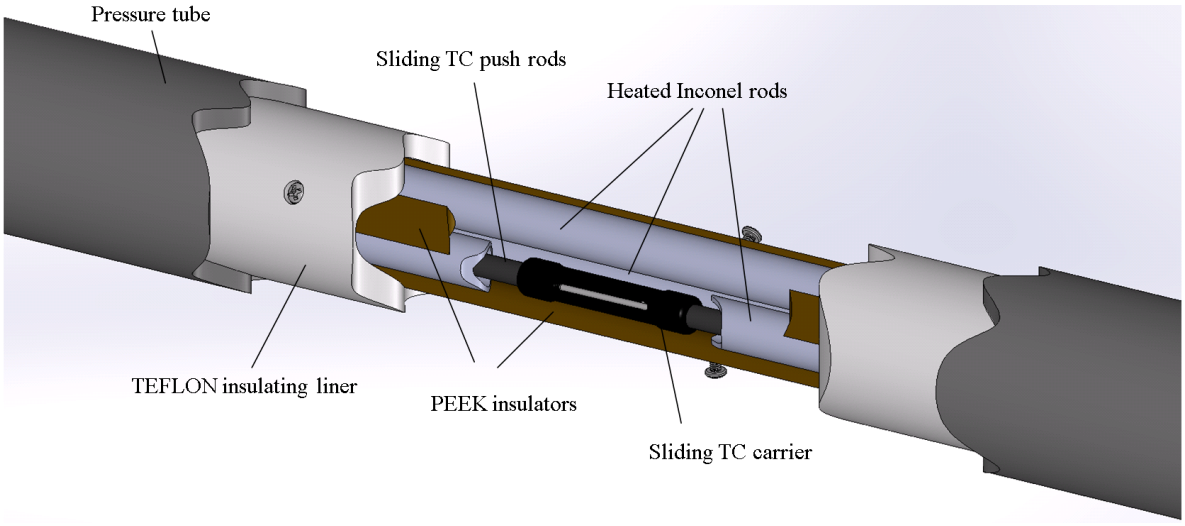

Figure 3.7 – Cutaway of the 3- rod bundle middle section

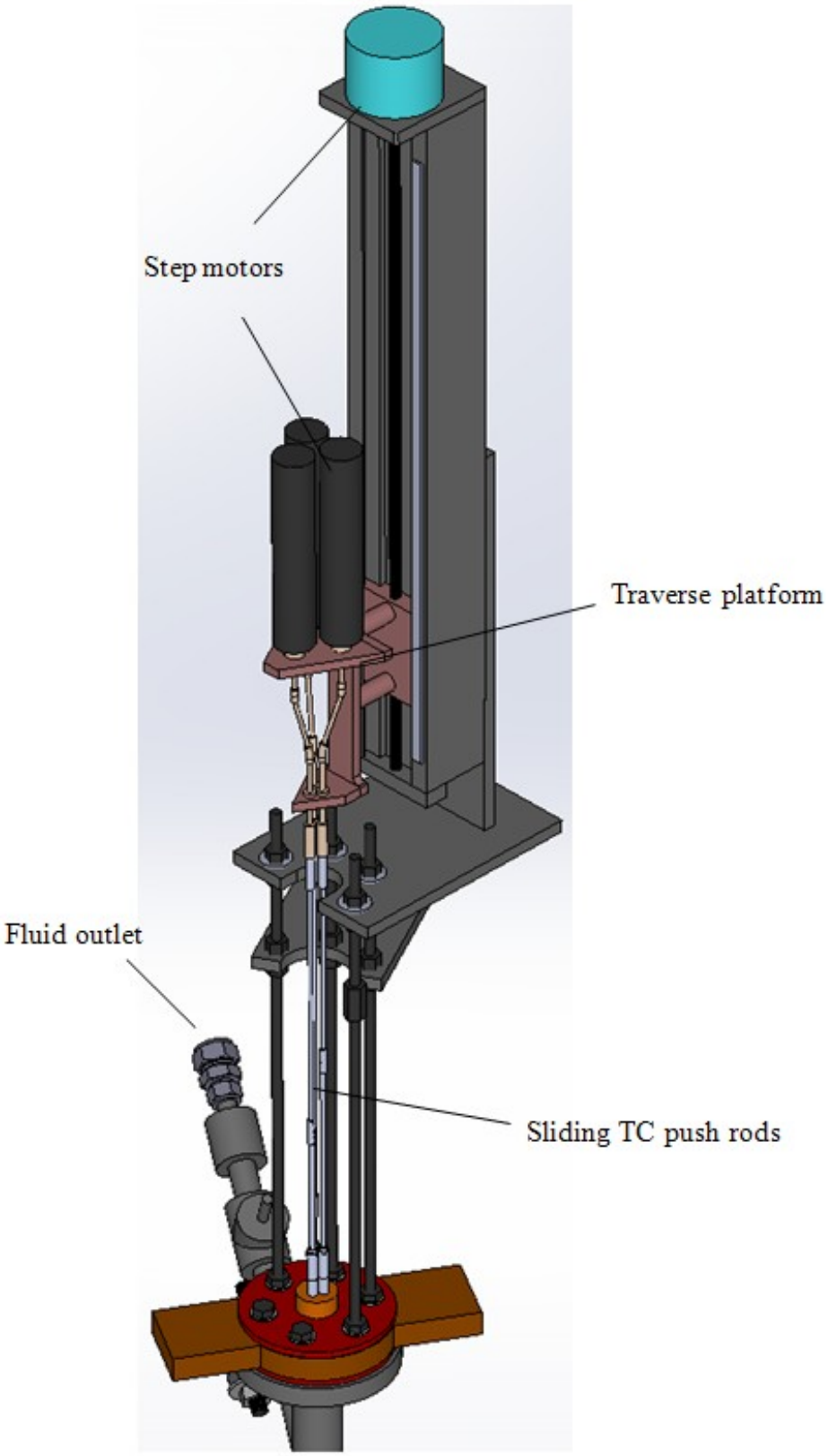

Figure 3.8 – 3-rod bundle traverse mechanism

Chapter 4 Measurement Procedures

4.1 General comments

As documented in Chapter 3, the sensors installed in SCUOL were capable of measuring TS inlet pressure, pressure drop across the TS, mass flux, heating power and TS wall temperature distribution. Some of these variables were parts of the equations for calculating the heat transfer coefficient, while others were used to evaluate thermophysical properties of CO_2 that were required in the equations.

The control parameters of the tests were loop pressure P, mass flux G, heat flux q and inlet temperature T_{in}. Tests with the same P and G values were usually grouped together and performed in sequence, starting with the lowest q value.

Each experiment started by charging the loop to the desired pressure and adjusting the mass flux by setting the appropriate pump frequency. Once the test conditions were set and a constant flow was established, one waited for the wall temperature readings in the test section to stop fluctuating with time and eventually become a plateau. Then the system was deemed to have reached steady state and the measurements were recorded.

4.2 Averaging of collected samples

It occurred occasionally that electronic and background noise were picked up by instruments and recorded. Hence, the data collected were subject to an outlier test. Samples too far away from the mean were marked and eliminated before the data set were properly averaged and used for calculations.

The 3-sigma rule states that 99.73% of the samples within a data set fall within 3 standard deviations of the mean, provided that the data set follows a normal distribution (Tavoularis, 2005). We considered this probability to be sufficient for the present study. Later results showed that the amount of outliers is insignificant (less than 1 in 200 samples). This indicated that the assumption of normal distribution is acceptable. The procedure was as follows:

- Calculate the arithmetic mean μ of all samples in a collected data set ($x_1, x_2, \ldots, x_N$):

$$\mu = \frac{1}{N}\sum_{i=1}^{N} x_i \tag{4.1}$$

- Calculate the standard deviation of the sample set:

$$\sigma = \sqrt{\frac{1}{N-1}\sum_{i=1}^{N}(x_i - \mu)^2} \tag{4.2}$$

- Identify a sample x_i as outlier if

$$3\sigma \leq |x_i - \mu| \tag{4.3}$$

- Remove all outliers from the sample set. Recalculate the arithmetic mean.

A sub-routine in the LabView interface was programmed specifically for performing this procedure automatically.

4.3 Approximation of test section thermal conductivity

When a test section was heated up by the electric current supplied by the power source, its temperature could rise to a few hundred degrees Celsius. We limited this temperature to a maximum of 225 °C, to avoid melting of the glue used to attach the thermocouples to the TS, which was rated for 260 °C.

The thermal conductivity k of Inconel alloys does not vary significantly within the temperature range that concerns the present study. However, for better accuracy we computed the value of k by the use of relationships curve fitted to the data supplied by the manufacturer (see Tables 3.3 and 3.4).

Using Microsoft Excel's LINEST, a linear fitting function, the equation for approximating k values of Inconel 600 and Inconel 625 alloys were found, respectively, as

$$k = 0.0146T + 14.509 \tag{4.4}$$

$$k = 0.0145T + 9.503 \tag{4.5}$$

where the unit of T is °C. Values approximated using these equations are listed in Tables 4.1 and 4.2 and compared to the provided values. The mean square differences calculated from these values for the two equations were 5.035×10^{-6} and 3.789×10^{-7} respectively, indicating good fits.

Table 4.1 – Curve fitting data for *k* of Inconel 600 alloy

Temperature [°C]	**Provided values [W/m·°C]**	**Approximated values [W/m·°C]**	**Difference %**
20	14.9	14.80	-0.491
100	15.9	15.97	0.071
200	17.3	17.43	0.066
300	19	18.89	-0.035

Table 4.2 – Curve fitting data for *k* of Inconel 625 alloy

Temperature [°C]	**Provided values [W/m·°C]**	**Approximated values [W/m·°C]**	**Error %**
21	9.8	9.81	0.040
38	10.1	10.05	-0.116
93	10.8	10.86	0.061
204	12.5	12.47	-0.013
316	14.1	14.10	0.001

4.4 Measurement of heating power and heat flux

The heating power supplied to a test section was determined as

$$Q = VI \tag{4.6}$$

where I was the electric current running through the TS and V was the measured voltage drop across the power clamps on the TS. Equation 4.3 can take the alternative forms

$$Q = \frac{V^2}{R} = I^2 R \tag{4.7}$$

Initially we attempted to measure the current by connecting a 50 mΩ shunt in the circuit and measuring the voltage drop across it. The current value would then be calculated using Ohm's Law. However, during the experiments the voltage readings fluctuated erratically and accurate values could not be obtained. We decided to use Equation 4.4 instead for calculating the heating power. For a conductor with uniform cross section and homogeneous properties throughout the length, such as the two tube test sections used for present study, the electrical resistance R was obtained using

$$R = \frac{\rho L_H}{A_{cs}} \tag{4.8}$$

where ρ is the electrical resistivity, L_h is the heated length and A_{cs} is the cross-sectional area of the test section. The values of these parameters can be found in Table 4.3.

Table 4.3 – Electrical properties of the 8 mm and 22 mm test sections

Test section	ρ **[μΩ·m]**	L_h **[mm]**	A_{cs} **[m^2]**	R **[Ω]**
8 mm tube (Inconel 600)	1.03	1940	2.827×10^{-5}	0.0707
22 mm tube (Inconel 625)	1.29	2000	1.107×10^{-4}	0.0233

As for the 3-rod bundle test section, its resistance was estimated as the equivalent of three 1.5 m long Inconel 600 rods connected in parallel (as depicted in Figure 4.3). Because the resistivity of copper (0.0168 μΩ·m at 20 °C) is significantly lower than that of Inconel 600, the resistance of the copper rods in the bundle was ignored in the calculation. The resistance of each Inconel 600 rod, calculated using Equation 4.5, is 0.0546 Ω. The total resistance of the 3-rod bundle test section was one third of that of a single rod, namely 0.0182 Ω. Independent measurements of the rod bundle resistance with the use of an oscilloscope (Tektronix® TDS1001B) gave a value of 0.018 Ω, indicating that the estimation was acceptable.

The available power supply produced a rectified AC instead of an ideal DC, so that voltage and current vary with time and the instantaneous power is

$$Q(t) = V(t)I(t) \tag{4.9}$$

The time-averaged power was computed as

$$Q_{avg} = V_{rms} I_{rms} = I_{rms}^2 R = \frac{V_{rms}^2}{R} \tag{4.10}$$

where *rms* denotes the root mean square value. For the present tests, the root mean square values of the voltage measurements V_{rms} were calculated by an rms function within the LabVIEW program and recorded.

The heat flux q, the rate of thermal energy transfer through a surface with unit area, was defined as

$$q = \frac{Q}{A_h} \tag{4.11}$$

where A_h is the heated area that was in contact with the fluid. For the tube test sections, $A_h = \pi d_i L_h$, where d_i is the inner diameter of the tube.

For example, if one measured V_{rms} = 10.0 V across the heated length of the 8 mm TS, the heating power would be 1.414 kW and the heat flux would be 29.0 kW/m^2.

The heat flux was used as a controlled parameter in our experiments to represent the level of heating, in lieu of the actual total heating power, as it takes into account both the total heating power and the area of the surface on which heat transfer took place.

4.5 Wall temperature measurement

When electrically heated, the 8 mm and 22 mm test sections were considered as long solid tubes, insulated at the outer radius r_o and cooled by CO_2 at the inner radius r_i, with a heated length of L_h and a uniform volumetric heat generation rate q_v in the solid (Figure 4.4)

$$q_v = \frac{Q}{\pi\left(r_o^2 - r_i^2\right)L_h} \tag{4.12}$$

The difference between outer wall surface temperature $T_{w,o}$ and inner wall surface temperature T_w was calculated using the following equation (Incropera, 2007):

$$T_w = T_{w,o} - q_v \cdot \frac{r_o^2}{2k} \cdot ln\left(\frac{r_o}{r_i}\right) + \frac{\left(r_o^2 - r_i^2\right)\cdot q_v}{4k} \tag{4.13}$$

where k is the thermal conductivity [W/(m•K)] of the test section approximated using either Equation 4.4 or 4.5, depending on the test section.

The outer wall surface temperature $T_{w,o}$ was measured with thermocouples placed in the patterns shown in Figure 4.1 (8-mm TS) and in Figure 4.2 (22-mm TS). Z_h, the axial locations of the TC within heat lengths of both TS are presented in Table 4.4 and Table 4.5. The sampling rate was 10 samples per second per thermocouple and each scan lasted 20 - 25 s after steady state was reached. The samples for each TC were averaged using the procedure stated in section 4.2. The temperature T_w of the inner wall surface where the convective heat transfer to the CO_2 coolant actually takes place was estimated and used to calculate the heat transfer coefficient, as will be explained in the next section. Figure 4.5 presents the measured

$T_{w,o}$ and estimated T_w values for a sample test performed in the 8 mm TS at the pressure of 8.36 MPa.

Table 4.4 – Axial locations of the wall temperature thermocouples in the 8 mm test section

TC #	04	05	06	07	08	09	10
Z_h, m	0.053	0.103	0.153	0.203	0.253	0.303	0.353
TC #	11	12	13	14	15	16	17
Z_h, m	0.403	0.453	0.503	0.553	0.603	0.653	0.703
TC #	18	19	20	21	22	23	24
Z_h, m	0.753	0.803	0.853	0.903	0.953	1.034	1.084
TC #	25	26	27	28	29	30	31
Z_h, m	1.134	1.184	1.234	1.284	1.334	1.384	1.434
TC #	32	33	34	35	36	37	38
Z_h, m	1.484	1.534	1.584	1.634	1.684	1.734	1.784
TC #	39	40	41				
Z_h, m	1.834	1.884	1.934				

Table 4.5 – Axial locations of the wall temperature thermocouples in the 22 mm test section

TC #	03	04	05	06	07	08	09
Z_h, m	0.02	0.07	0.12	0.17	0.22	0.27	0.32
TC #	10	11	12	13	14	15	16
Z_h, m	0.37	0.42	0.47	0.52	0.57	0.62	0.67
TC #	17	18	19	20	21	22	23
Z_h, m	0.72	0.77	0.82	0.87	0.92	0.97	1.02
TC #	24	25	26	27	28	29	30
Z_h, m	1.07	1.12	1.17	1.22	1.27	1.32	1.37
TC #	31	32	33	34	35	36	37
Z_h, m	1.42	1.47	1.52	1.57	1.62	1.67	1.72
TC #	38	39	40	41	42		
Z_h, m	1.77	1.82	1.87	1.92	1.97		

4.6 Calculation of convective heat transfer coefficient

The convective heat transfer coefficient h from a heated wall surface of area A and temperature T_w to a surrounding fluid with local bulk temperature T_b was calculated as

$$h = \frac{Q}{A\left(T_w - T_b\right)} = \frac{q}{T_w - T_b} \tag{4.14}$$

The bulk fluid temperature T_b at any location in the TS was evaluated from the local fluid enthalpy H_b using the NIST fluid properties database (Lemmon et al., 2002). H_b was extrapolated as

$$H_b = H_{in} + \frac{Z_h}{L_h}\left(H_{out} - H_{in}\right) \tag{4.15}$$

Where Z_h is the axial coordinate of the location along the heated length, H_{in} and H_{out} are the enthalpy values at TS inlet and outlet respectively. Since the bulk fluid temperatures at these locations were measured, H_{in} and H_{out} were obtained using the NIST database as well. Figure 4.6 presents the estimated T_w, T_b and calculated h values for one of the tests performed in the 8 mm TS.

4.7 Heat balance

The first law of thermodynamics states that energy cannot be created nor destroyed. This means that the amount of energy entering a control system (in our case the test section) equals that leaving the system:

$$Q - Q_{loss} = \dot{m}(H + \frac{v^2}{2} + gZ)_{out} - \dot{m}(H + \frac{v^2}{2} + gZ)_{in} + \frac{dE}{dt} \quad (4.16)$$

where Q_{loss} is the sum of heat loss through imperfect insulation and axial conduction along the test section tube. E is the energy of the solid materials inside the control system. For steady-state processes, $\dot{m}$ is constant and dE/dt is zero. The axial location of the inlet and outlet, Z_{in} and Z_{out}, are pre-determined. CO_2 enthalpy values H_{in} and H_{out} were evaluated by the LabVIEW interface, using real-time measurements of inlet and outlet fluid temperatures. Flow velocity v_{in} and v_{out} were calculated from flow rate $\dot{m}$, flow area and density values evaluated at inlet and outlet. Although the fluid density varied vastly from inlet to outlet, the change of the kinetic components of Equation 4.17 (on the order of tens of watts) was miniscule compared to the total energy (on the order of kilowatts) and therefore ignored.

For instance, during one of the experiments performed in the 8 mm test section at 8.46 MPa, $\dot{m}$ and Q were measured as 0.075 kg/s and 17.06 kW respectively. T_{in} = 10.3 °C, H_{in} = 213.7 kJ/kg, T_{out} = 51.8 °C, H_{out} = 433.1 kJ/kg and Q_{loss} was found to be 0.600 kW. This amounts to a percentage loss of 3.52%, which indicates that the TS insulation was adequate and that the instrumentation performed properly.

4.8 Calculation of hydraulic diameter of the 3-rod bundle test section

The hydraulic diameter of a non-circular channel was defined as

$$D_{hy} = \frac{4A_f}{P} \tag{4.17}$$

where P is the wetted perimeter[4] and A_f is the cross-sectional area of the channel that is occupied by the fluid. The values for the present experiments were

P = 0.183 m (as calculated using SolidWorks software package)

A = 0.000187 m^2 (as calculated using SolidWorks software package)

D_h = 4.08 mm

[4] This includes surfaces that are in direct contact with the fluid, except those of the wire wrap; in the present rod bundle, these are the surfaces of the TEFLON insulating liner, PEEK partial rods and heated Inconel 600 rods (see Section 3.2.4).

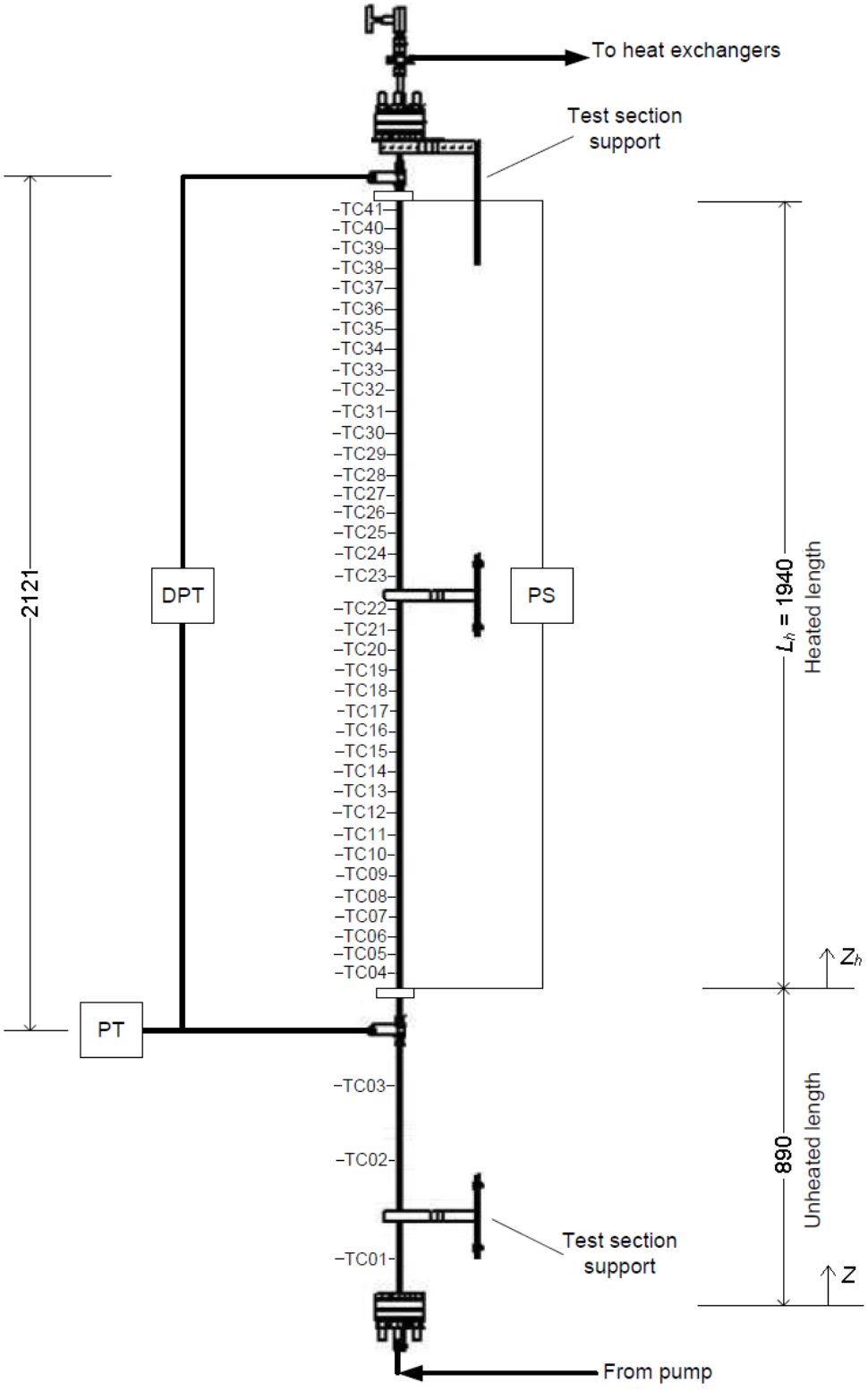

Figure 4.1 – 8 mm test section thermocouple locations

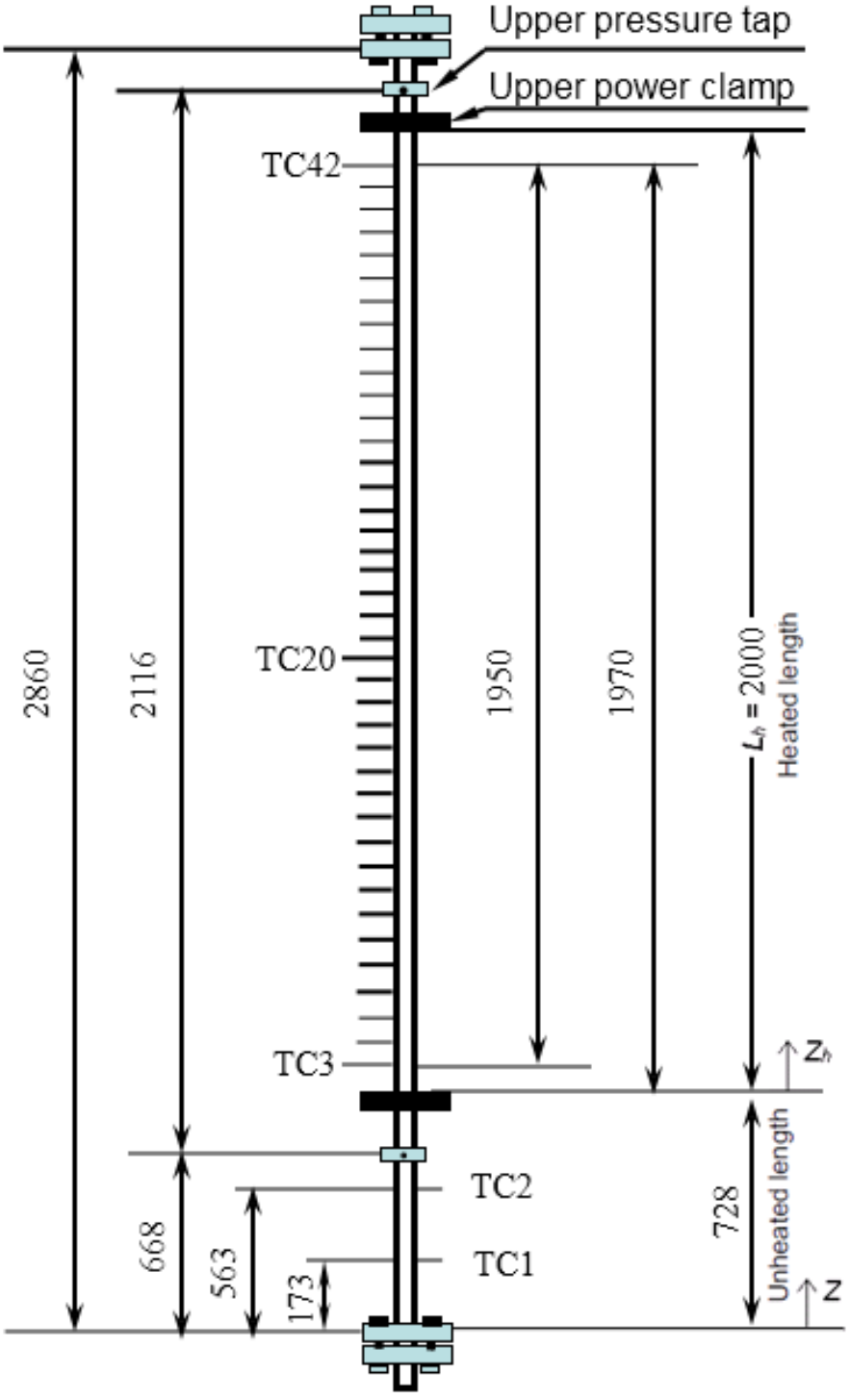

Figure 4.2 – 22 mm test section thermocouple locations

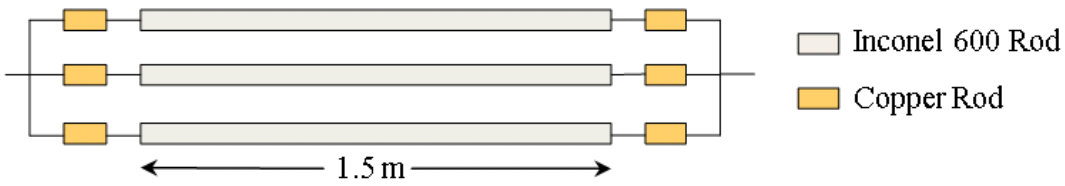

Figure 4.3 – Electrical elements of the 3-rod bundle test section

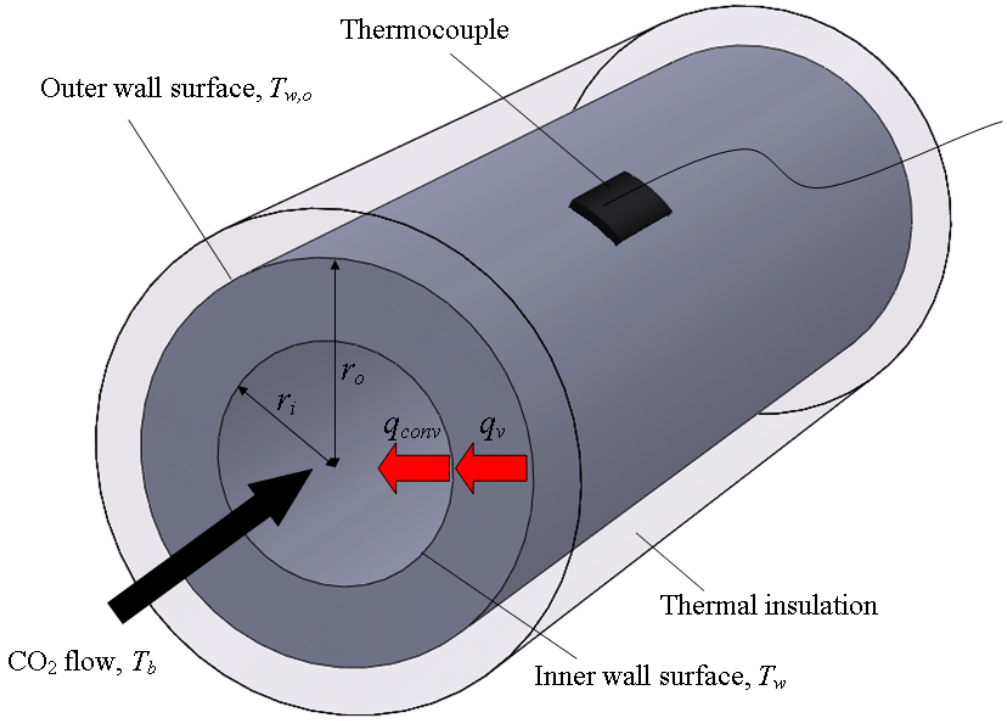

Figure 4.4 – Heat transfer in a heated tube cooled by an internal coolant

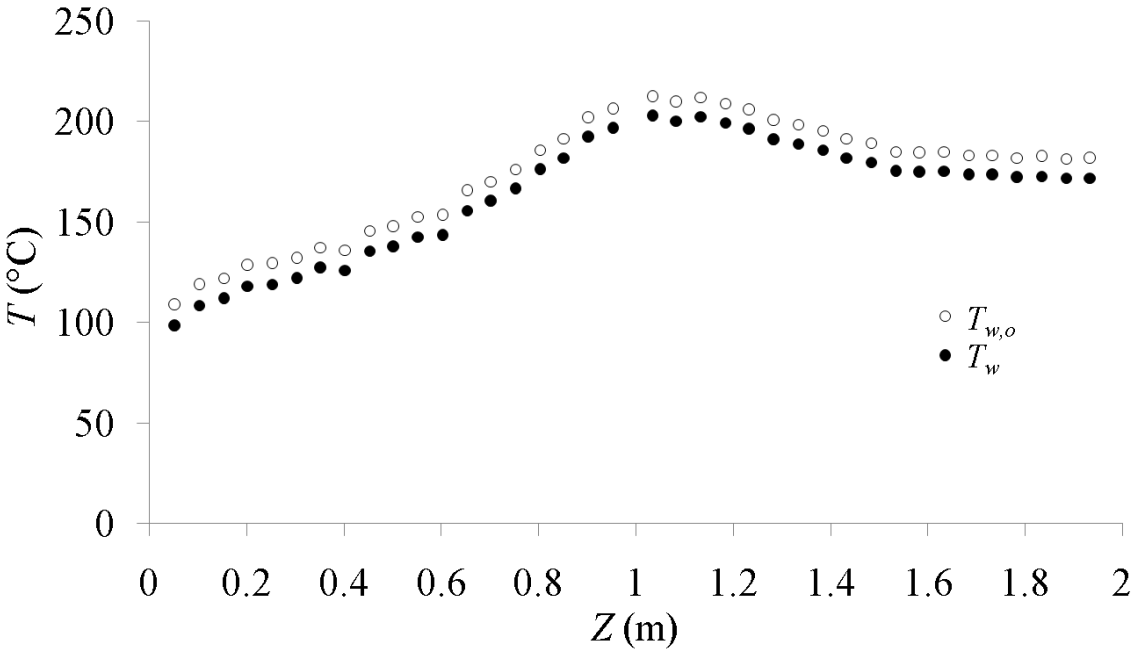

Figure 4.5 – $T_{w,o}$ and T_w for a test in the 8 mm test section with P = 8.36 MPa, G = 1500 kg/m^{2}s, q = 360 kW/m^2 and T_{in} = 7.8 °C

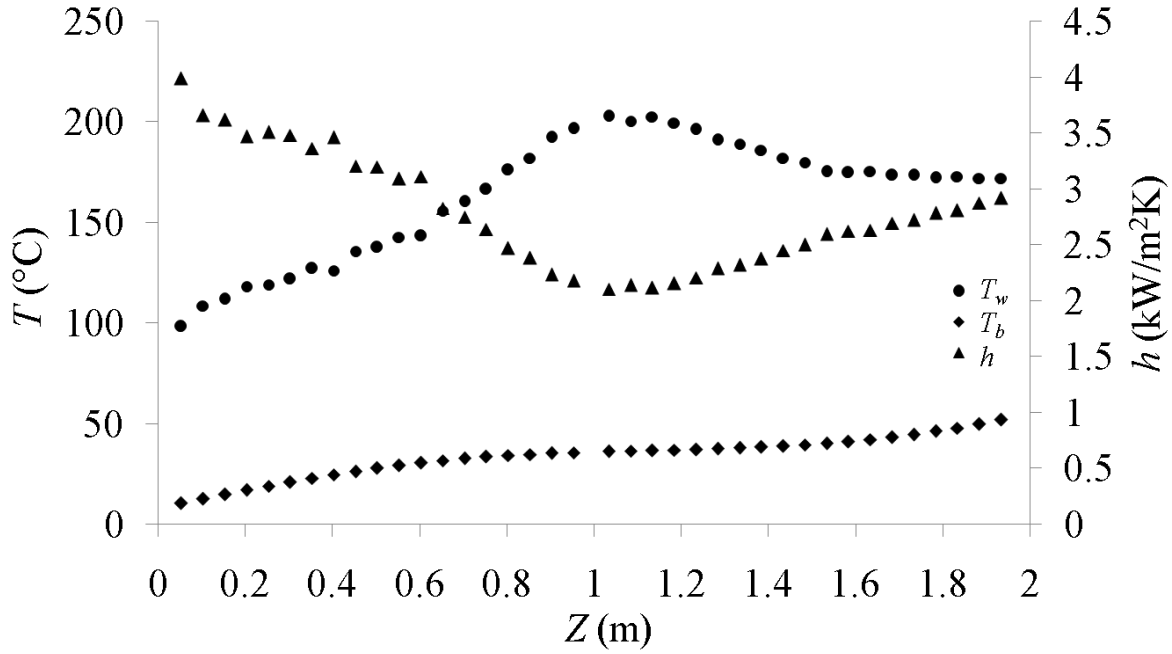

Figure 4.6 – T_w, T_b and h for a test in the 8 mm test section with P = 8.36 MPa, G = 1500 kg/m^{2}s, q = 360 kW/m^2 and T_{in} = 7.8 °C

Chapter 5 Experimental Results

5.1 Experimental flow conditions

Experiments at SCUOL have been performed by the research team using upward-flowing CO_2 in the three test sections under wide ranges of high-subcritical, near-critical and supercritical conditions. In this thesis, two groups of representative results at supercritical pressures in the 8 mm tube are selected, presented and discussed.

The first group includes a number of tests performed at experimental conditions comparable to those used by Fewster and Jackson (2004) and Song et al. (2008) (Table 5.1). The results of our replicate tests were compared to those published by said researchers. Values and discussion can be found in Section 5.2.

Table 5.1 – Flow Conditions in selected tests from the literature and in present replicate tests

Authors	D (mm)	L_h (mm)	P (MPa)	G (kg/s m^2)	q (kW/ m^2)	T_{in} (ºC)
Fewster and Jackson (2004)	7.9	1,185	7.58	398	33.6	14.5
Present	8.0	1,940	7.61	402	33.9	13
Song et al. (2008) - Case B1	9.0	2,650	8.12	400	30	7.5
Present	8.0	1,940	8.14	405	29.9	13.4
Song et al. (2008) - Case B3	9.0	2,650	8.12	1200	50	6.4
Present	8.0	1,940	8.14	1210	50.1	9.0

The second group covers a series of tests performed at different heat fluxes, pressures and mass fluxes. The effects of these conditions on supercritical heat transfer are discussed in Section 5.3.

5.2 Comparison with results of previous researchers

Wall temperature measurements methodology has been documented in previous sections. All results presented here are inner wall surface temperatures T_w estimated with the procedure introduced in section 4.5 and averaged using the methodology explained in section 4.2. The wall temperature measurements are plotted in Figures 5.1 - 5.3. The heat transfer coefficients (HTC) calculated from wall temperature measurements are presented in Figure 5.4 - Figure 5.6.

In Figure 5.7 and Figure 5.8, our wall temperature and HTC results respectively are plotted alongside those presented by Fewster and Jackson (2004). The locations where significant heat transfer deterioration (characterized by sharp increase of wall temperature and drop in heat transfer coefficient) happened are almost identical. The enthalpy range covered for our study was larger due to the relatively longer heated length. Similarly Figure 5.9 and Figure 5.10 illustrate fair agreement between the present results and those of Song et al. (2008). The discrepancy could be attributed to slight differences in the experimental setup and the actual flow conditions including tube diameters, heated lengths and inlet temperatures. It was demonstrated that the facility was operational and the measurements it produced were trustworthy and could be reproduced.

It is worth mentioning that while replicating the test case B2 from Song et al (2008), we observed oscillations of all loop readings (Figure 5.11); similar oscillations have been occasionally reported by other researchers (Pioro and Duffey, 2007). Unsteady test case have not been included in the reported results.

5.3 Effects of flow conditions on supercritical heat transfer

Figure 5.12 to Figure 5.15 present the T_w and HTC results obtained from tests at increasing heat flux and mass flux conditions at the relatively low supercritical pressure of 8.14 ± 0.16 MPa. Figure 5.12 shows that for the low mass flux G = 507 ± 10 kg/m^{2}s, T_w and HTC increased monotonically with increasing q for $q \leq 40$ kW/m^2. For the test with q = 50

kW/m^2, a temperature peak and a drop in HTC were observed, indicating the occurrence of HTD. When G was increased to 1004 ± 9.95 kg/m^{2}s, as shown in Figure 5.13, no temperature peak appeared within the measured bulk fluid enthalpy range. T_w values again increased monotonically as q increased. In Figure 5.14, G was further increased to 1502 ± 9.95 kg/m^{2}s. Temperature peaks were once again observed in tests with $q \geq 250$ kW/m^2. The peaks were much less pronounced and occurred further downstream in the test section compared to the one observed in the test shown in Figure 5.12. Figure 5.15 shows that when G was increased to 1999 ± 9.95 kg/m^{2}s, no temperature peak was present within the measured bulk fluid enthalpy range. For tests with q values of 200 kW/m^2 or higher, HTC values started to decrease around mid-test section. It could not be determined if the same would have happened to the tests with lower q values, had the heated length been longer and the achievable bulk fluid enthalpy range were wider.

In order to show the effect of pressure on supercritical heat transfer, a number of tests were performed at the higher pressure of 8.53 ± 0.04 MPa; these results are shown in Figure 5.16. Compared to tests in Figure 5.14, which had approximately the same mass flux, there was no temperature peak observed for those in Figure 5.16. This might be due to the fact that changes in thermophysical properties in supercritical fluid near the pseudo-critical temperature are less drastic at higher pressures. The values of HTC were also higher for the same q.

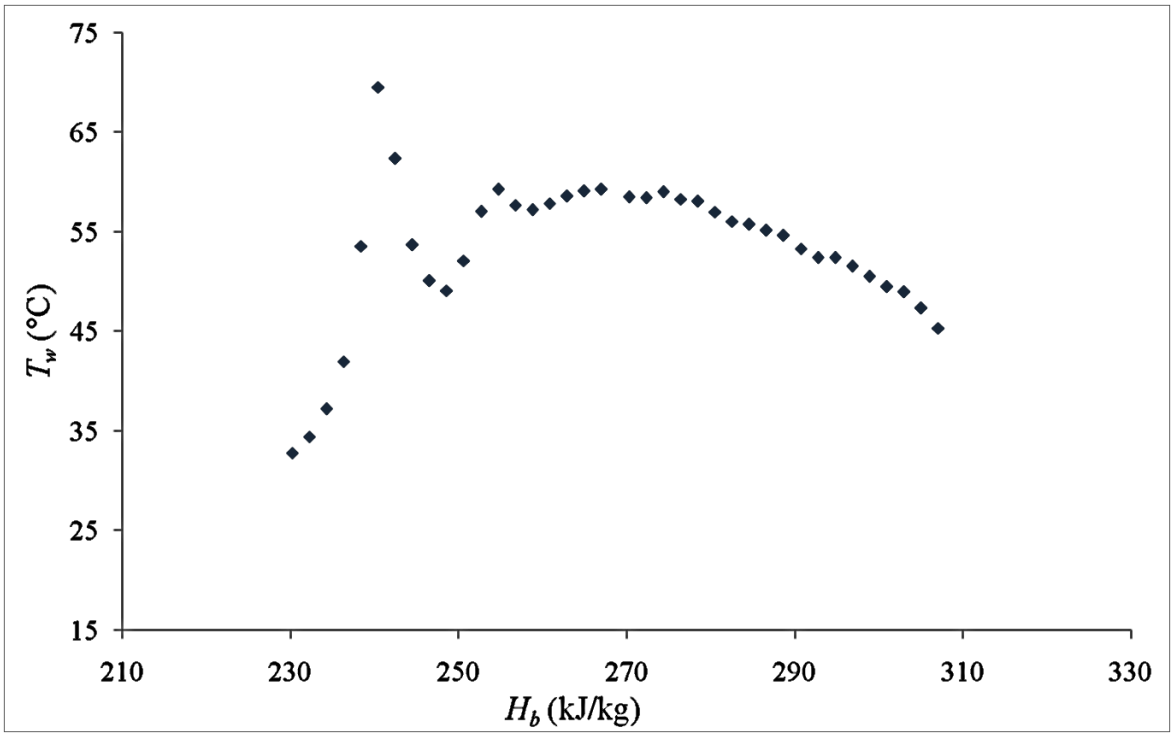

Figure 5.1 – Test section wall temperature variation for G = 402 kg/m^{2}s, P = 7.66 MPa, q = 34.0 kW/m^2 and T_{in} = 13.0 °C, replicating the condition of Fewster and Jackson (2004)

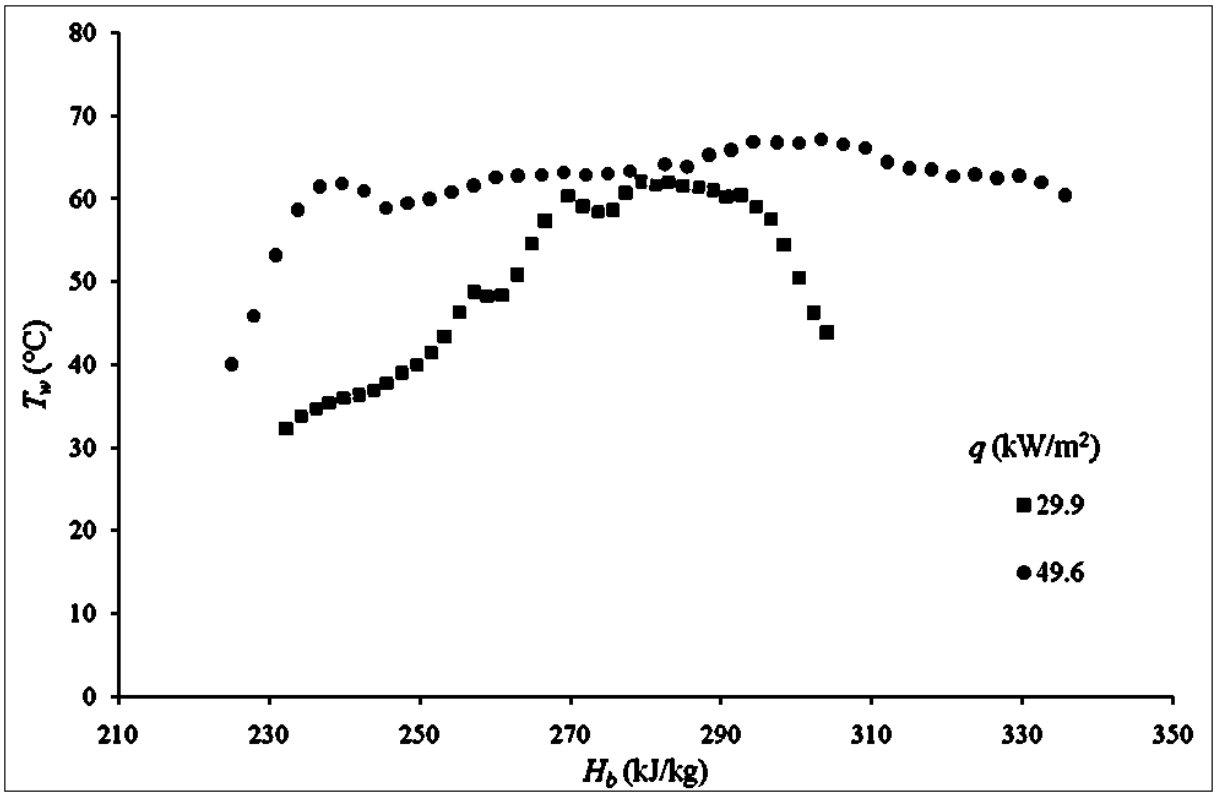

Figure 5.2 – Test section wall temperature variations for G = 408.5 ± 3.5 kg/m^{2}s and P = 8.15 ± 0.01MPa, replicating experimental cases B1 and B2 of Song *et al*. (2008)

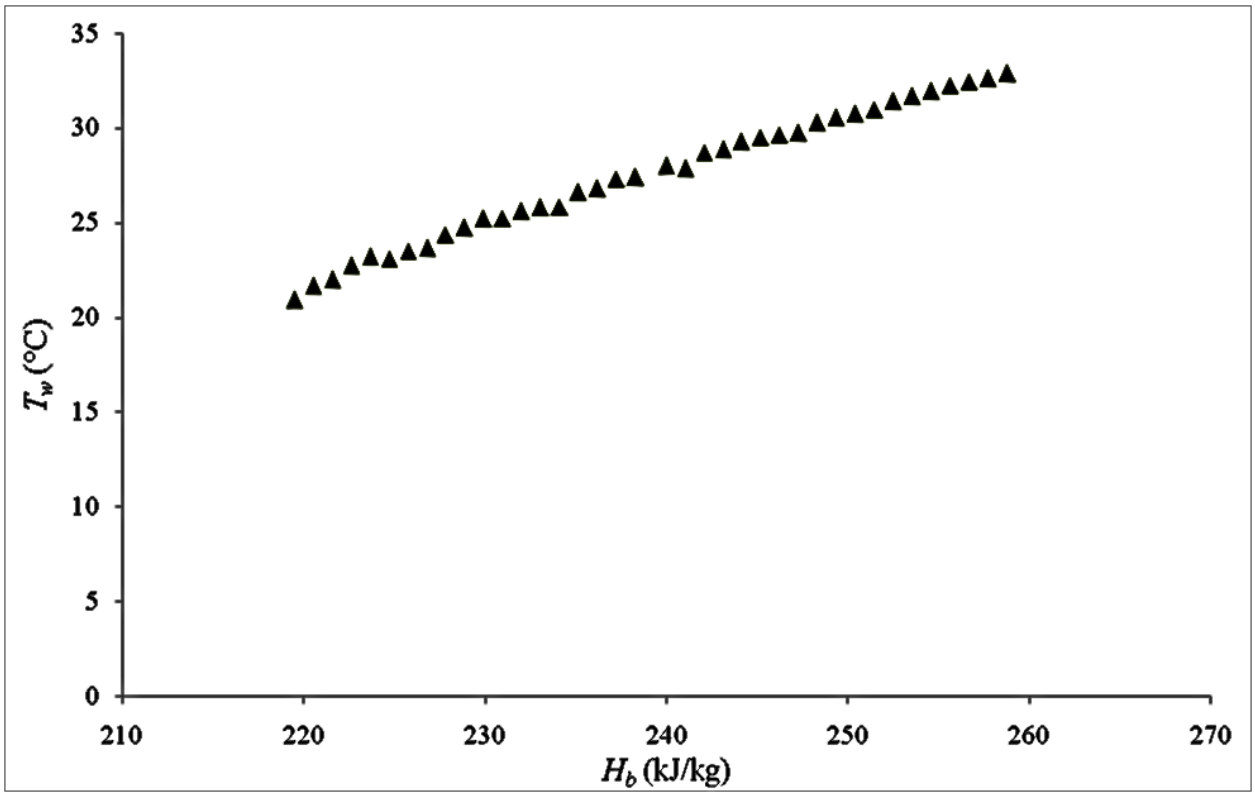

Figure 5.3 – Test section wall temperature variation for G = 1120 kg/m^{2}s, P = 8.14MPa and q = 50.0 kW/m^2, replicating experimental case B3 of Song *et al*. (2008)

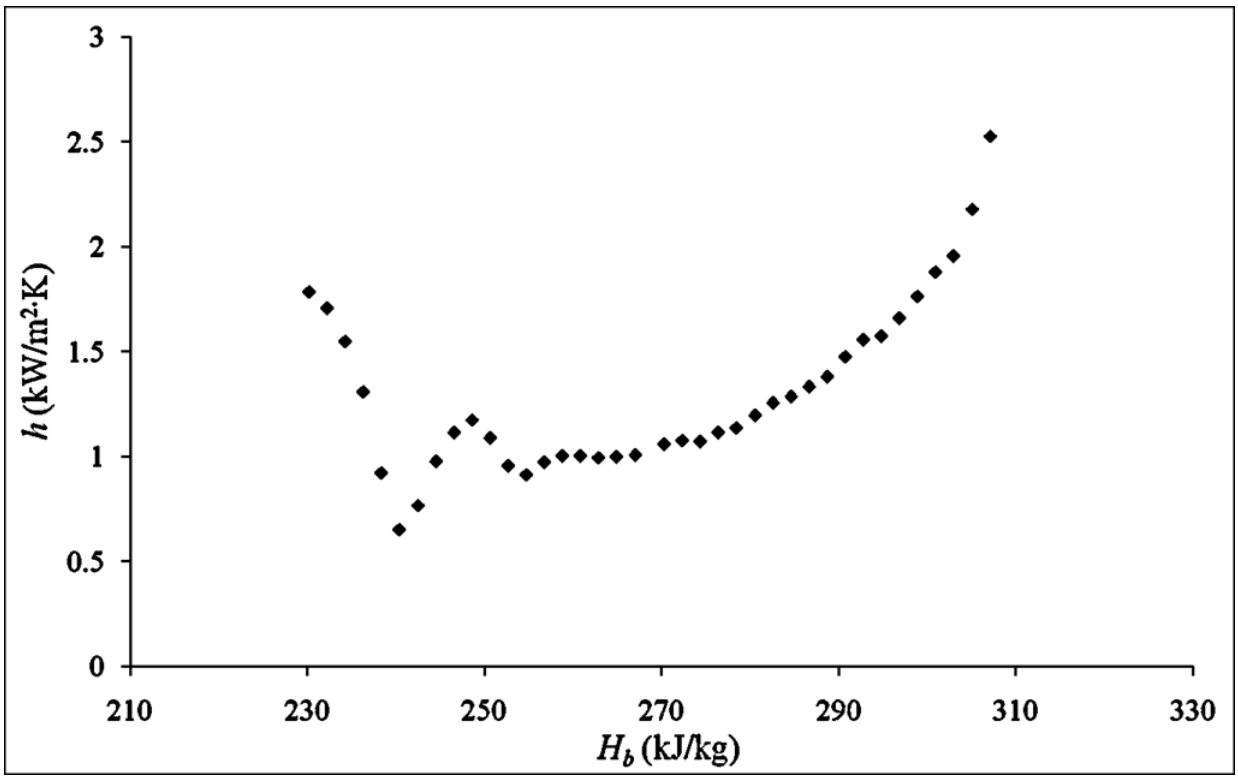

Figure 5.4 – Heat transfer coefficient variation for G = 402 kg/m^{2}s, P = 7.66MPa, q = 34.0 kW/m^2 and T_{in} = 13.0 °C, replicating the condition of Fewster and Jackson (2004)

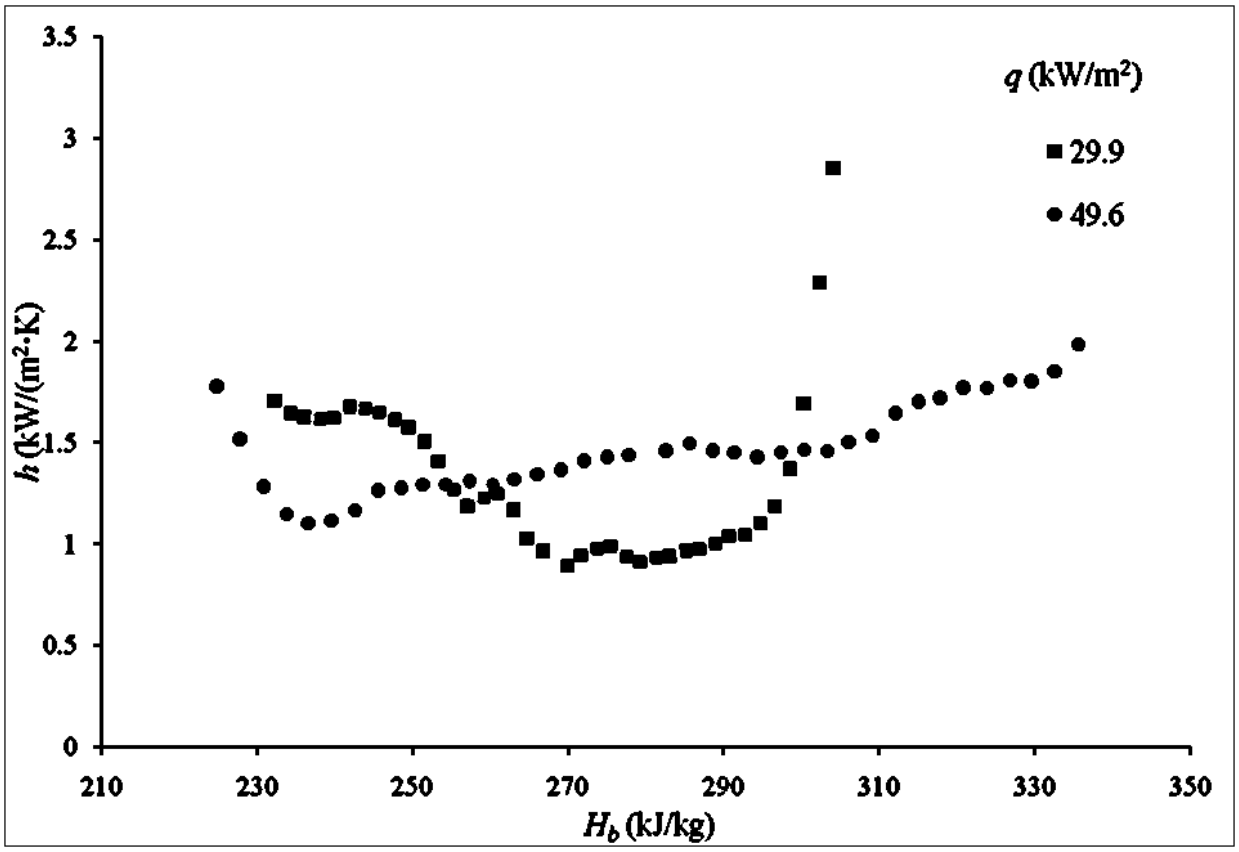

Figure 5.5 – Heat transfer coefficient variations for G = 408.5 ± 3.5 kg/m^{2}s and P = 8.15 ± 0.01MPa, replicating experimental cases B1 and B2 of Song *et al*. (2008)

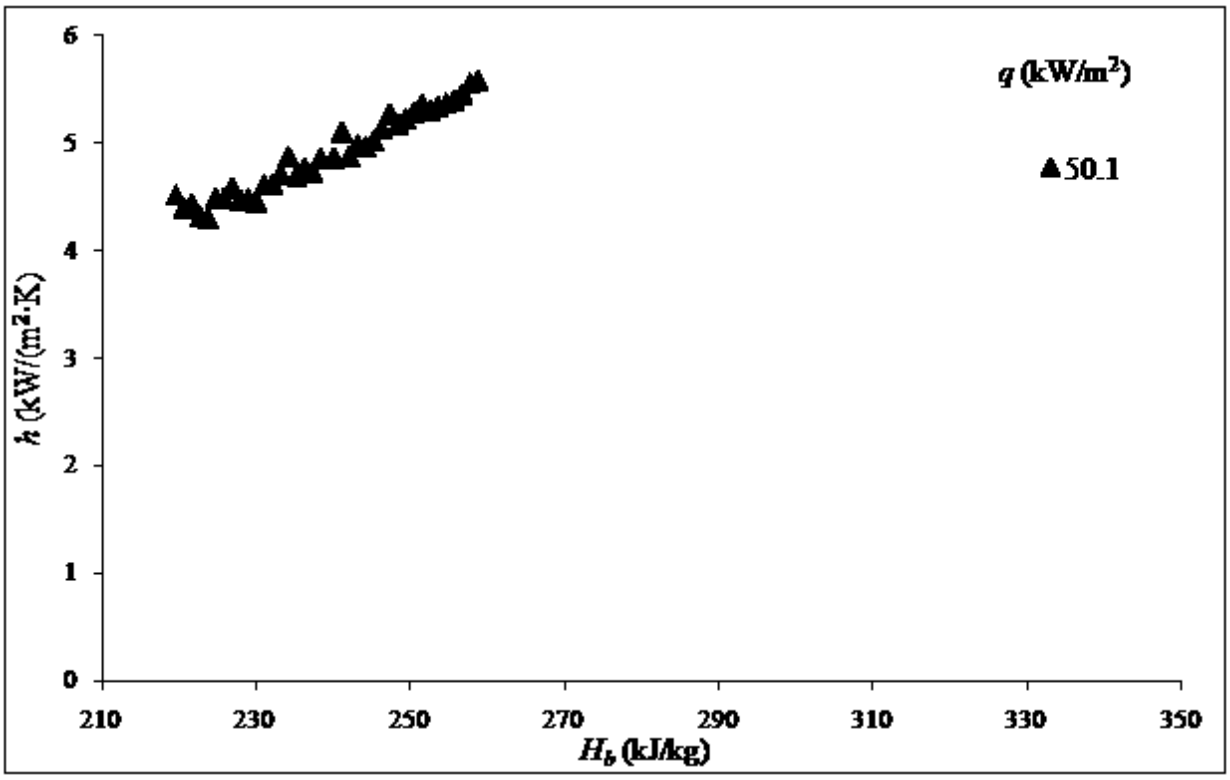

Figure 5.6 – Heat transfer coefficient variations for G = 1120 kg/m^{2}s, P = 8.14 ± 0.01MPa and q = 50.0 kW/m^2, replicating experimental case B3 of Song *et al*. (2008)

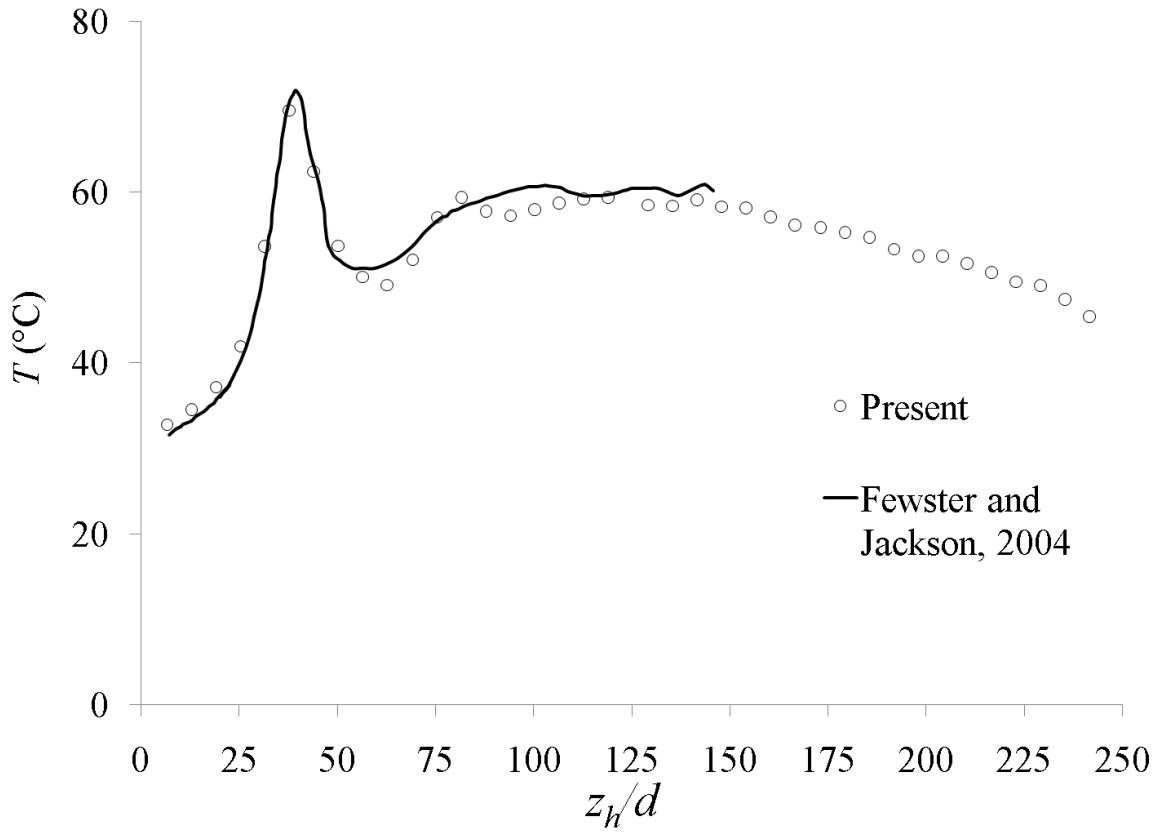

Figure 5.7 – Wall temperature variations reported by Fewster and Jackson (2004) and of present study under conditions listed in Table 5.1.

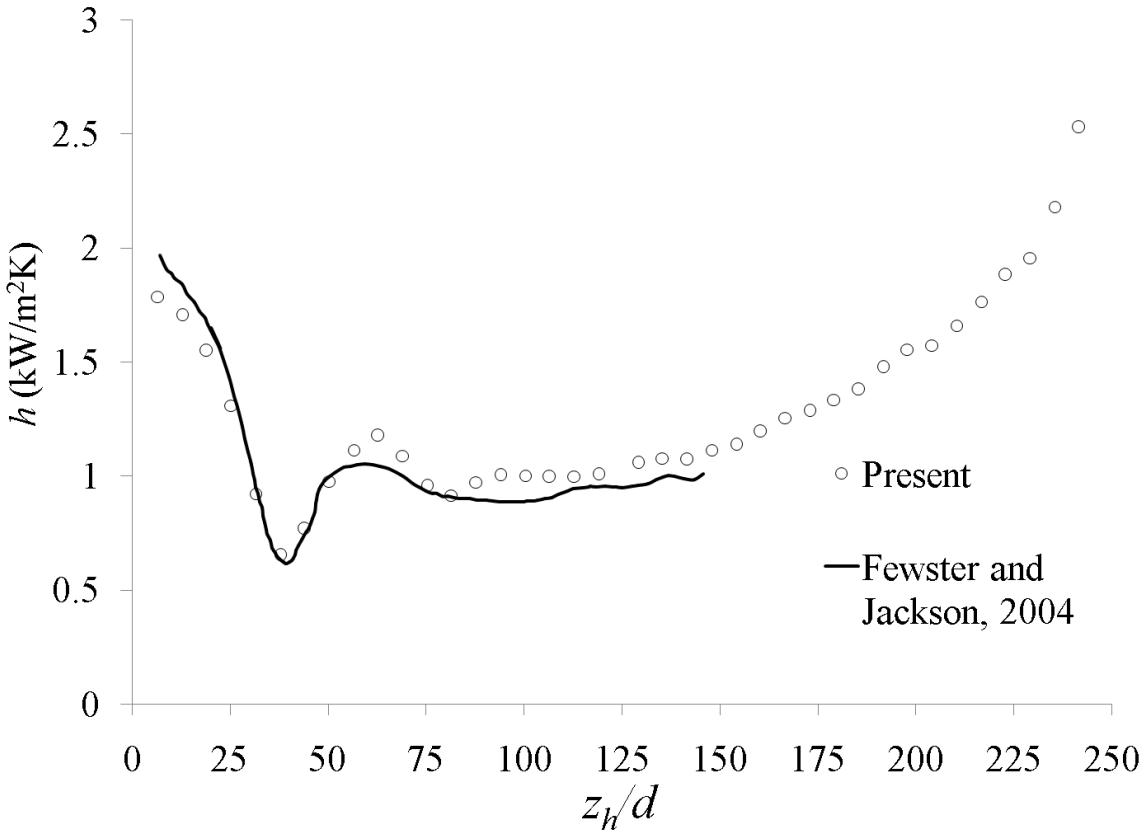

Figure 5.8 – Heat transfer coefficient variations reported by Fewster and Jackson (2004) and of present study under conditions listed in Table 5.1.

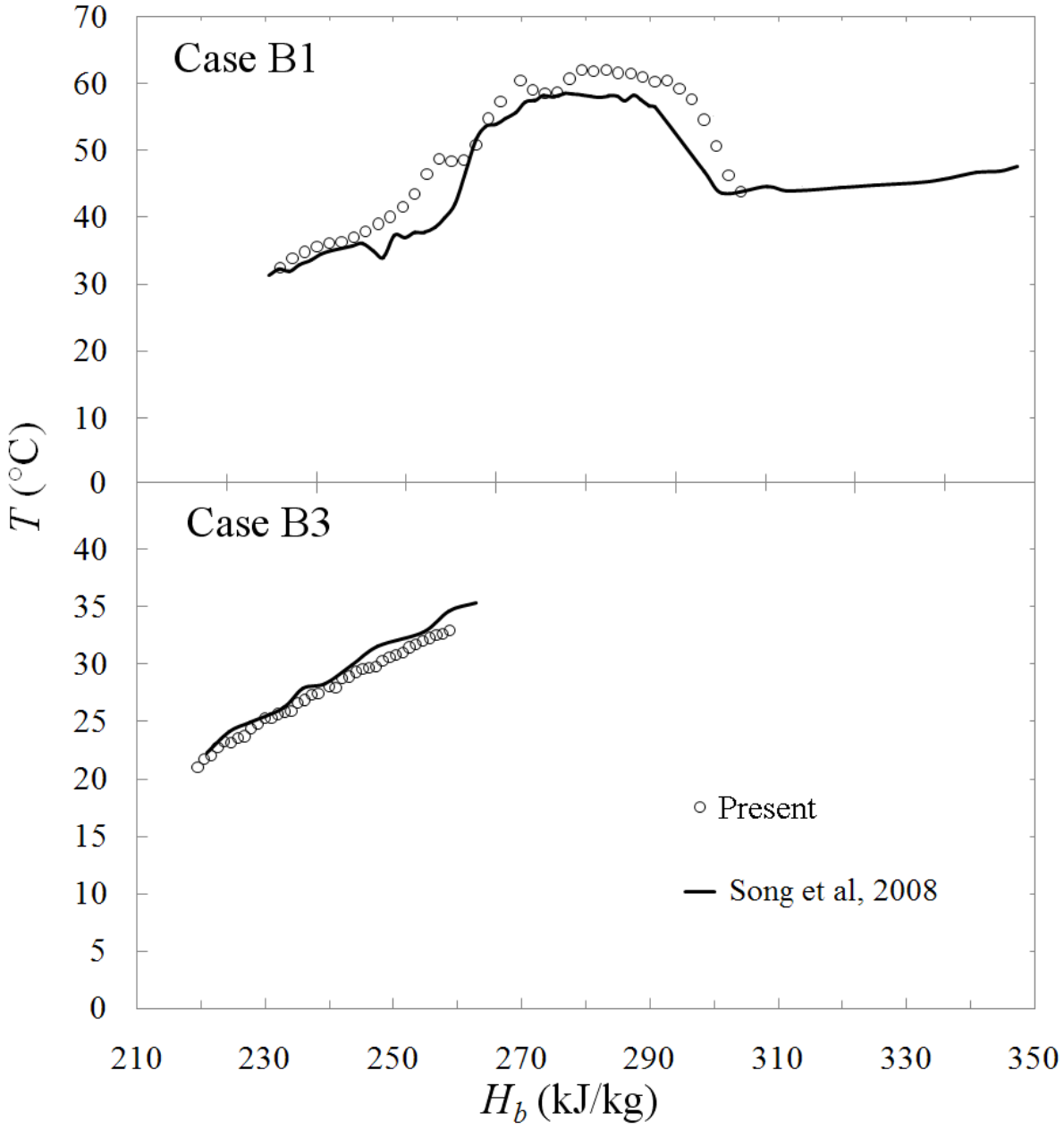

Figure 5.9 – Wall temperature measurements reported by Song et al. (2008) and of present study under conditions listed in Table 5.1.

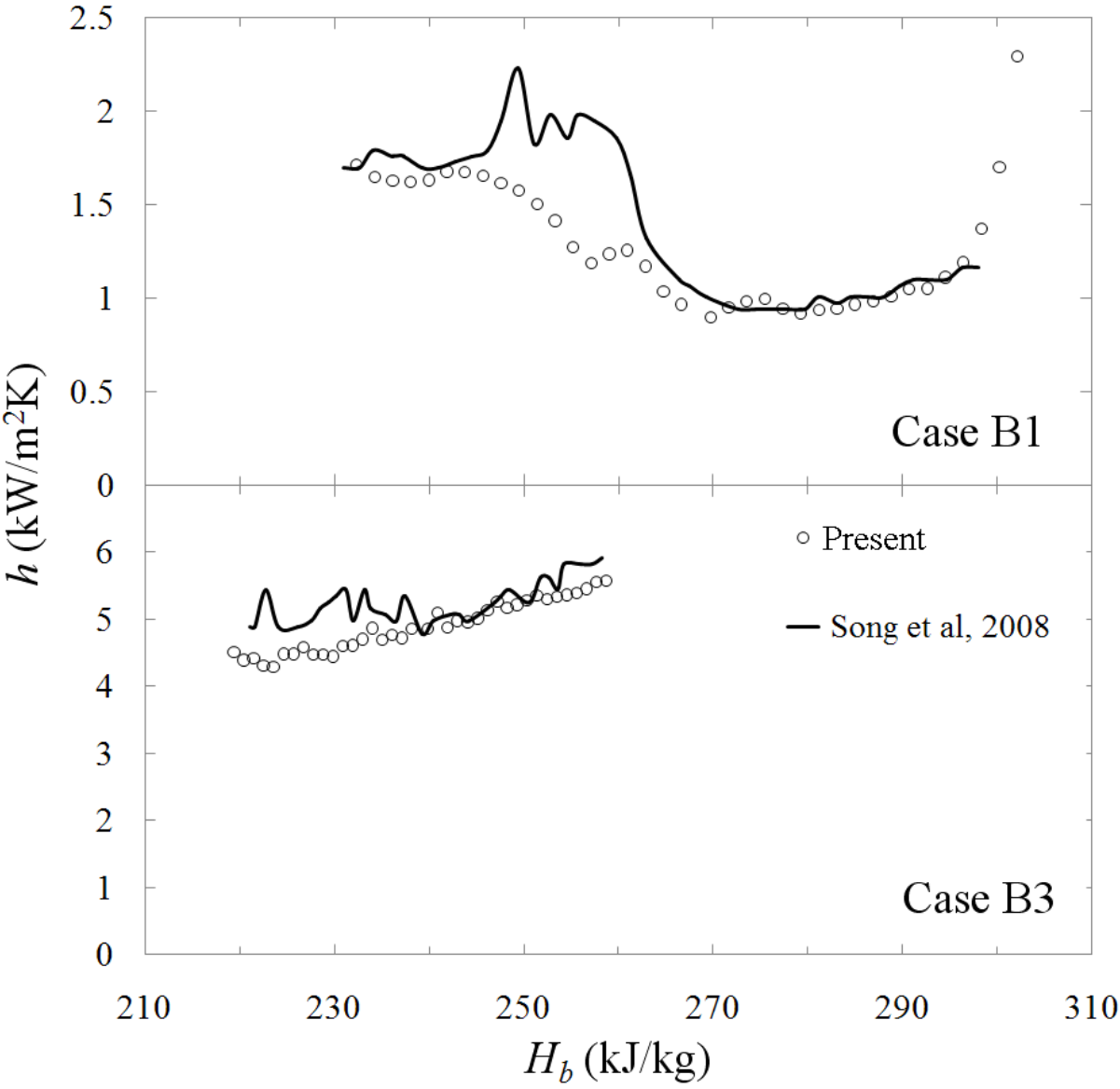

Figure 5.10 – Heat transfer coefficient variations reported by Song et al. (2008) and of present study under conditions listed in Table 5.1.

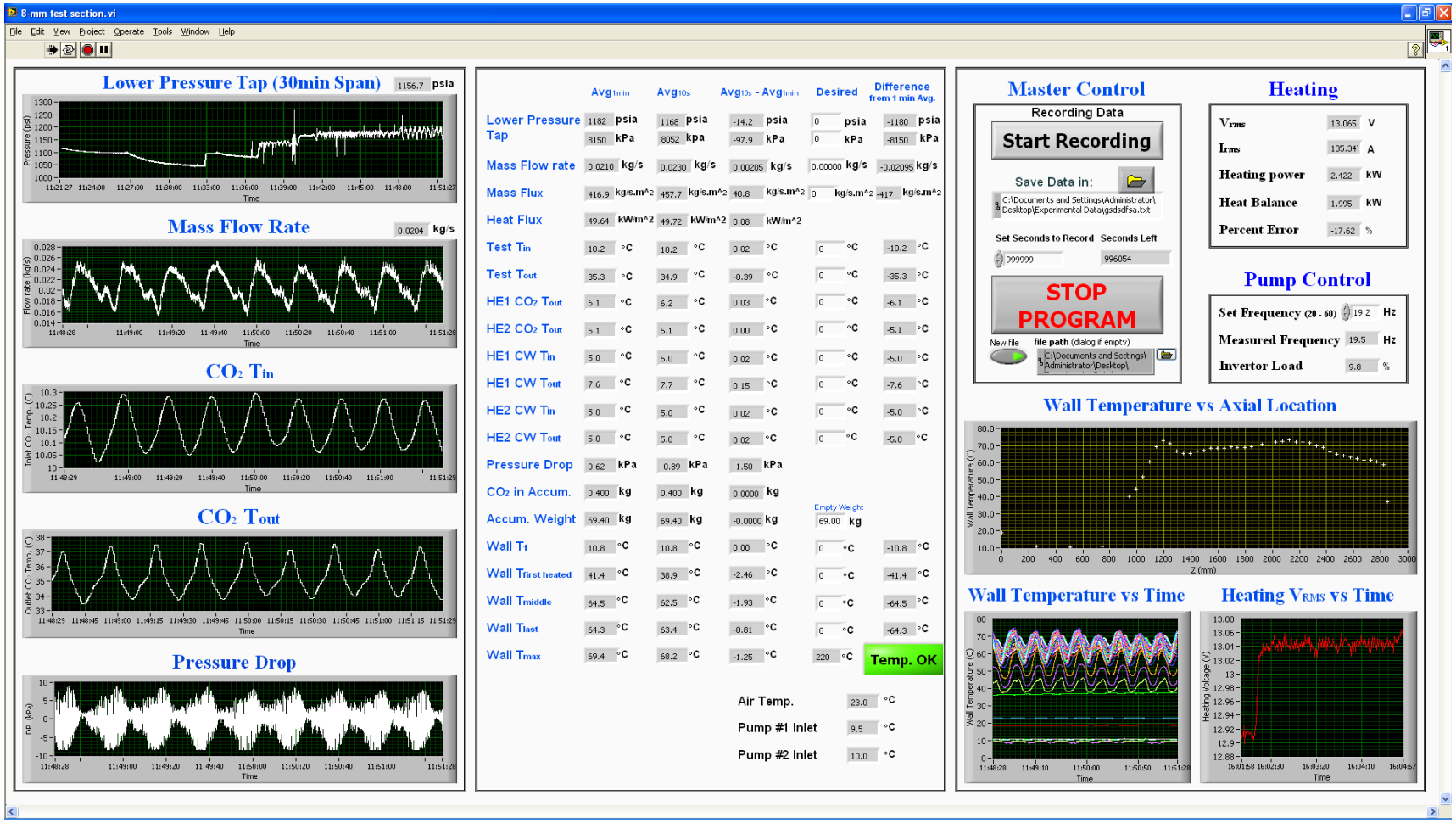

Figure 5.11 – Oscillation observed during the replication of test case B2 from Song et al. (2008)

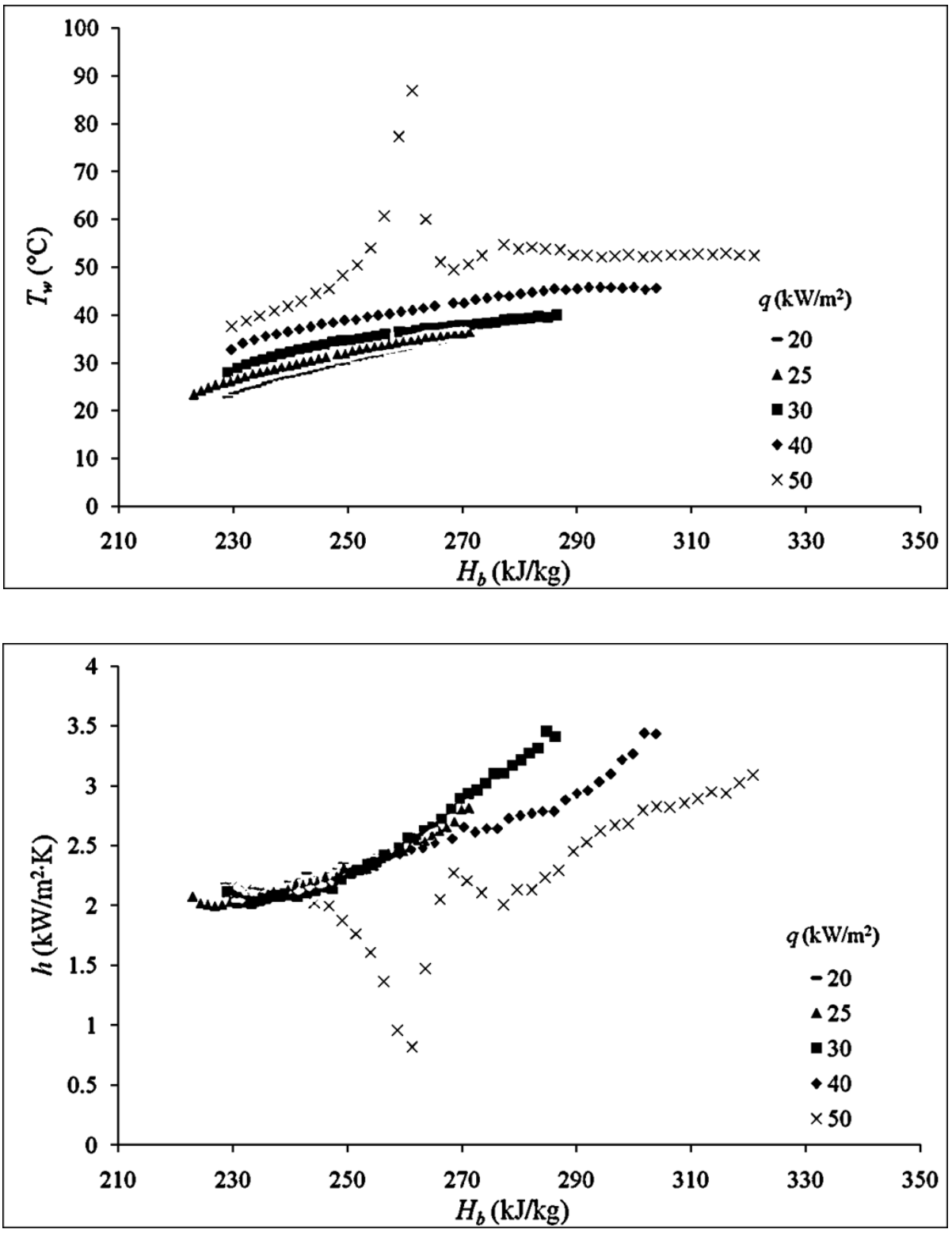

Figure 5.12 – Test section wall temperature (top) and heat transfer coefficient (bottom) variations for $G = 507 \pm 10$ kg/m^{2}s and $P = 8.43 \pm 0.07$ MPa

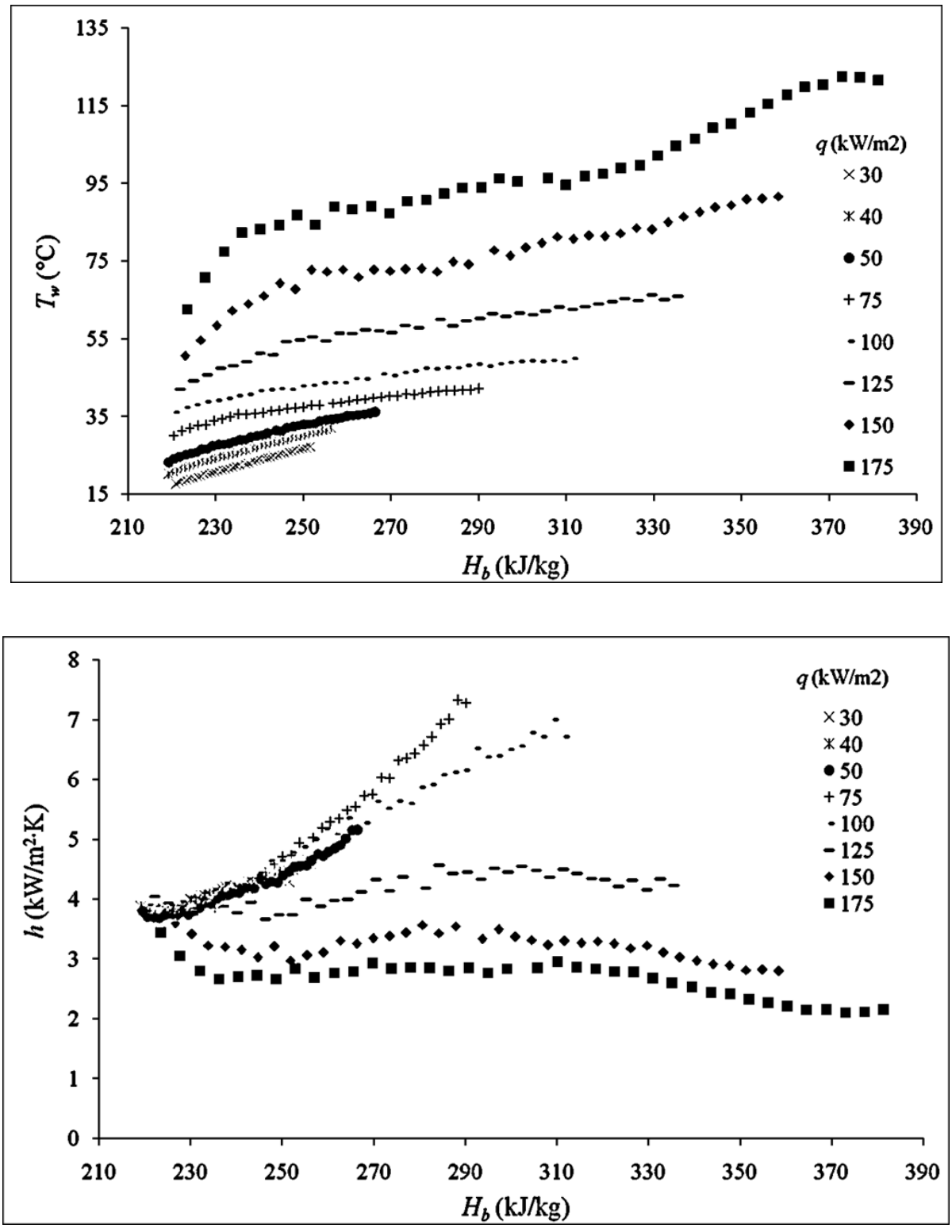

Figure 5.13 – Test section wall temperature (top) and heat transfer coefficient (bottom) variations for $G = 1004 \pm 9.95$ kg/m^{2}s and $P = 8.35 \pm 0.11$ MPa

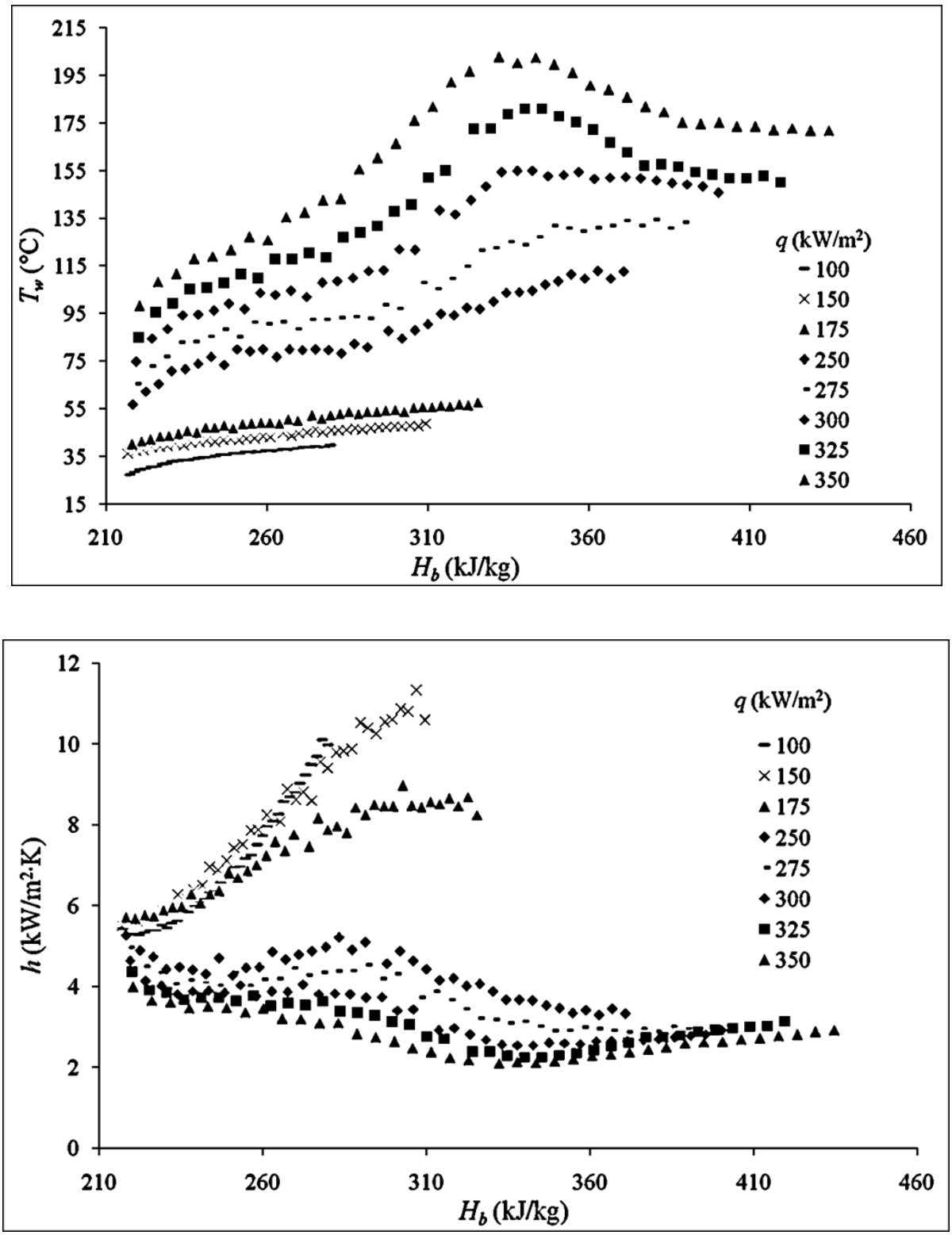

Figure 5.14 – Test section wall temperature (top) and heat transfer coefficient (bottom) variations for $G = 1502 \pm 9.95$ kg/m^{2}s and $P = 8.34 \pm 0.11$ MPa

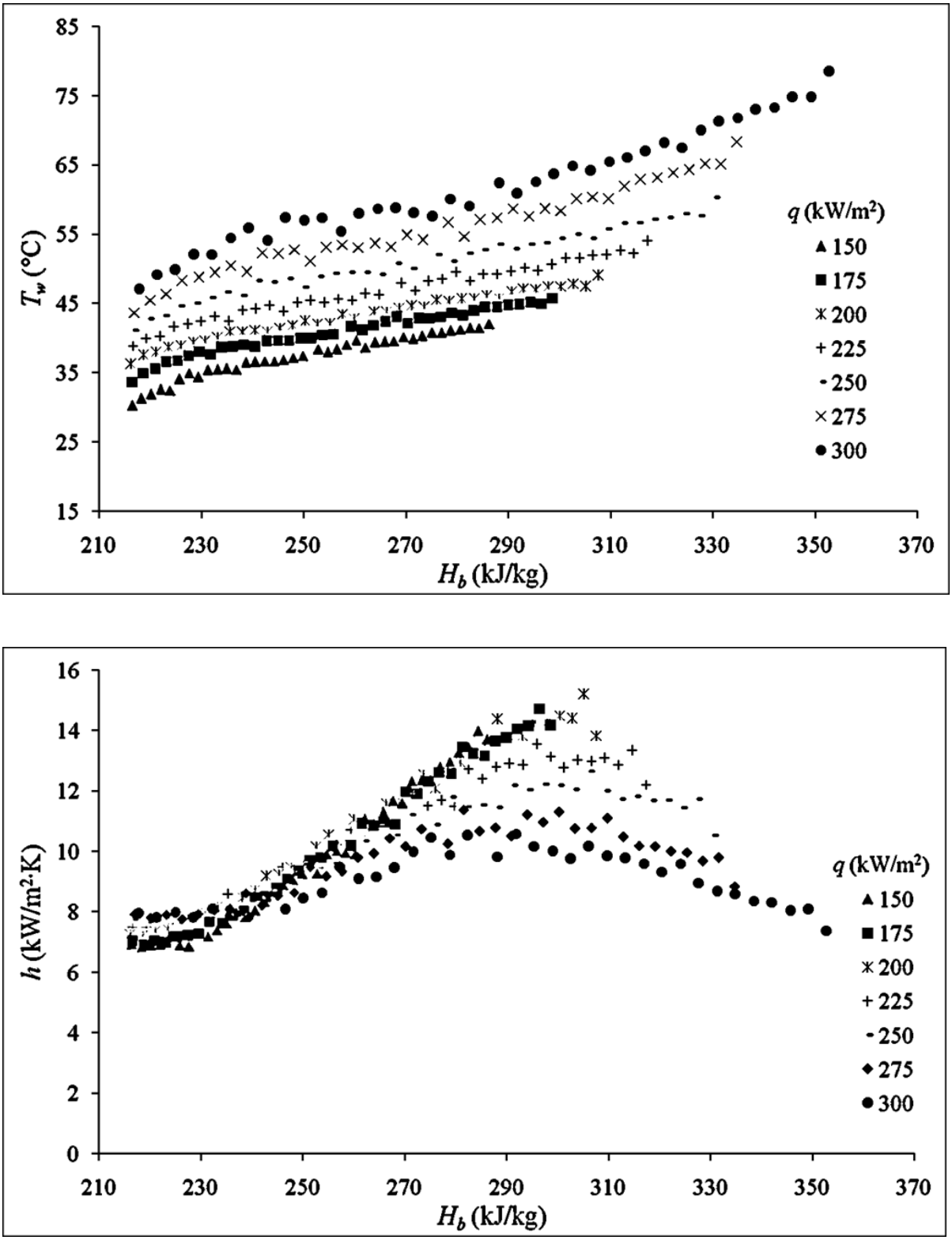

Figure 5.15 – Test section wall temperature (top) and heat transfer coefficient (bottom) variations for $G = 1999 \pm 9.95$ kg/m^{2}s and $P = 8.48 \pm 0.08$ MPa

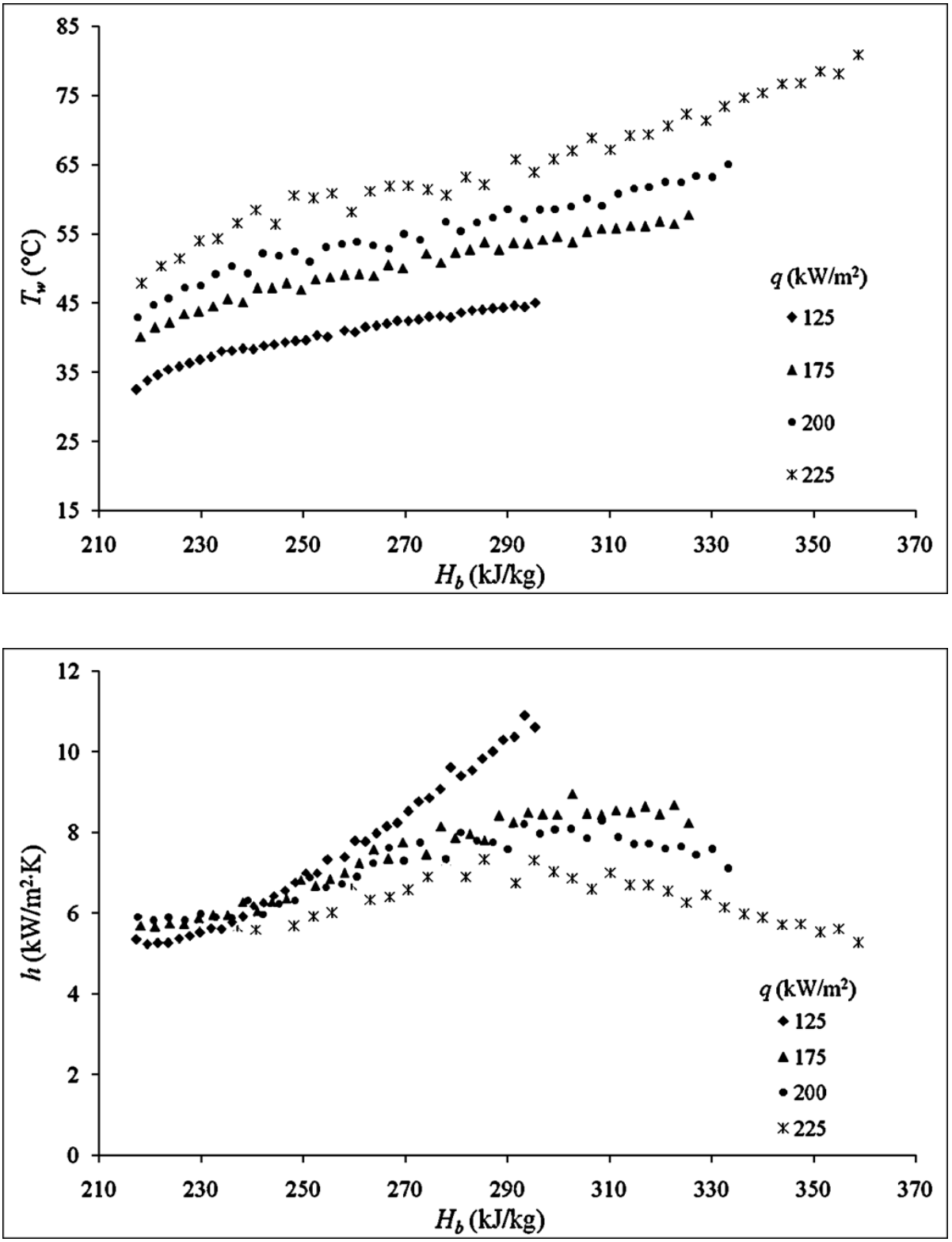

Figure 5.16 – Test section wall temperature (top) and heat transfer coefficient (bottom) variations for $G = 1502 \pm 9.95$ kg/m^{2}s and $P = 8.53 \pm 0.04$ MPa

Chapter 6 Past Publications

During my involvement in the University of Ottawa supercritical heat transfer research project, I had the opportunity to attend conferences, workshops and symposia relevant to the research activities of the team. I also contributed in the authoring of a number of publications, as listed in this chapter and attached in Appendix B.

In March 2011, I attended the 5th International Symposium on Supercritical-Water-Cooled Reactors in Vancouver, British Columbia, Canada and co-authored the papers by Jeddi et al. (2011). For this article I provided the description of the experimental facility, its components and the 3-rod bundle test section; I also produced 3D CAD drawings to be used in the article and later in the presentation at the symposium.

In June 2012, I attended the 3rd Annual Conference of the Canadian Nuclear Society in Saskatoon, Saskatchewan, Canada and published the paper by Jiang et al. (2011). In this paper I provided an up-to-date status of the facility modifications and some results from the commissioning tests.

In March 2013, I co–authored the paper by Zahlan et al. (2013). My contribution to this article is the latest information regarding the facility and instrumentation upgrades. I also wrote about some measurements that were taken to repeat past research efforts, and compared our results to those previously reported.

Chapter 7 Summary and Recommendations

7.1 Summary

The Supercritical University of Ottawa Loop has been built to support the thermalhydraulic research required for the development of the next generation Canadian Supercritical-Water-Cooled Reactor. The design and construction of the facility have been explained in previous chapters. The functions and detailed specifications of the main components and the test sections have been described.

The procedure and results of the commissioning and preliminary measurements have been documented. Experiments conducted by previous researchers using carbon dioxide were reviewed and some of them repeated at the SCUOL facility. Comparison between our results and those previously published has shown good agreement, which demonstrates that the facility is operational and the data it generates are trustworthy and reproducible. The effects of mass flux and pressure on supercritical heat transfer were observed during the tests and discussed.

7.2 Recommendations for further research

The test section inlet temperatures of the experiments conducted so far were limited by the temperature of the chilled water supplied to the heat exchangers. It tends to fluctuate over time and adds an uncertainty to the experimental results. After I left the team, a preheater was installed, which has the ability to regulate the fluid temperature at the inlet to the test sections. Future researchers should take full advantage of the preheater to explore the effect of inlet temperature on heat transfer.

Severe condensation around the piping has occurred during some hotter summer days when the fluid temperature was lower than the dew point in the lab. Water dripping on the floor could cause corrosion to metal components, or, more dangerously, short-circuit electronic equipment. It is recommended to have all the piping completely insulated to reduce the exposure to the atmosphere. A dehumidifier could be added in the room. Alternatively, experiments could be scheduled to avoid being conducted during the time when the air is hot and humid.

References

Aoki, N., Murakami, Y., Mori, H., and Ohno, M. (2006). "Transient heat transfer in a sub-bundle channel during pressure reduction from supercritical to subcritical pressure", Proc., 11th Power and Energy Technology Sym. of the Japan Society of Mechanical Engineers, Tokyo, Japan, June 29-30, 2006, Page 257-258.

Bae, Y.Y., Kim, H.Y., and Yoo, T.H. (2011). "Effect of a helical wire on mixed convection heat transfer to carbon dioxide in a vertical circular tube at supercritical pressures", *International Journal of Heat and Fluid Flow*, 32, 340–351, 2011.

Chun, S.Y., Shin, C.H., Hong, S.D. and Song, C.H. (2009). "Heat transfer characteristics near the critical pressure in a rod bundle cooled by R-134a fluid during pressure transient", Proc. 4th Intern. Sym. on Supercritical Water-Cooled Reactors, Heidelberg, Germany, March 8-11, 2009.

Ezato, K., Seki, Y., Dairaku, M., Suzuki, S., Enoeda, M., Akiba, M., Mori, H., and Oka, Y. (2009). "Heat transfer in a seven-rod test bundle with supercritical pressure water – (1): Experiments", Proc. Intern. Congress on Advances in Nuclear Power Plants 2009 (ICAPP 2009), Shinjuku, Tokyo, Japan, May 10-14, 2009, Paper No.9487, Page 1786.

Fewster, J. and Jackson, J.D. (2004). "Experiments on Supercritical Pressure Convective Heat Transfer having Relevance to SPWR", Proceedings of ICAPP'04, Paper 4342, Pittsburgh, PA USA, June 13-17. 2004.

Grabezhnaya, V.A. and Kirillov, P.L. (2004). "Heat Transfer in Pipes and Rod Bundles during Flow of Supercritical-Pressure Water," *Atomic Energy*, Vol. 96, No. 5, 2004

Guellouz, M.S. (1989). "Heat transfer in rod bundle subchannels", Master's thesis, University of Ottawa, Ottawa, Ontario, Canada, 1989.

Jackson, J.D. and Hall W.B. (1979). "Forced convection heat transfer to fluids at supercritical pressure", in *Turbulent Forced Convection in Channels and Bundles*, edited by Kakaç, S. and Spalding, D. B., Vol. 2, pp. 563–611, Hemisphere, Washington, USA, 1979.

Jeddi, L., Jiang, K., Tavoularis, S., and Groeneveld, D.C. (2011). "Preliminary tests at the University of Ottawa supercritical CO_2 heat transfer facility", 5th International Symposium on Supercritical-Water-Cooled Reactors (ISSCWR-5), Vancouver, British Columbia, Canada, March 13-16, 2011.

Jiang, K., Zahlan, H., Tavoularis, S. and Groeneveld, D.C. (2012). "Commissioning tests of the University of Ottawa Supercritical CO_2 Facility", 3rd Annual Conference of the Canadian Nuclear Society, Saskatoon, Saskatchewan, June 10 – 13, 2012.

Kim, J.K., Jeon, H.K., Yoo, J.Y., and Lee, J.S. (2005). "Experimental study on heat transfer characteristics of turbulent supercritical flow in vertical circular/non-circular tubes", 11thInternational Topical Meeting on Nuclear Reactor Thermal-Hydraulics (NURETH-11), Popes' Palace Conference Center, Avignon, France, October 2-6, 2005.

Kim, H., Kim, H.Y., Song, J.H., and Bae, Y.Y. (2006). "Heat transfer to supercritical pressure carbon dioxide flowing upward through tubes and a narrow annulus passage", Korea Atomic Energy Research Institute, South Korea, 2006

Kim, H.Y., Kim, H., Kang, D.J., Song, J.H., and Bae, Y.Y. (2007). "Heat transfer experiments for an upward flow of supercritical pressure CO_2 in a narrow annulus", 3rd Int. Symposium on SCWR-Design and Technology, Shanghai, China, March 12-15, 2007.

Lemmon, E.W., M.O. McLinden and Friend, D.G. (2002). "Thermophysical Properties of Fluid Systems", NIST Standard Reference Database Number 69, NIST Reference Fluid Thermodynamic and Transport Properties Database: Version 7.0, 2002.

Leung, L.K.H., Yetisir, M., Diamond, W., Martin, D.,Pencer, J.,Hyland, B., Hamilton, H., Guzonas D., and DuffeyR. (2011). "A next generation heavy water nuclear reactor with supercritical water as coolant", Int. Conf. Future of HWRs, Paper No. 042, Ottawa, Ontario, Canada, Oct. 02-05, 2011

Li, H.Z., Wang, H.J., Luo, Y.S., Gu, H.F., Shi, X.B., Chen, T.K., Laurien, E., and Zhu, Y. (2004). "Experimental investigation on heat transfer from a heated rod with a helically wrapped wire inside a square vertical channel to water at supercritical pressures", *Nucl. Eng. Des.* , 231, 187-197, 2004.

Mori, H., Yoshida, S., Morooka, S., and Komita, H. (2005). "Heat transfer study under supercritical pressure conditions for single rod test section", Proc. Intern. Congress on Advances in Nuclear Power Plants (ICAPP/05), Seoul, Korea, May 15-19, Paper No.5404, 9 pages, 2005.

Mori, H., Kaida, T., Ohno, M., Yoshida, S. and Hamamoto Y. (2012). "Heat transfer to a supercritical pressure fluid flowing in sub-bundle channels", *Journal of Nuclear Science and Technology*, Vol. 49, No. 4, pp. 373-383, 2012.

Ouma, B.H. (1988). “Experiments in rod bundle subchannel flow with varying rod-wall proximity”, Master’s thesis, University of Ottawa, Ottawa, Ontario, Canada, 1988.

Pioro, I.L., Duffey, R.B. (2003). “Literature Survey of Heat Transfer and Hydraulic Resistance of Water, Carbon Dioxide, Helium and Other Fluids at Supercritical and Near-Critical Pressures”, Chalk River Laboratories, Chalk River, Ontario, Canada, 2003

Pioro, I.L., Duffey, R.B. and Dumouchel, T.J. (2004).“Hydraulic resistance of fluids flowing in channels at supercritical pressures (survey)”,*Nucl. Eng. Des.*,231, 187-197, 2004.

Pioro, I.L. and Duffey, R.B. (2007). “Heat transfer and hydraulic resistance at supercritical pressures in power engineering applications,” ASME Press, New York, NY, USA, 334 pages, 2007.

Richards, G., Milner, A., Pascoe, C., Patel, H., Peiman, W., Saltanov, Eu, Pometko, R.S., Opanasenko, A.N., Shelegov, A.S., Kirillov, P.L. and Pioro, I.L. (2010). “Heat transfer in a vertical 7-element bundle cooled with supercritical Freon-12,” Proc. 2nd Canada-China Joint Workshop on Supercritical Water-Cooled Reactors, Toronto, Canada, April 25-28, 10 pages, 2010.

Richards, G., Shelegov, A.S., Kirillov, P.L., Pioro, I.L. and Harvel, G. (2011). “Temperature profiles of a vertical bare 7-element bundle cooled with supercritical Freon-12”, Proc. ICONE19, Chiba, Japan, May 16-19, 2011a.

Richards, G., Shelegov, A.S., Kirillov, P.L., Pioro, I.L. and Harvel, G. (2011). “Heat transfer profiles of a vertical, bare, 7-element bundle cooled with supercritical Freon-12”, Proc. NURETH-14, Toronto, Ontario, Canada, September 25-30, 2011b.

Rummens, H. (2001). “Supercritical CO2 test loop facility description”, Atomic Energy Canada Limited, Chalk River, Ontario, Canada, 2001.

Silin, V.A., Voznesensky, V.A. and Afrov, A.M. (1993). “The light water integral reactor with natural circulation of the coolant at supercritical pressure B-500 SKDI”, *Nucl. Eng. Des.*, Vol. 144, pp. 327-336, 1993.

Song, J.H., Kim, H.Y., Kim, H., and Bae, Y.Y. (2008). “Heat transfer characteristics of a supercritical fluid flow in a vertical pipe”, *Journal of Supercritical Fluids*, Vol. 44, pp. 164–171, 2008.

Tavoularis, S. (2005). "Measurement in Fluid Mechanics." CambridgeUniversity Press, Cambridge, UK.

Tavoularis, S. (2011).“Rod bundle vortex networks, gap vortex streets, and gap instability: a nomenclature and some comments on available methodologies,” *Nucl. Eng. Des.*, 241, 2624-2626, 2011.

Yamashita, Y., Murakami, Y., Mori, H., and Ohno, M. (2006). “Heat transfer to a supercritical pressure fluid flowing downward in sub-bundle channel”, Proc., 11th Power and Energy Technology Sym. of the Japan Society of Mechanical Engineers, Tokyo, Japan, June 29-30, 2006, Page 255-256.

Yu, J.Y., Wang S.T. and JiaB.S. (2007). “Development of sub-channel analysis code for super critical CANDU type reactor”, Proc. 3rd Int. Sym. on SCWR-Design and Technology, Shanghai, China, March l2-15, 2007a.

Yu, J.Y., Wang, S.T. and Jia, B.S. (2007). “Development of sub-channel analysis code for CANDU-SCWR, *Prog. Nucl. Ener.,* 49, 334–350, 2007b.

Zahlan, H., K. Jiang, S. Tavoularis and D. Groeneveld, 2013. Measurements of Heat Transfer Coefficient, CHF and Heat Transfer Deterioration in Flows of CO2 at Near-critical and Supercritical Pressures, 6th International Symposium on Supercritical Water-Cooled Reactors (ISSCWR-6), Shenzhen, China, March 3-7, 2013.

Appendix A Supplemental Information

Figure A.1 – Swagelock® stainless steel fittings, assorted

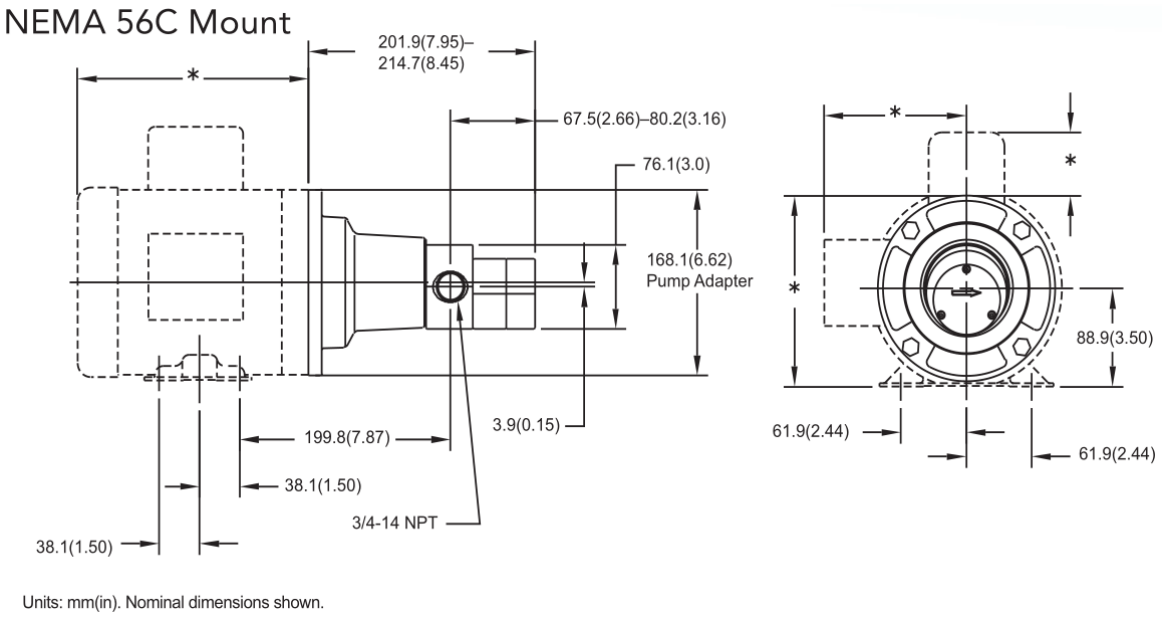

Figure A.2– Gear pump-motor assembly with NEMA 56C Mount

Figure A.3– Micropump® GL series gear pump

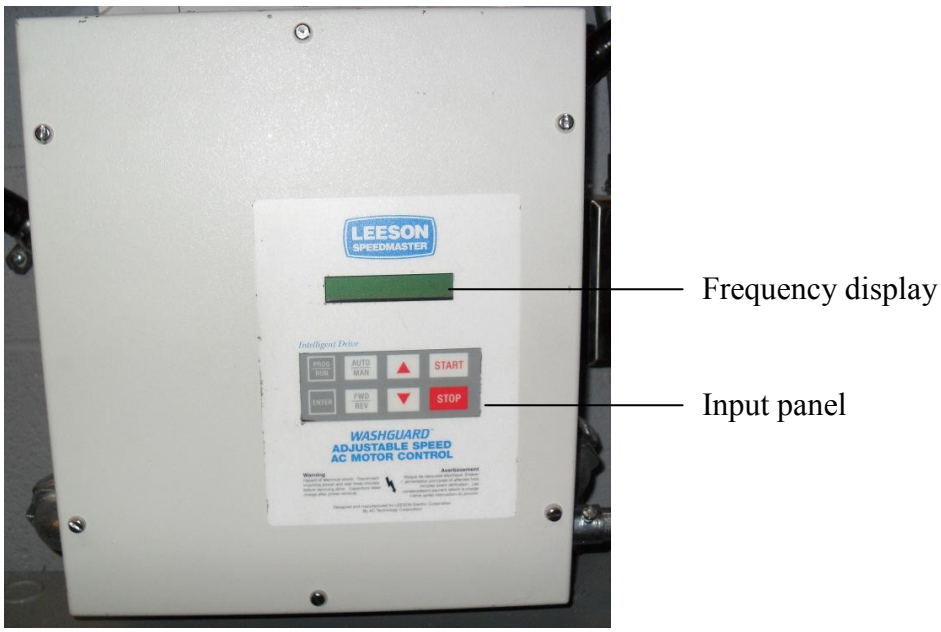

Figure A.4– Power inverter for CO_2 pumps

Figure A.5– FlexicraftHydropad®accumulator

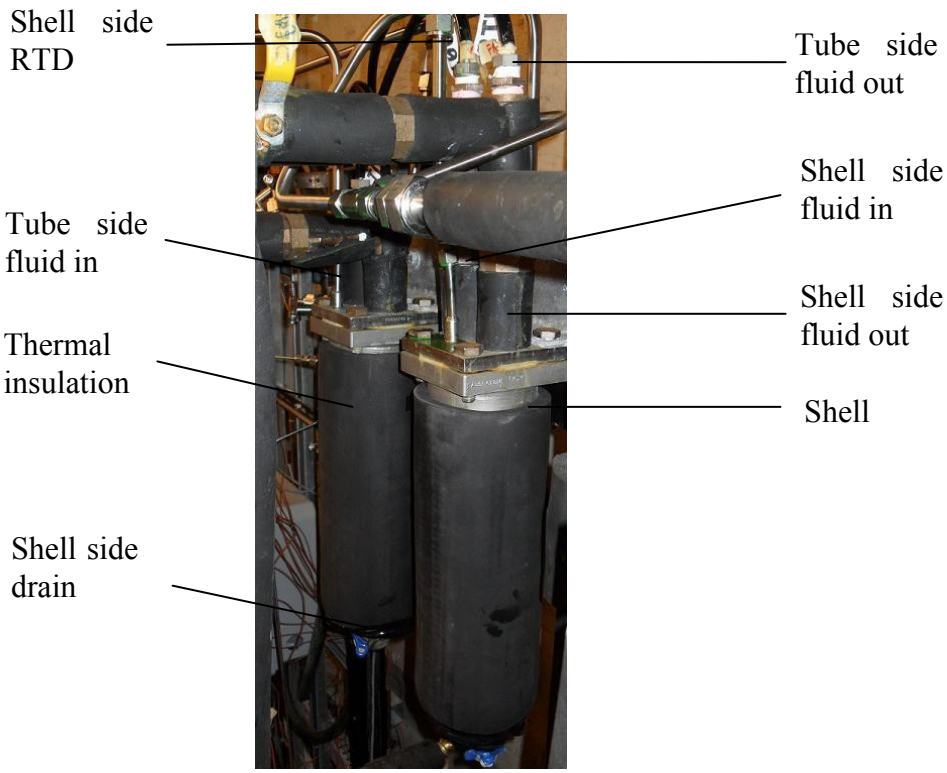

Figure A.6– Sentry® FXF6223U heat exchangers

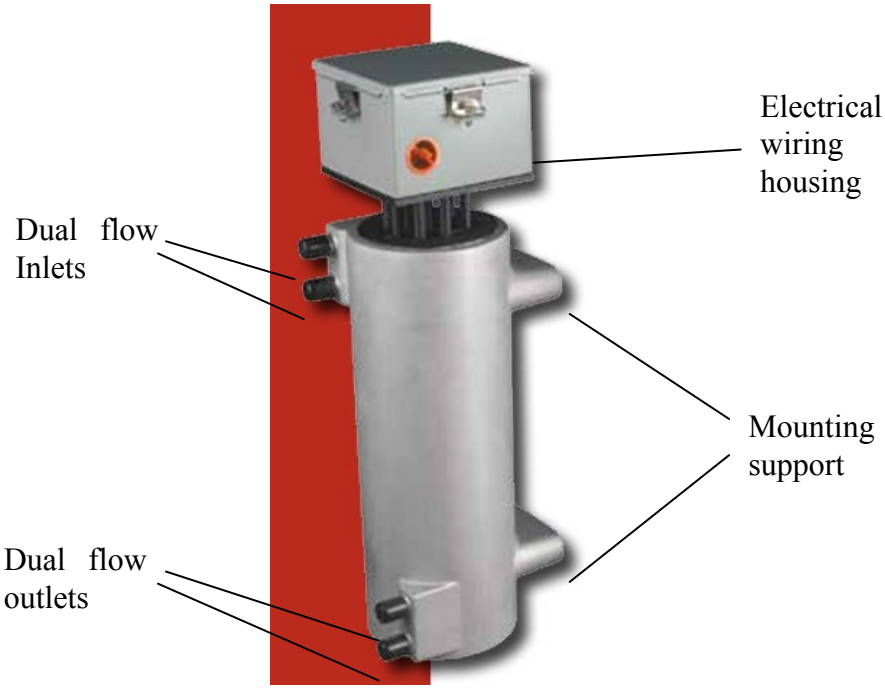

Figure A.7 – CAS CAST-X 3000 preheater

Figure A.8– DC Power Supply

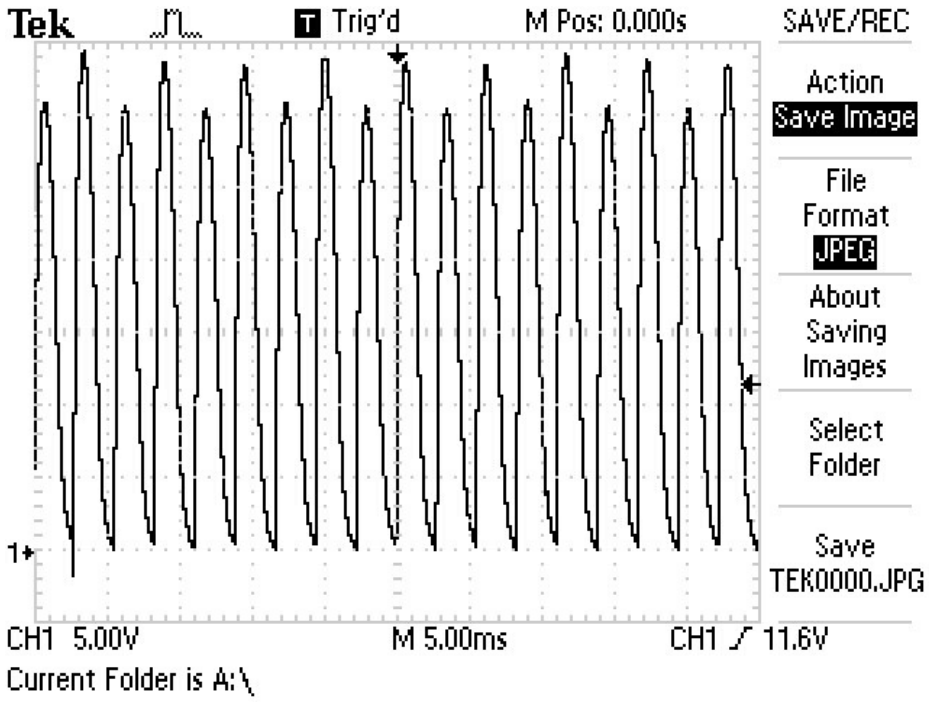

Figure A.9– Power supply output waveform obtained with a Tektronix® TDS1001B oscilloscope

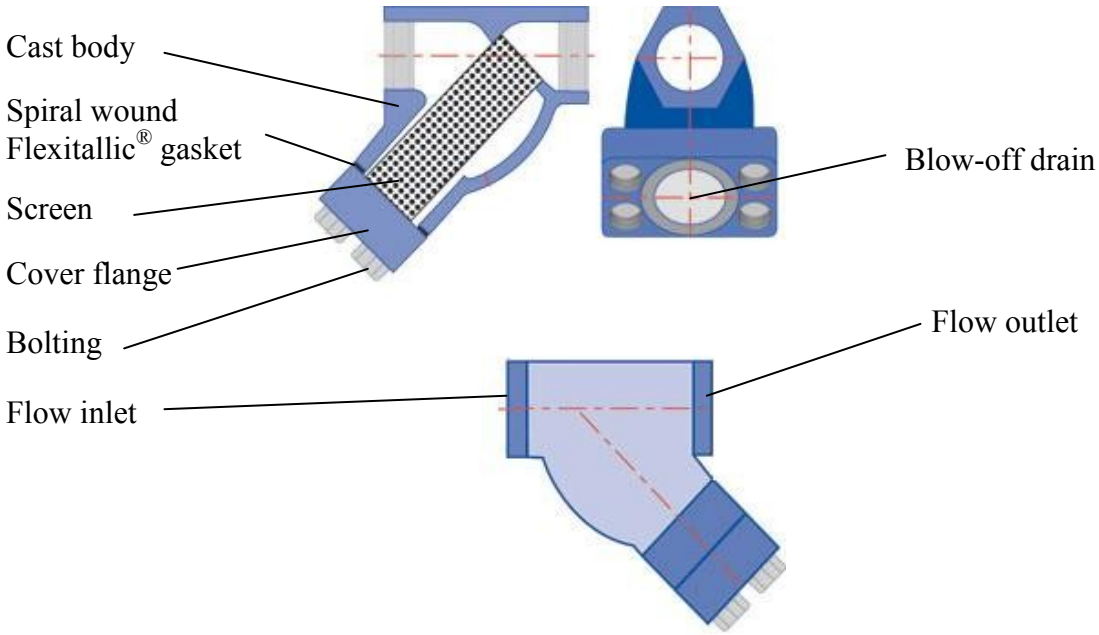

Figure A.10– Sure Flow® YT1500SSBC series strainer

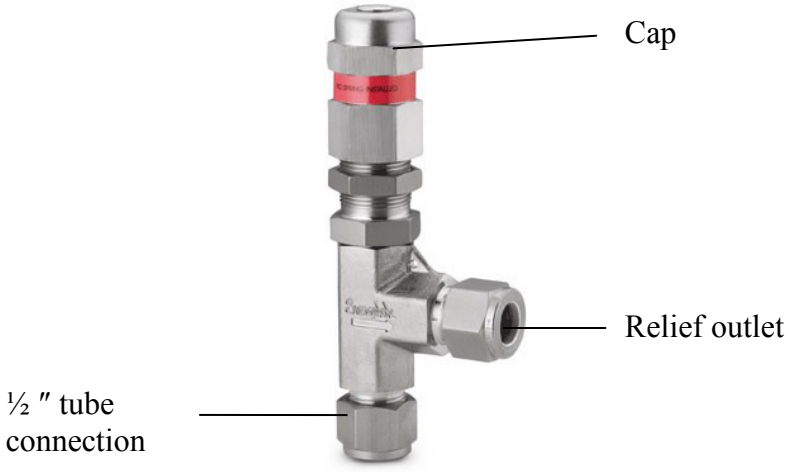

Figure A.11 – Swagelok® SS-R4S8 proportional pressure relief valve

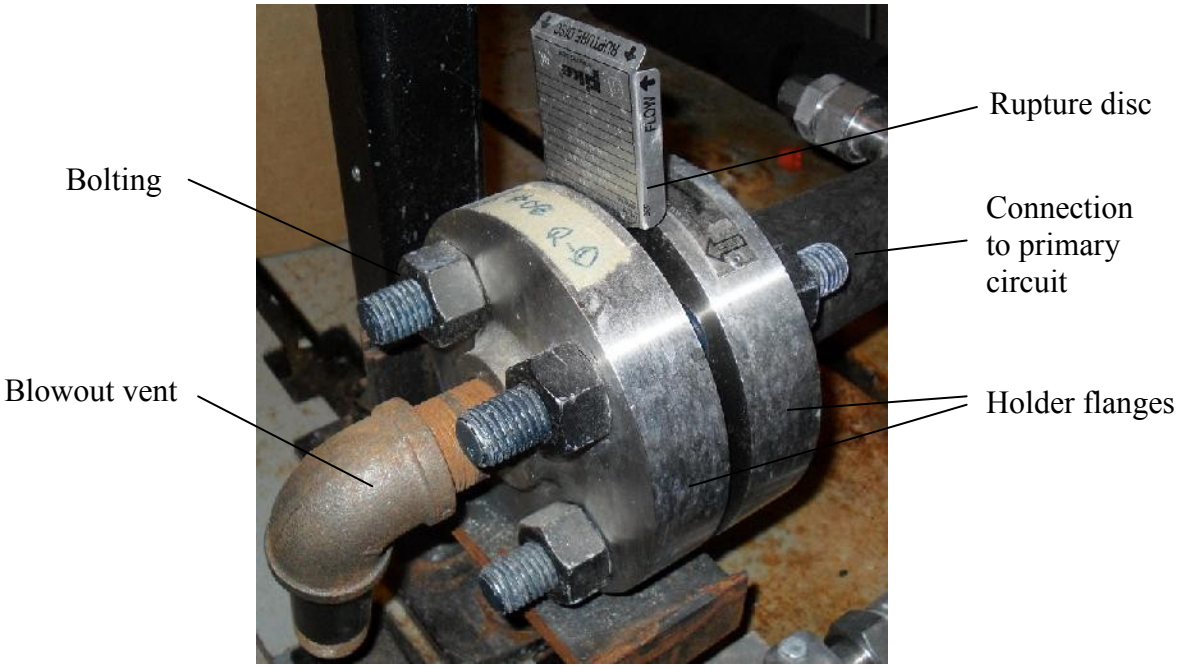

Figure A.12– Rupture disc holder

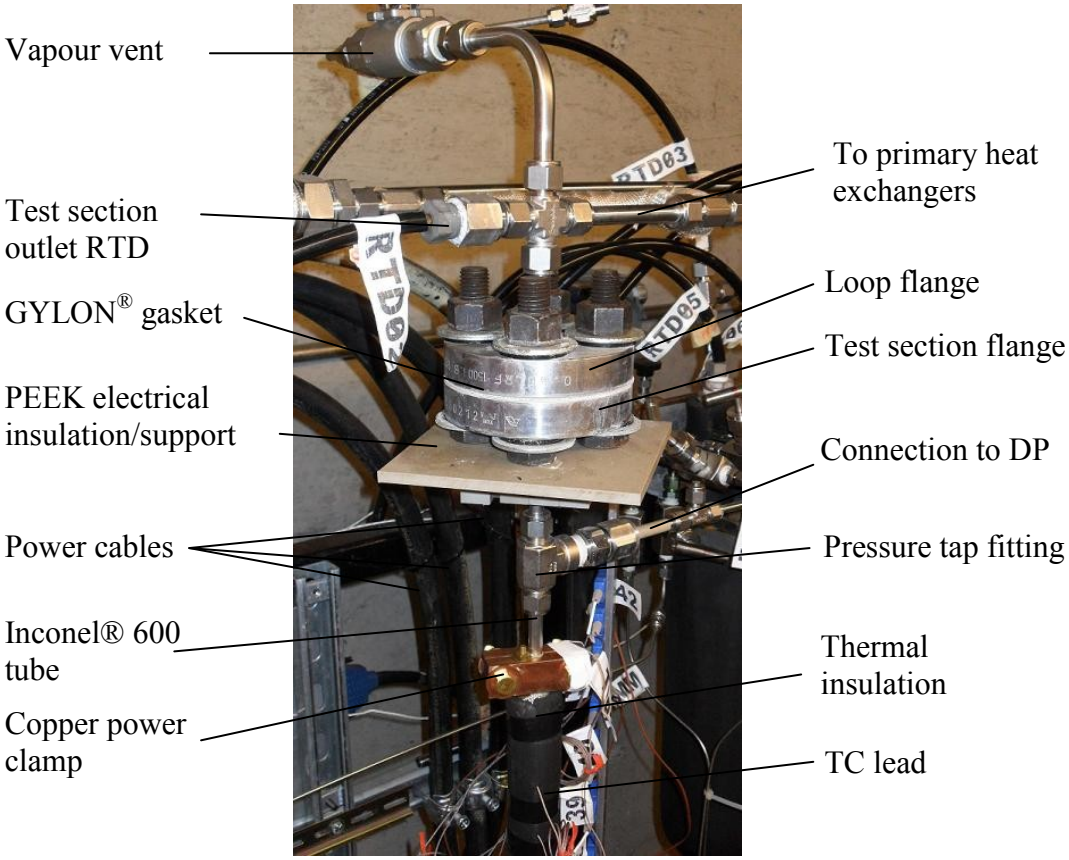

Figure A.13– Upper part of the 8-mm test section

Figure A.14 – National Instruments PXIe-1065 PXI Express chassis

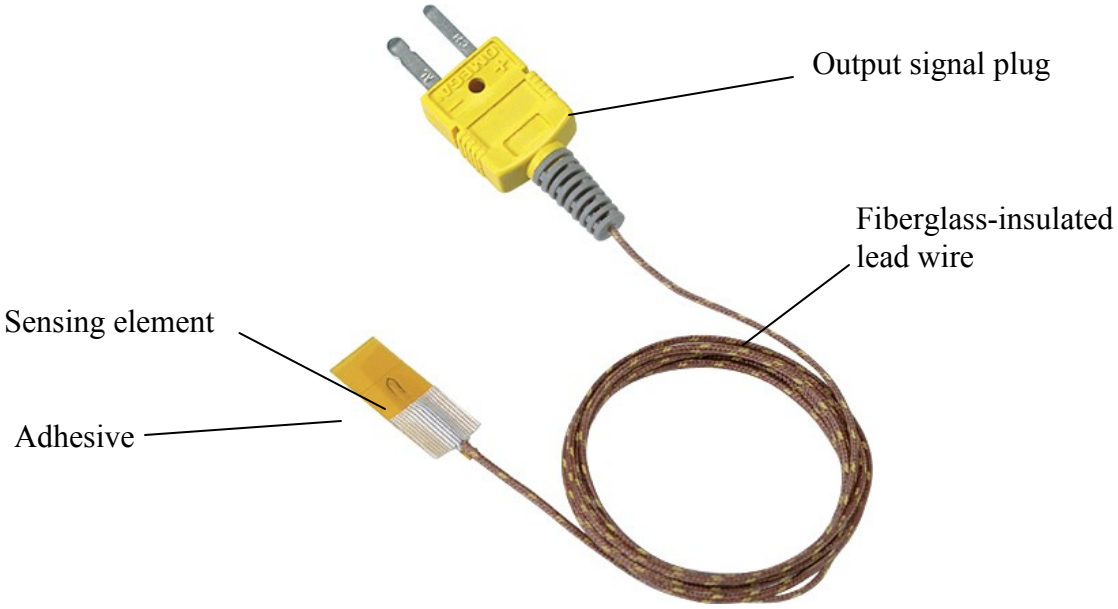

Figure A.15– Omega® SA1XL series thermocouple

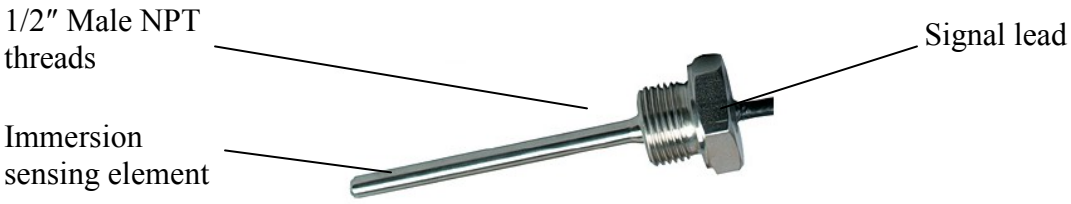

Figure A.16– Omega® P-M-1/10-1/8-5-1/2-G-15 in-flow ultra precise RTD sensors

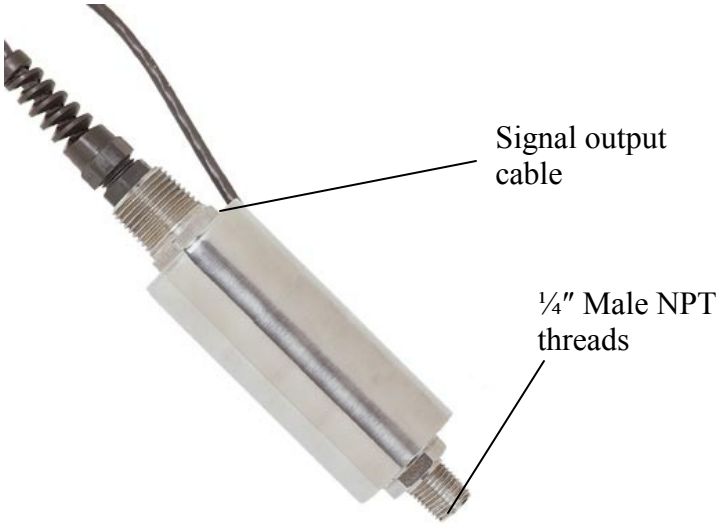

Figure A.17– Omega® PX01C1-3KA5T pressure transducer

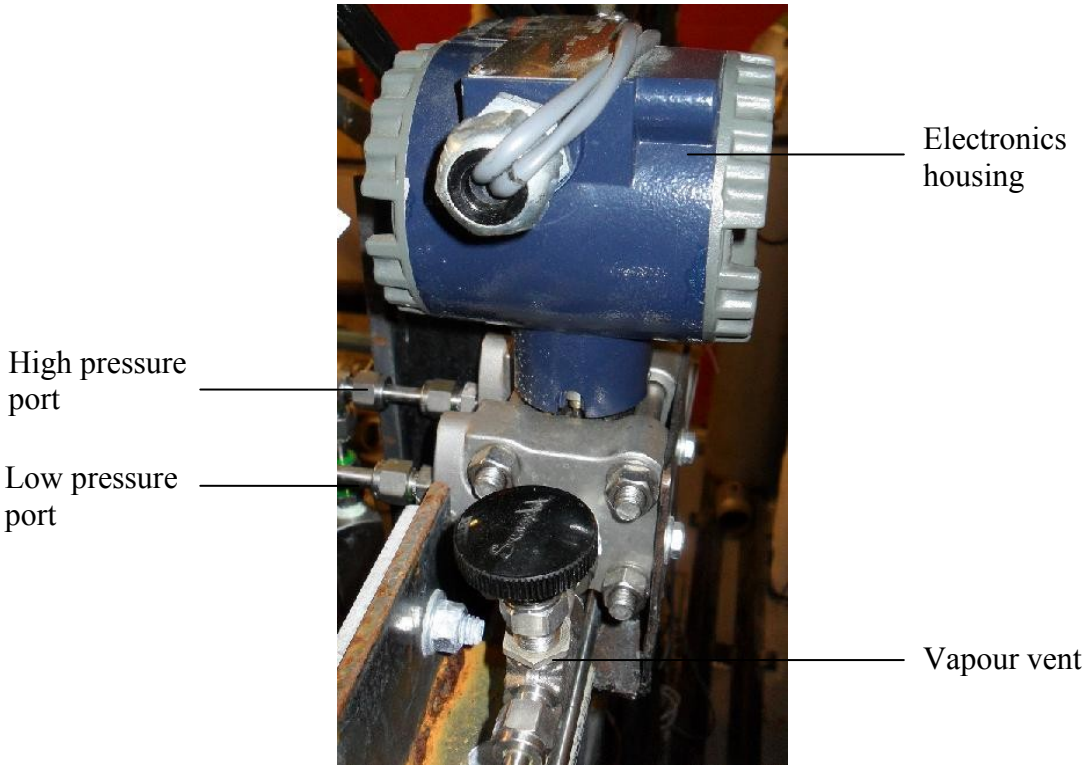

Figure A.18– Omega® PX771A-300DI differential pressure transmitter

Figure A.19– Micro Motion® Elite®coriolis flow meter

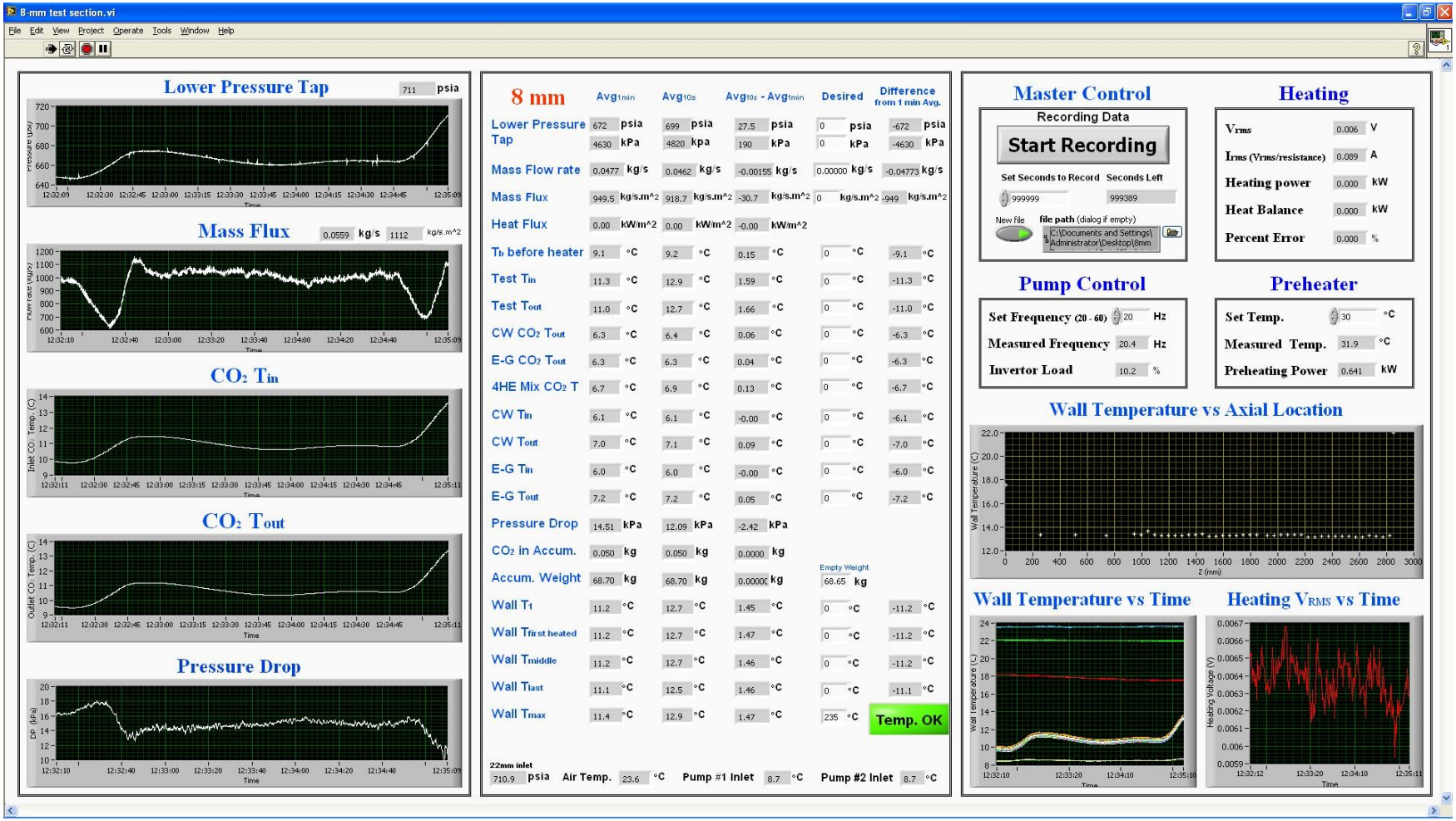

Figure A.20 –LabVIEW®[®] interface for parameter control, data monitoring and logging

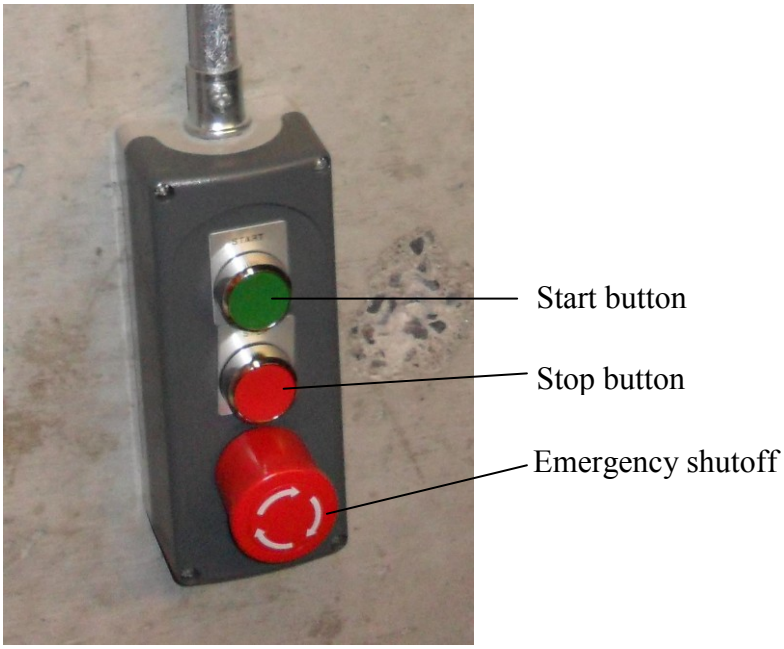

Figure A.21 – CO_2 pump on/off switch

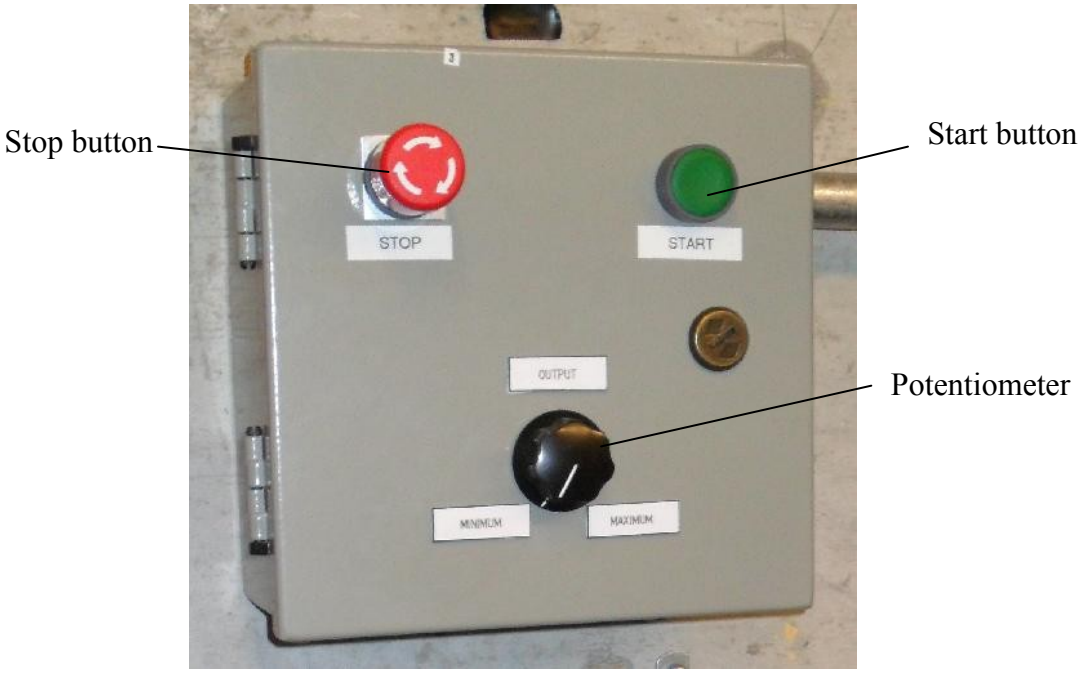

Figure A.22 – Heating power control

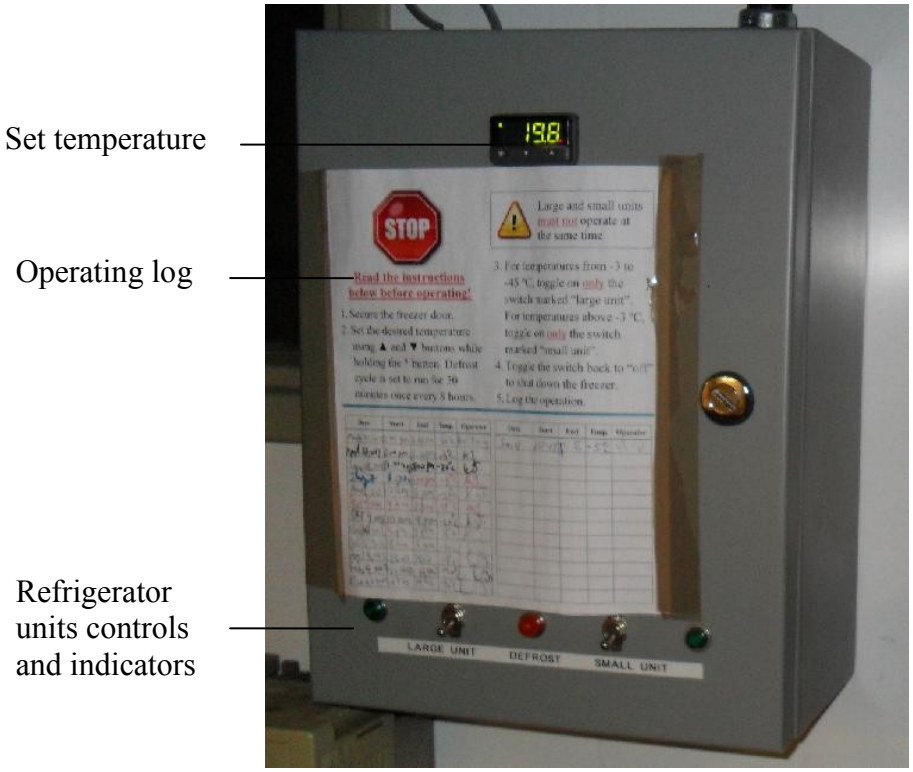

Figure A.23 – Freezer chamber temperature control box

Figure A.24– Preheater control panel

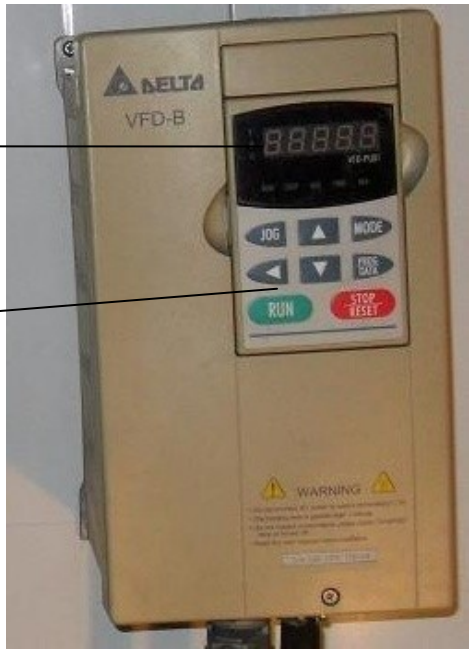

Figure A.25 – Power inverter for freezer chamber pump #1

Figure A.26– Temperature controller for freezer chamber pump #2

Appendix B Past Publications

Jeddi, L., Jiang, K., Tavoularis, S., and Groeneveld, D.C. (2011). "Preliminary tests at the University of Ottawa supercritical CO_2 heat transfer facility", 5th International Symposium on Supercritical-Water-Cooled Reactors (ISSCWR-5), Vancouver, British Columbia, Canada, March 13-16, 2011.

Jiang, K., Zahlan, H., Tavoularis, S. and Groeneveld, D.C. (2012). "Commissioning tests of the University of Ottawa Supercritical CO_2 Facility", 3rd Annual Conference of the Canadian Nuclear Society, Saskatoon, Saskatchewan, June 10 – 13, 2012.

Zahlan, H., K. Jiang, S. Tavoularis and D. Groeneveld, 2013. Measurements of Heat Transfer Coefficient, CHF and Heat Transfer Deterioration in Flows of CO2 at Near-critical and Supercritical Pressures, 6th International Symposium on Supercritical Water-Cooled Reactors (ISSCWR-6), Shenzhen, China, March 3-7, 2013.

PRELIMINARY TESTS AT THE UNIVERSITY OF OTTAWA SUPERCRITICAL CO_2 HEAT TRANSFER FACILITY

L. Jeddi, K. Jiang, S. Tavoularis and D.C. Groeneveld
University of Ottawa, Ontario, Canada

Abstract

This article describes the new supercritical heat transfer test facility that has been constructed at the University of Ottawa and preliminary tests for its commissioning. The facility uses CO_2 as a medium and has three test sections: a tube with an 8 mm ID, to serve as a reference for comparisons with literature, a second tube with a 22 mm ID, and a rod bundle. The facility is designed for tests in the ranges of pressure, heat flux and mass flux that correspond to normal, enhanced and deteriorated heat transfer under conditions relevant to supercritical water cooled reactor designs. Some preliminary measurements of the heat transfer coefficient under subcritical and supercritical conditions in the 8 mm tube are presented and compared to representative correlations. This article also discusses plans for heat transfer measurements in the rod bundle and measurements of turbulence properties and temperature fluctuations using hot- and cold-wire probes in the 22 mm tube.

1. Introduction

The present research is in support of the Canadian National Program on Generation IV Energy Technologies for the development of a Super Critical Water-cooled Reactor (SCWR), which, compared to existing nuclear reactors, is expected to have increased safety, lower-cost electricity production, more compact size and reduced volume of nuclear wastes. The operation of such reactors requires heat transfer to the cooling fluid at pressures higher than the critical pressure. At this pressure, the heat transfer behaviour is quite different from that at subcritical pressure because of the drastic variations of the physical properties near the pseudo-critical temperature [1]. Thus, an accurate prediction of the heat transfer coefficient is necessary for a thermal-hydraulic reactor design.

A heat transfer test facility which can be operated at subcritical and supercritical pressures using carbon dioxide as a surrogate for water has been built at the University of Ottawa. Carbon dioxide was chosen as working fluid because of its inertness and its lower critical pressure and temperature compared to those of water (see Table 1); this reduced the safety requirements as well as the loop construction and operating costs. The following sections describe the loop and provide some preliminary results for heat transfer in an 8 mm tube at two different pressures. The heat transfer coefficients estimated from the tests are compared with corresponding predictions of existing heat transfer correlations.

Table 1 Critical conditions for water and carbon dioxide.

Parameter	Symbol	Unit	H_2O	CO_2
Critical pressure	P_c	MPa	22.1	7.4
Critical temperature	T_c	°C	374.1	31.0
Critical density	ρ_c	kg m^{-3}	315	468

2. Test facility

2.1 General description of the loop

A schematic diagram of the loop is shown in Figure 1. The loop was designed for a maximum pressure of 15 MPa and a nominal operating pressure of 10 MPa.

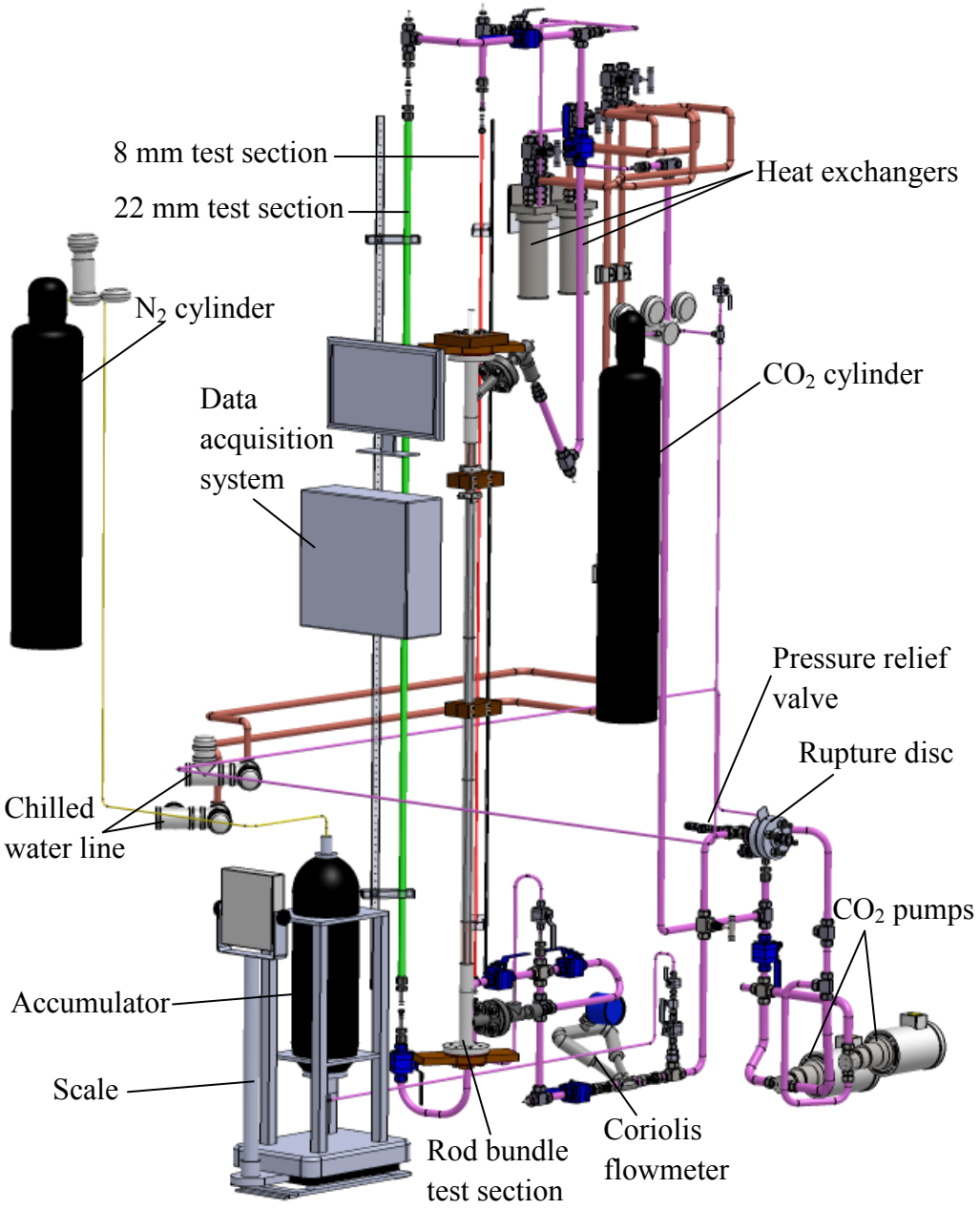

Figure 1 Schematic diagram of the supercritical CO_2 loop.

The loop is filled with CO_2 from cylinders with an internal pressure of 13 MPa through a regulating valve. CO_2 flow is driven by a gear pump (Cole-Palmer, Model GLH23.JVS;E.M2N1CH15). A second

pump is available for operation in parallel with the first one so that higher flow rates can be achieved; additional pumps can be installed for even higher flow rates. A gear pump design was adopted to keep flow fluctuations as low as possible.

A bladder accumulator is used to maintain the loop pressure at the desired value during its operation. The inner side of the bladder is connected to a pressurized nitrogen cylinder, whereas its outer side is connected to the CO_2 in the loop downstream of the pump. The accumulator is mounted on a scale so that the weight of liquid or liquid-like CO_2 in it can be monitored.

The flow rate in the loop is regulated by adjusting the pump speed using a single inverter (Cole-Parmer, Model 3PH Nema 4VFD7.5HP). A pressure relief device and a rupture disc are installed to prevent over-pressurization of the loop.

The test sections are heated electrically by passing direct current through their walls; power is provided by a DC power supply rated at a maximum voltage of 60 V and a maximum current of 2833 A.

The CO_2 leaving the test section is cooled by passing through two single helical tube heat exchangers (Sentry Equipment Corp., Model FXF-6223U) connected in series. In this preliminary stage of the tests, the secondary sides of both heat exchangers are connected to the central chilled water supply, whose specifications are summarized in Table 2. In later stages of the work, and in order to reach lower test section inlet temperatures, the second heat exchanger will use Dowtherm J synthetic organic heat transfer fluid (Dow Chemical Co.), which has a relatively low viscosity at low temperatures (e.g., 1.8×10^{-3} kg m^{-1} s^{-1} at -20 °C; this value is much lower than that of glycol or other commonly used low-temperature liquids); nominal specifications for this coolant are also presented in Table 2. The Dowtherm J fluid is stored in a tank in a walk-in freezer (Figure 2) and pumped to the CO_2 loop using a low-temperature pump (Dynapump Corp., Model JSB-2HP-1S, rated at 75 l/min). The same fluid is recirculated by a separate pump (Dynapump Corp., Model JSB-2HP-1S, rated at 38 l/min) to two radiators (Heat Innovations, Inc., 2-Row, 36x36) inside the freezer to maintain its temperature at a low level. Both pumps are located outside the walk-in freezer. All coolant supply lines are thermally insulated to keep heat losses to the surroundings as low as possible.

Table 2 Cooling system specifications.

Parameter	**Unit**	**Nominal Value**
Chilled water system:		
Inlet temperature	°C	10 (winter), 5 (summer)
Flow rate	l/min	166
Cooling capacity	kW	215 (winter), 274 (summer)
Dowtherm J system:		
Inlet temperature	°C	-35 (higher for continuous operation)
Flow rate	l/min	180
Cooling capacity	kW	92

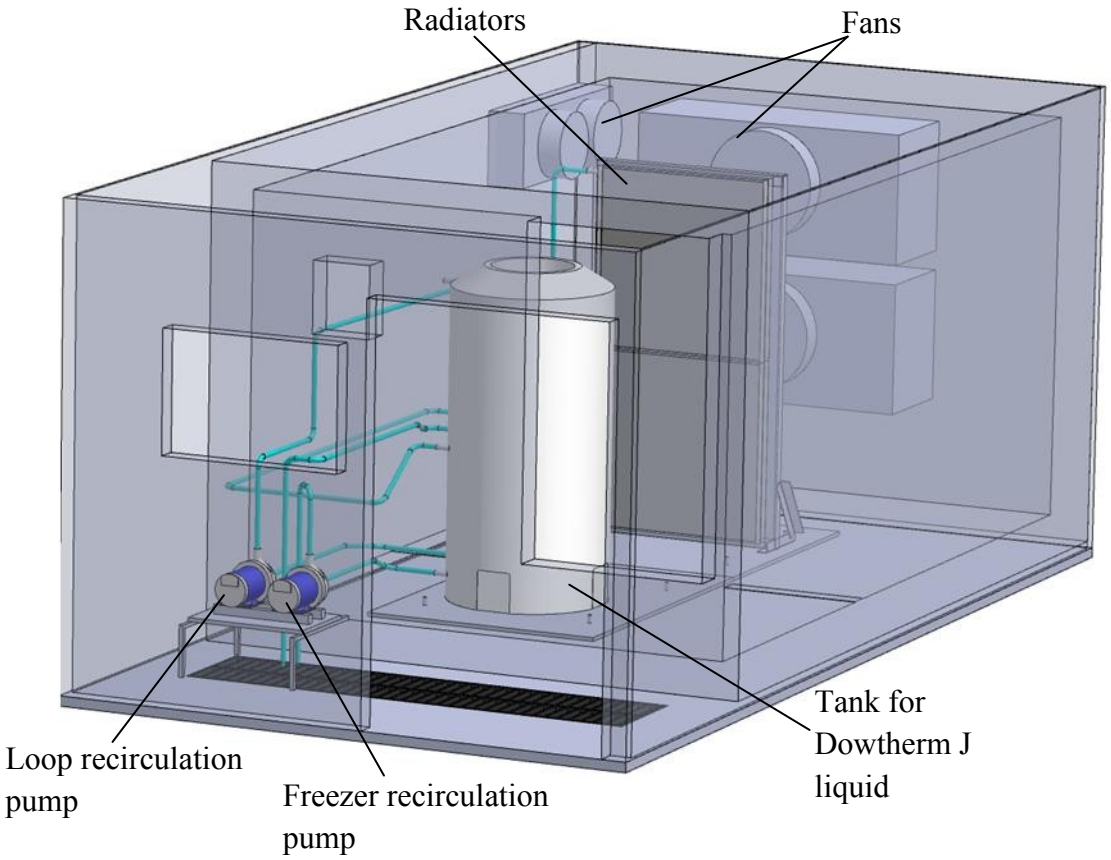

Figure 2 Schematic diagram of the walk-in freezer and the secondary cooling system.

2.2 Test section design

Three interchangeable test sections are connected to the loop: a tube with an 8 mm ID, a second tube with a 22 mm ID, and a rod bundle, all mounted vertically for upward flow. Figure 3 shows the first test section design, which consists of a circular tube made of Inconel 625 with an ID of D = 8.0 mm, a wall thickness of 1.0 mm and a length of 3.05 m. This tube is connected to the loop using electrically insulating connectors and to the power supply using two clamped electric terminals, whose position along the tube can be adjusted. The nominal heated length of the tube was L_h = 1.87 m and follows an unheated length of at least 1 m (i.e., 125 diameters), which allows the flow to develop without complications due to heating.

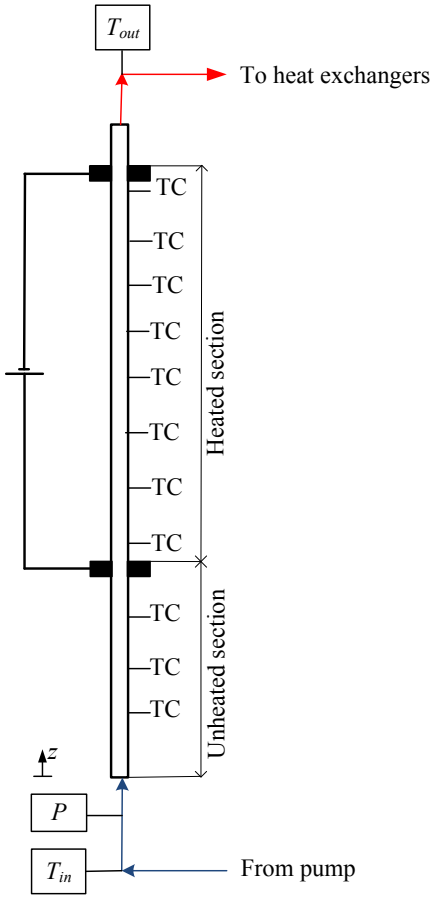

Figure 3 Schematic diagram of the 8 mm tube test section.

2.3 Instrumentation

For the particular tests reported here, 11 T-type thermocouples (Omega Engineering, Inc., Model SA1XL-T-SRTC) were installed along the 8 mm tube test section at distances of 254 mm from each other. For the main tests, many more thermocouples, as well as several RTDs, will be installed along each of the two tubes. The CO_2 temperatures T_{in} at the inlet and T_{out} at the outlet of each of the three test sections are measured by platinum, ultra-precise, long-stem RTDs (Omega Engineering, Inc., Model P-M-1/10-8-5-1/2-G-15). The pressure in the loop is measured using a pressure transducer (Omega Engineering, Inc., Model PX01C1-3KA5T), which is installed near the inlets of the three test sections. A Coriolis-type flow meter (Micro Motion, Model CFM050M320N0A2E2ZZ) is also installed near the inlets of the test sections to measure the mass flow rate. The ranges and uncertainties of these instruments are summarized in Table 4.

Table 4 Instrument range and uncertainty.

Instrument	Unit	Range	Uncertainty
Coriolis flow meter	kg s^{-1}	0 – 25	0.05%
Thermocouples	°C	-73 – 260	0.5 (to be reduced by calibration)
In-flow RTDs	°C	-73 – 400	0.03 + 0.0005|T|
Pressure transducer	MPa	0 – 20	0.05%

2.4 Data collection

All signals from the sensors, the flowmeter and the scale are monitored, recorded and processed using a dedicated data acquisition and processing system (National Instruments) along with a Labview 2009 software interface. This system consists of a 1.73 GHz quad-core embedded controller ((NI PXIE-8133) installed in a PXIE 1065 chassis that can hold up to 18 modules. Currently, they are three 32 channel thermocouple modules (NI PXI 4353) used for temperature measurement, three high precision temperature and voltage modules (NI PXI 4351) used for temperature measurement with RTDs and one high-accuracy multifunction M Series data acquisition (DAQ) module (NI PXI 6289) used for voltage measurement (flowmeter, pressure transducer and scale).

3. Preliminary loop commissioning tests

In the following, we will present three sets of preliminary measurements collected during pilot tests in preparation for the loop commissioning. Shortly after these measurements were taken, equipment malfunction interrupted the testing. The reaction of supercritical CO_2 with some materials in the pumps and the accumulator and the presence of undesirable gas in the loop have been investigated among the possible sources of problems and are currently been eliminated so that loop operation may resume in the near future.

3.1 Test conditions

The test conditions are summarized in Table 5. These include the loop pressure P and its ratio with the critical pressure P_c, the inlet temperature T_{in}, the mass flux G and the heat flux q. Tests A and B were at a subcritical pressure and test C was at a supercritical one. The saturation temperature T_{sat} for the subcritical tests and the pseudo-critical temperature T_{pc} for the supercritical tests have also been included in Table 5. In all cases, the mass flux was kept at the same moderate value, whereas the heat flux was adjusted so that different heat transfer regimes could be examined.

Table 5 Conditions for the present tests.

Parameter	Units	Test A	Test B	Test C
P	MPa	6.70	6.70	7.68
P/P_c	-	0.90	0.90	1.04
T_{in}	°C	7.84	8.15	8.74
T_{sat}	°C	26.76	26.76	–
T_{pc}	°C	–	–	32.75
G	kg/m² s	500	500	500
q	kW/m²	5	50	90

3.2 Data reduction

The local thermophysical properties of CO_2 at the loop pressure and the local bulk fluid temperature were calculated using NIST software RefProp 7.0. The bulk temperature T_b of CO_2 at each downstream location in the tube was calculated from the loop pressure and the local bulk specific enthalpy i_b of the fluid. The bulk specific enthalpy for all three tests was assumed to increase linearly along the flow direction, as

$$i_b = \frac{(i_{out} - i_{in})}{L_h} z + i_{in} \quad (1)$$

Analysis taking into account heat conduction through the tube wall demonstrated that the temperature difference between the inner and outer wall surfaces was much lower than the overall temperature measurement uncertainty. The heat transfer coefficient h was estimated as

$$h = \frac{q \pm q_{loss}}{T_w - T_b} \quad (2)$$

for the cases for which no boiling was detected to occur and as

$$h = \frac{q \pm q_{loss}}{T_w - T_{sat}} \quad (3)$$

for cases for which boiling was present. Because during these specific preliminary tests the test section was not insulated, there was heat transfer to or from the surroundings and so a rough estimate of heat flux q_{loss} to or from the exterior of the tube was used to correct the estimate of h.

3.3 Heat transfer correlations used for comparisons

At this preliminary stage of the work, we present comparisons of our results with representative correlations for subcritical and supercritical pressures. For forced convection in circular tubes at subcritical pressures, we considered the widely used Dittus-Boelter (D-B) correlation [2]:

$$\mathrm{Nu}_b = 0.0243\ \mathrm{Re}_b^{0.8}\ \mathrm{Pr}_b^{0.4} \quad (4)$$

When it was assessed that film boiling occurred in the tube, the following Dougall-Rohsenow (D-R) form of the D-B correlation was used

$$\mathrm{Nu}_{fb} = hD/k_v = 0.0243\mathrm{Re}_{\mathrm{hom}}^{0.8}\ \mathrm{Pr}_v^{0.4} \quad (5)$$

where the Reynolds number for homogeneous fluid is

$$\mathrm{Re}_{\mathrm{hom}} = \frac{GD}{\mu_g}\left[x_e + (1 - x_e)\frac{\rho_g}{\rho_f}\right] \quad (6)$$

For supercritical pressures, we considered as representative the correlation devised by Jackson and Fewster (J-F correlation) [3]:

$$\mathrm{Nu}_b = 0.0183\ \mathrm{Re}_b^{0.82}\ \overline{\mathrm{Pr}}_b^{0.5} \left(\frac{\rho_w}{\rho_b}\right)^{0.3} \quad (7)$$

All symbols used in these correlations are defined in the nomenclature.

4. Preliminary results

Figures 4, 5 and 6 present measurements of the wall temperatures and estimates of the heat transfer coefficients in the 8 mm tube test section for tests A, B and C, respectively, under conditions summarized in Table 5. Corresponding predictions of correlations for the heat transfer coefficients are also presented in these figures.

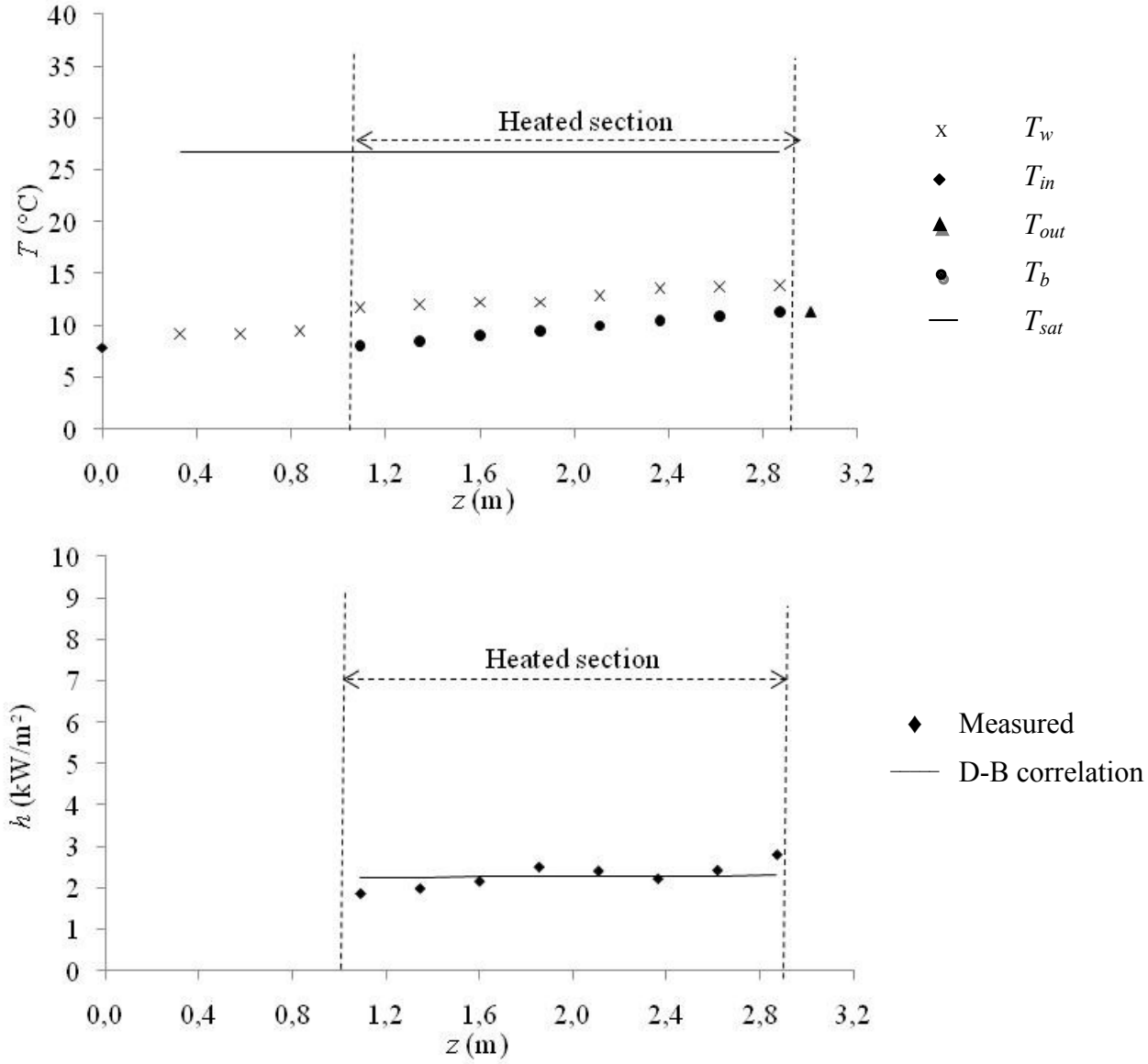

Figure 4 Measured wall temperatures and estimated heat transfer coefficients for subcritical test A (see Table 5 for test conditions).

During subcritical test A, the heat flux was sufficiently low for the wall temperature and the bulk temperature of CO_2 to be significantly lower than the saturation temperature (Figure 4). Consequently, the CO_2 remained a subcooled liquid at the exit of the test section and the heat transfer was within the normal regime for single-phase flow. The heat transfer coefficients estimated from the experimental data were in fair agreement with predictions of the Dittus-Boelter correlation.

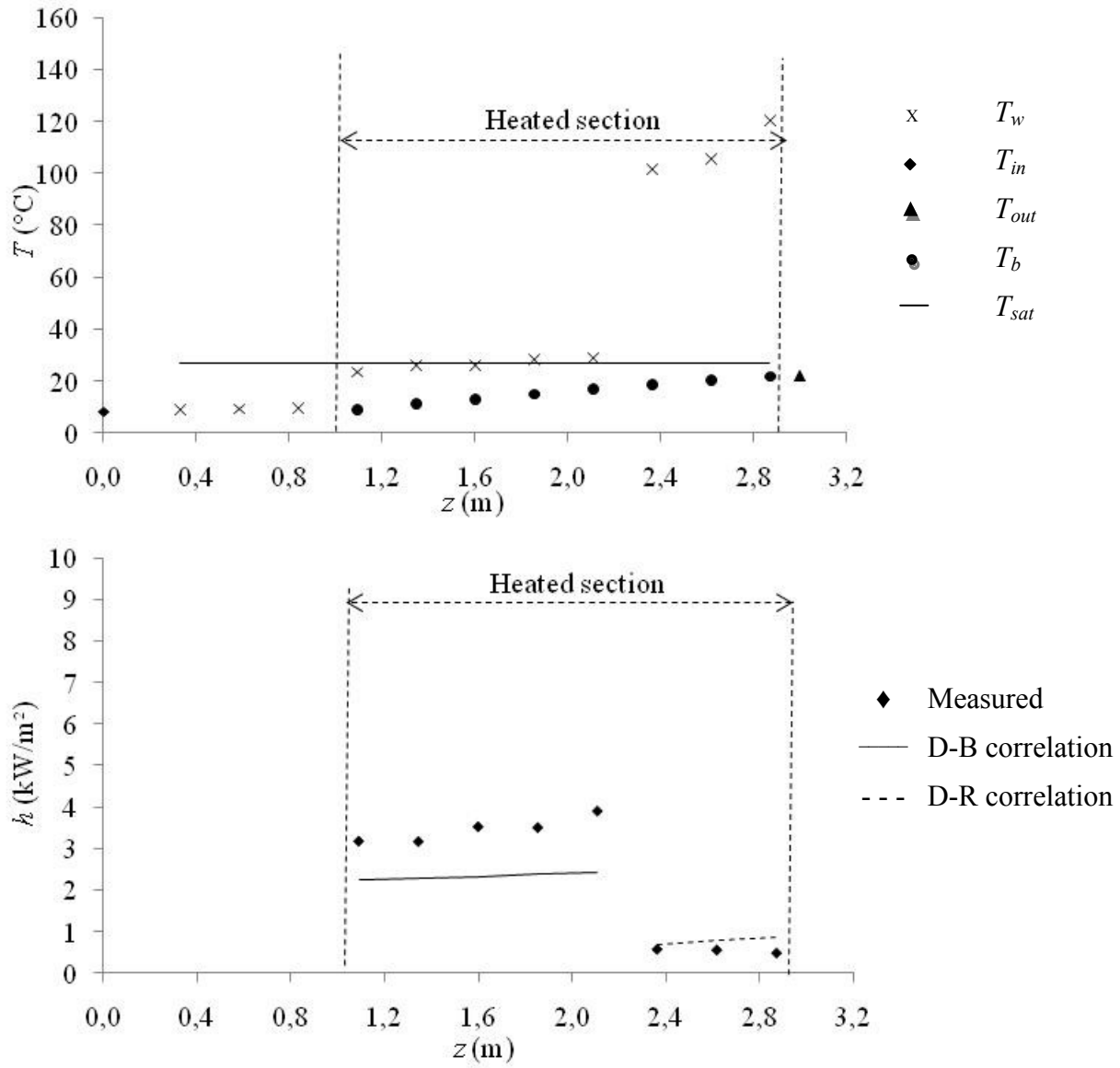

Figure 5 Measured wall temperatures and estimated heat transfer coefficients for subcritical test B (see Table 5 for test conditions).

During subcritical test B, which is at a much higher heat flux than test A, it is evident that, at a certain elevation, the heated wall temperature that exceeded the saturation temperature (Figure 5). For axial locations $0.8 < z < 2.2$ m, the heat transfer coefficient was significantly higher than the Dittus-Boelter prediction, which indicates the presence of pre-CHF boiling. The measurements suggest that CHF occurred at $z = 2.2$ m, because the wall temperature profile displayed a temperature rise that is typical of initiation of film boiling heat transfer. At locations $2.2 < z < 2.9$ m, developing film boiling conditions prevailed. The experimental film boiling heat transfer coefficient and the one calculated from the D-R correlation are in fair agreement.

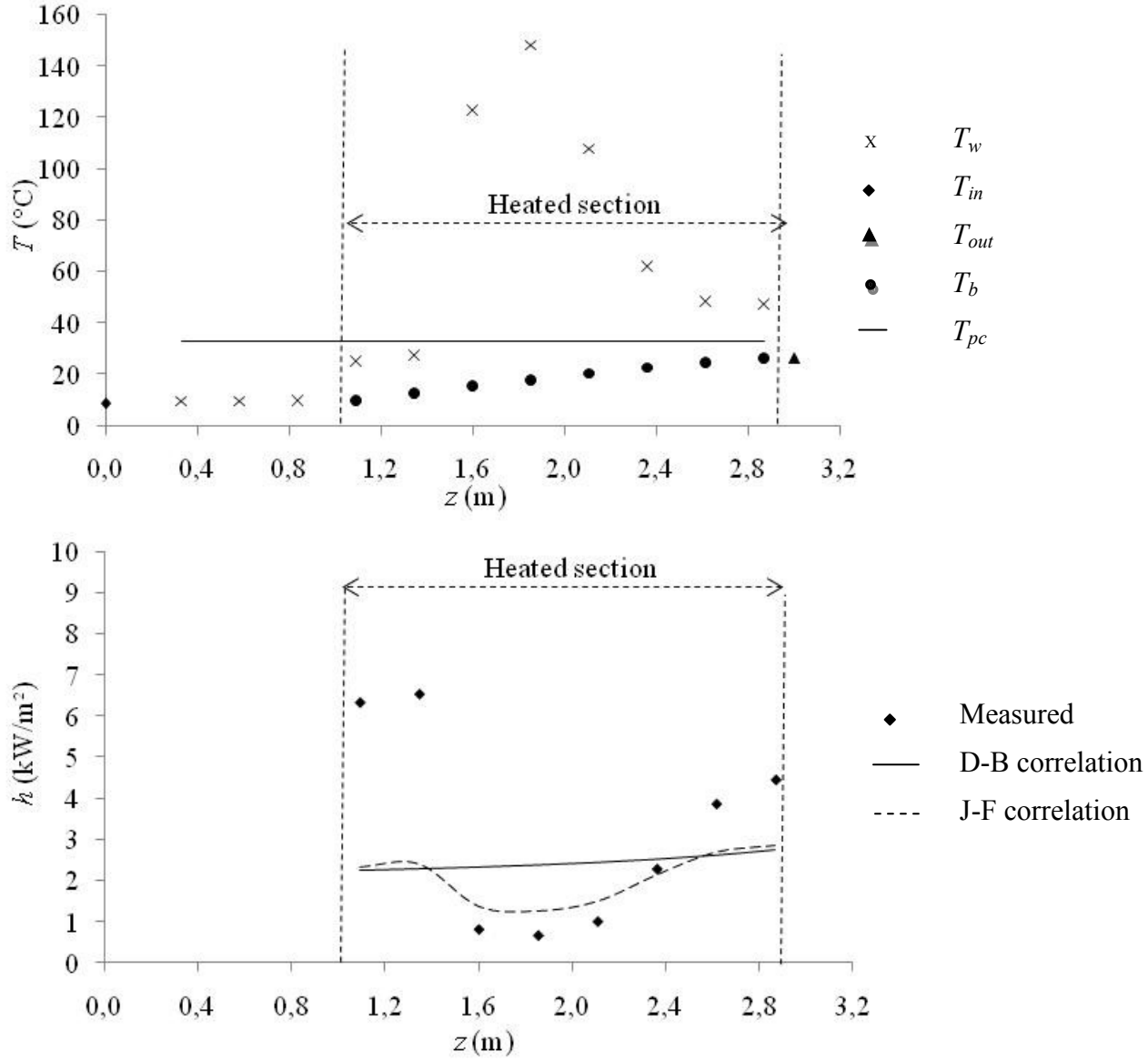

Figure 6 Measured wall temperatures and estimated heat transfer coefficients for supercritical test C (see Table 5 for test conditions).

Figure 6 shows the wall temperatures and the heat transfer coefficients for the supercritical test C. It is shown that these coefficients were relatively high near the inlet of the heated section, where the wall temperature and the bulk temperature of CO_2 were both lower than the pseudo-critical temperature. Further downstream, the heat transfer deteriorated and the wall temperature exceeded the pseudo-critical temperature while the bulk temperature remained below the pseudo-critical value. The Dittus-Boelter correlation deviated from the experimental results both in values and trend, whereas the predictions of the Jackson and Fewster correlation have some qualitative resemblance with the measurements, but also deviated in values.

5. Ongoing work

5.1 Loop commissioning tests

The installation of additional instrumentation and controls is in progress. To refine the measurement resolution, additional T-type thermocouples and also wall RTDs (RDF Corp., Model 29223 - three-wire type) are being installed along the 8 mm tube at distances of 50 mm from each other. To reduce the measurement uncertainty, the thermocouples will be calibrated against the wall RTDs. In addition, a differential pressure transmitter (Omega Engineering, Inc., Model PX771A-300WCDI) will be installed to measure the pressure drop from the inlet to the outlet of the test section.

As part of the loop commissioning process, a series of tests using the 8 mm tube will be performed for a few additional representative sets of conditions, within the nominal ranges which have been summarized in Table 6. Heat balance tests will be conducted for each test by comparing electrical power input into the test section with thermal power given to the fluid, determined from the flow rate, loop pressure and enthalpy rise across the test section.

Table 6 Proposed test conditions.

Parameter	Unit	Range for CO_2 tests	Equivalent range in water
Inlet pressure	MPa	6.60, 7.36, 8.36, 8.80	19.8, 22.1, 25.1, 26.4
Inlet temperature	°C	5 – 30	320 – 350
Outlet temperature	°C	20 – 60	350 – 435
Mass flux	kg m^{-2} s^{-1}	800, 1000, 1500	594, 1188, 1782
Heat flux	kW m^{-2}	20 – 500	150 – 3800

5.2 Heat transfer and pressure drop measurements in the 8 and 22 mm tube test sections

Detailed measurements of wall temperature will be conducted in the 8 and 22 mm tubes over the nominal ranges of conditions that have been specified in Table 6. The full ranges of mass flux and heat flux may not be covered simultaneously for the 22 mm tube, because of limitations in the loop capabilities. The results will be compared to existing measurements in tubes and will complement and expand the available database. They will also serve as reference for comparisons with measurements in the rod bundle test section under the same conditions. In addition, these two test sections will be modified with the additions of two pressure taps each, one just before and a second one just after the heated sections, so that pressure drop can be measured under the test conditions. The pressure drop will be measured with a differential pressure transmitter (Omega Engineering, Inc., Model PX771A-300WCDI), having a range from 0 to 75 kPa and an uncertainty of 0.1%.

5.3 Heat transfer and pressure drop measurements in a rod bundle

The available rod bundle subassembly, shown in Figure 7, comprises a pressure tube with an inner diameter of 25.4 mm, which contains three directly heated rods and three wall inserts. The rod bundle has five sections, each 500 mm long, connected in series and separated from the neighbouring sections by endplates. Pads are positioned between the rods and on the rod sides that face the pressure tube at regular intervals to ensure that the gaps remain as uniform as possible. The first and last sections of the rod bundle are made of copper, whereas the three sections in the middle are made of Inconel, so that only these three sections are subject to significant direct heating. The rod diameter is 10.0 mm and the

pitch to diameter ratio is 1.14. The hydraulic diameter of the rod bundle is 6.7 mm and the flow area is 177 mm^2. The ends of the three rods are fastened on copper plates, which are connected to the power supply. The inner surface of the pressure tube is electrically insulated. Each of the three rods in the last heated section of the rod bundle contains a sliding thermocouple assembly, as shown in Figure 8. This assembly consists of a carriage rod, near the upstream end of which two insulated K-type thermocouples are mounted across from each other. A loaded spring pushes each thermocouple against the heated surface to ensure good thermal contact. Each thermocouple may be rotated within the rod over 360° and traversed along the rod over a distance of 378 mm.

Heat transfer and pressure drop measurements in the rod bundle will be conducted over the same ranges of conditions as those listed in Table 6. The axial and azimuthal variations of wall temperature in the three rods of the last heated section will be measured and used to calculate the heat transfer coefficient. These results will be compared to available measurements in tubes and predictions of empirical correlations. Of particular interest will be to determine whether deteriorated heat transfer occurs in flow under supercritical pressures in rod bundles, and, if so, the conditions under which it does.

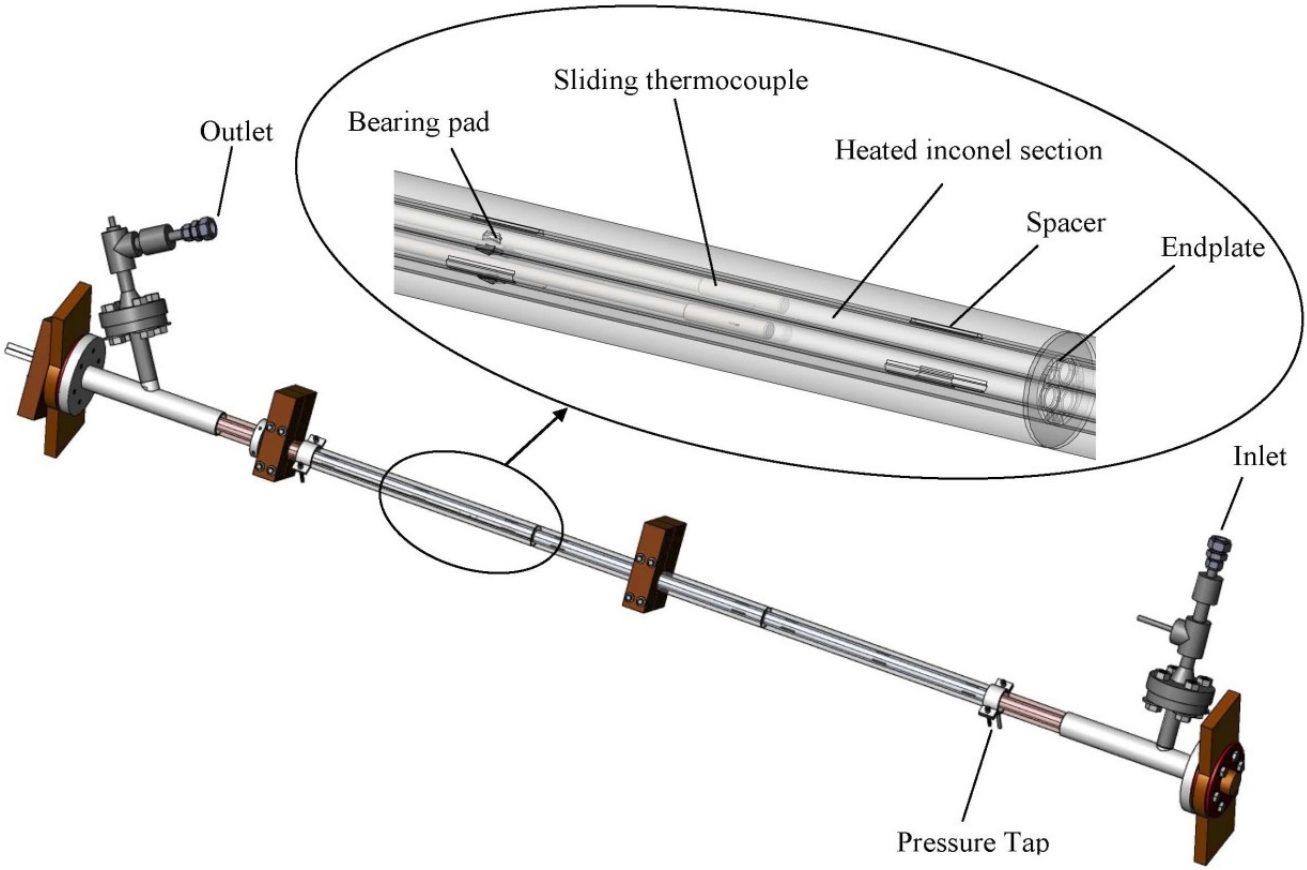

Figure 7 Rod bundle test section.

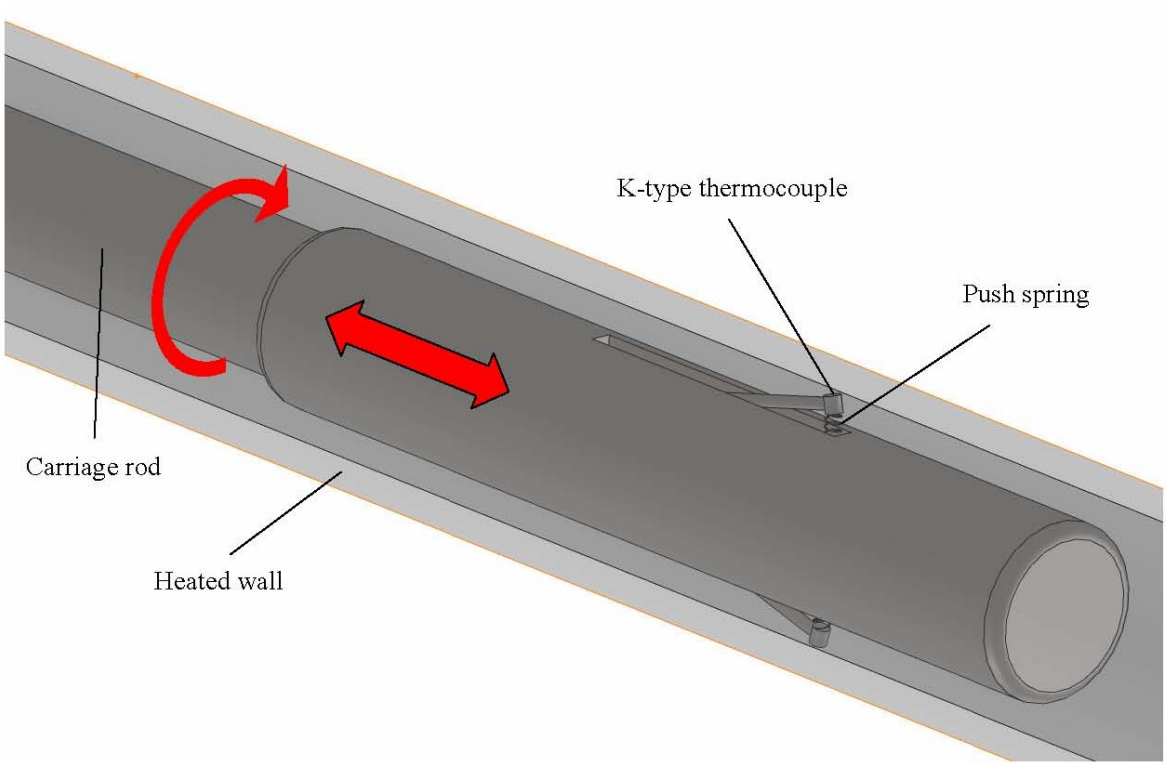

Figure 8 Sliding thermocouple assembly for rod-bundle.

5.4 Measurements of turbulence and in-flow temperature in the 22 mm tube

Finally, the velocity and temperature fluctuations in the 22 mm ID test section will be measured with hot- and cold-wire probes, respectively. The velocity sensor will be operated in the constant temperature mode and the temperature sensor will be operated in the constant current mode. The design of these probes will be similar to the one used by Vukoslavčević et al. [4], who have also presented results of probe calibration and response under ranges of conditions comparable to those of interest in this work. Flanges mounted on the test section as shown in Figure 9 will be used for probe insertion. The probes will be electrically insulated from the test section as well as sealed to a pressure of at least 10 MPa. The calibration of the probes will be performed in situ against a micro-Pitot tube and a micro-thermocouple or micro-thermistor, which will be inserted and traversed in the test section together with the hot- and cold-wire probes. This set of measurements of velocity and temperature fluctuations are expected to contribute to the understanding of the complex phenomena of heat transfer enhancement and deterioration, which occur under certain conditions of interest to SCWR, and to serve as benchmarks for the validation of analytical models and numerical simulations.

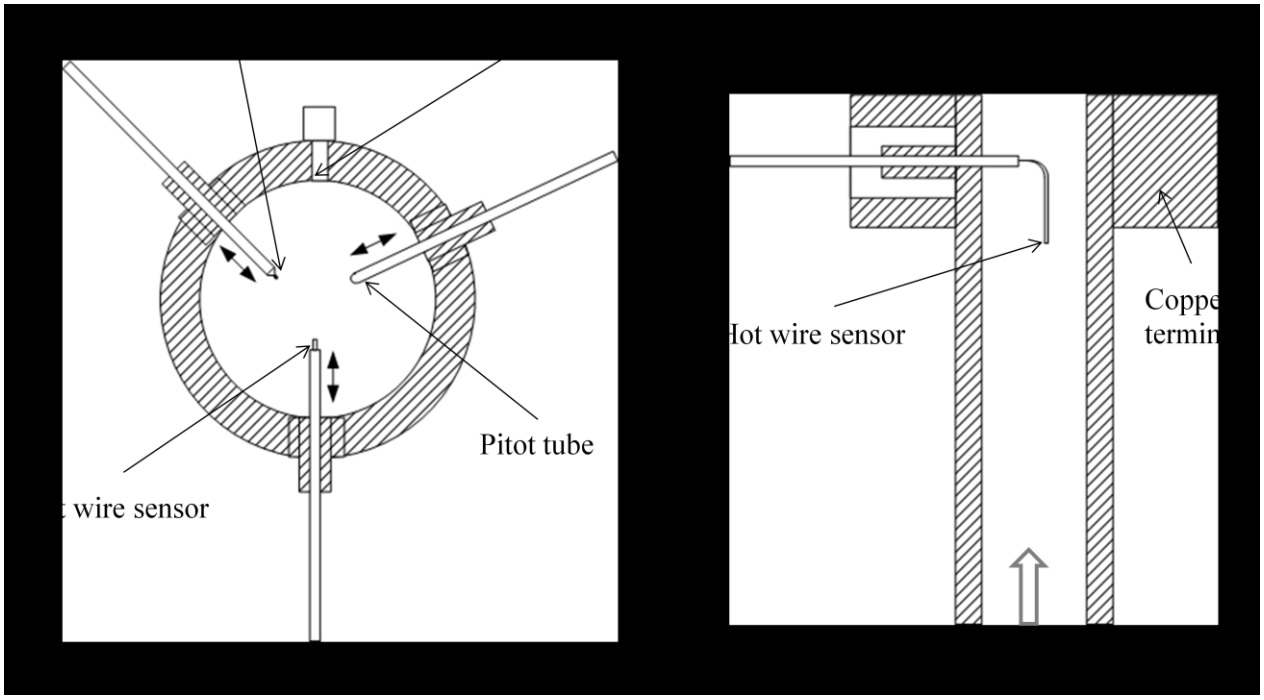

Figure 9 Schematic diagram of the probe insertion arrangement.

6. Summary

In this article we presented a detailed description of a new supercritical heat transfer facility using carbon dioxide as a medium. As part of the loop commissioning procedure, the heat transfer coefficient was measured for a relatively low mass flux in upward flow along a vertical 8 mm tube under both subcritical and supercritical conditions.

Under subcritical conditions, two heat transfer regimes were reproduced. For a relatively low heat flux, the fluid remained in the liquid phase and the heat transfer coefficient that was estimated from the experimental data was in fair agreement with predictions of the Dittus-Boelter correlation. For a higher heat flux, the fluid near the heated wall apparently boiled at some location in the test section, beyond which the experimental heat transfer coefficient was in fair agreement with predictions of the Dougall-Rohsenow correlation that applies to the film-boiling regime.

Under supercritical conditions with relatively low heat and mass fluxes, we observed an enhancement of heat transfer in the inlet region, where the wall temperature and the bulk temperature of CO_2 were both lower than the pseudo-critical temperature, and strong heat transfer deterioration further downstream. The streamwise variation of the experimental heat transfer coefficient had some qualitative resemblance with the predictions of the Jackson and Fewster correlation.

The article further describes our plans for measuring wall temperature variation and pressure drop in upward flows along tubes with inner diameters of 8 and 22 mm and a simple rod bundle under a variety of supercritical conditions, as well as plans for measuring turbulence and temperature fluctuations in the 22 mm tube.

Acknowledgments

The financial support of NSERC, NRCan and AECL is gratefully acknowledged. We thank Noam Lightstone and Rachel Anderson for assisting us with the drawings and Hussam Zahlan for assistance with the analysis.

References

[1] I. L. Pioro and R. B. Duffey, "Heat Transfer and Hydraulic Resistance at Supercritical Pressures in Power-Engineering Applications", ASME Press, New York, 2007.

[2] F. W. Dittus and L. M. K. Boelter, "Heat transfer in automobile radiators of the tubular type", University of California, Berkeley, Publications on Engineering, Vol. 2 (13), pp. 443-461, 1930.

[3] I. Pioro, H. F. Khartabil and R. B. Duffey, "Heat transfer to supercritical fluids flowing channels – empirical correlations (survey)", Nuclear Engineering and Design, Vol. 230, pp. 69-91, 2004.

[4] P. V. Vukoslavčević, I. M. Radulovic and J. M. Wallace, "Testing of a hot- and cold-wire probe to measure simultaneously the speed and temperature in supercritical CO_2 flow", Experiments in Fluids, Vol. 39 (4), pp. 703-711, 2005.

Nomenclature

C_p	specific heat at constant pressure (J kg^{-1} K^{-1})
$\bar{C}_p = \frac{i_w - i_b}{T_w - T_b}$	average specific heat (J kg^{-1} K^{-1})
G	mass flux (kg m^{-2} s^{-1})
h	heat transfer coefficient (kW m^{-2} K^{-1})
i	specific enthalpy of CO_2 (kJ kg^{-1})
D	inner diameter of test section (mm)
k	thermal conductivity (W m^{-1} K^{-1})
L_h	heated length (m)
P	pressure (MPa)
q	heat flux (W m^{-2})
T	temperature (°C)
x_e	equilibrium quality
z	axial coordinate (m)

Greek letters

μ	dynamic viscosity (kg m^{-1} s^{-1})
ρ	density (kg m^{-3})

Non-dimensional numbers

$\mathrm{Nu} = \frac{hD}{k}$	Nusselt number

$\mathrm{Pr} = \frac{\mu C_p}{k}$	Prandtl number
$\overline{\mathrm{Pr}} = \frac{\mu \bar{C}_p}{k}$	average Prandtl number
$\mathrm{Re} = \frac{G D}{\mu}$	Reynolds number

Subscripts

b	bulk
c	critical
f	saturated liquid
fb	film boiling
g	gas
hom	homogeneous
in	inlet
loss	heat loss to or gain from the surroundings
out	outlet
pc	pseudo-critical
sat	saturation
v	vapour property evaluated at (T_w + T_{sat})/2
w	wall

Commissioning Tests of the University of Ottawa Supercritical CO_2 Facility

K. Jiang, H. Zahlan, S. Tavoularis and D.C. Groeneveld
Department of Mechanical Engineering,
University of Ottawa, Ottawa, Ontario K1N 6N5, Canada

Summary

An experimental facility supporting the Canadian Super Critical Water-cooled Reactor (SCWR) research efforts has been constructed at the University of Ottawa. Loop commissioning tests have been performed, during which a number of heat transfer phenomena were observed. The measured heat transfer coefficients are compared with predictions of available correlations. The test results demonstrated that the facility operates within design specifications.

1. Introduction

The present research is in support of the Canadian National Program on Generation IV Energy Technologies for the development of a Super Critical Water-cooled Reactor (SCWR), which, compared to existing nuclear reactors, is expected to have increased safety, lower-cost electricity production, more compact size and reduced volume of nuclear wastes. The operation of such reactors requires heat transfer to the cooling fluid at pressures higher than the critical pressure. At critical and supercritical pressures, the heat transfer behaviour is quite different from that at subcritical pressures because of the drastic variations of the physical properties near the pseudo-critical temperature [1]. An accurate prediction of the heat transfer coefficient in rod bundles under near-critical and supercritical (SC) conditions is necessary for the design and preliminary analysis of SCWR, but the available information is not sufficient for these purposes. A heat transfer test facility which can be operated at subcritical and supercritical pressures using carbon dioxide as a surrogate fluid for water has been built at the University of Ottawa. CO_2 was chosen as working fluid because of its inertness and its lower critical pressure and temperature compared to those of water. Therefore, by comparison to a SC water loop, the proposed facility has lower safety requirements and lower construction and operating costs. Commissioning tests for the loop have been conducted under conditions covering subcritical, near-critical and SC pressures.

2. The experimental facility

Figure 1 is a schematic diagram of the test facility. The loop was designed for a maximum pressure of 15 MPa and a nominal operating pressure of 10 MPa. The CO_2 flow in the loop is maintained by one or more gear pumps connected in parallel. Loop pressure is stabilized by a group of bellow-type accumulators containing nitrogen. An oxygen depletion monitor has been

installed to ensure that the air in the laboratory has sufficient oxygen concentration even near the floor. Three test sections can be connected in the loop: an 8 mm ID tube, a 22 mm ID tube and a three-rod bundle. The wall of each test section is heated electrically by a low-voltage/high-current DC power supply. The recirculating fluid is cooled using two helical-tube heat exchangers. Two cooling mechanisms are available: chilled water supplied by the University and a refrigeration system using Dowthem J (a type of organic refrigerant) for reaching lower cooling temperatures.

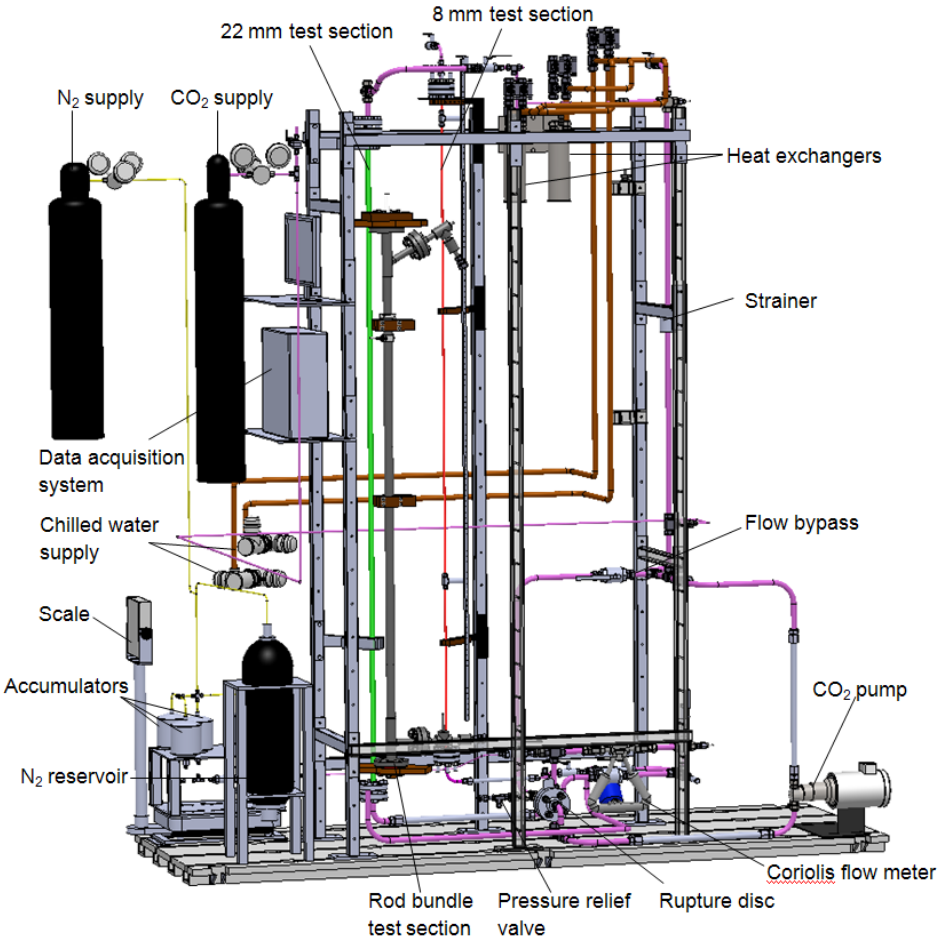

Fig. 1: Schematic diagram of the CO_2 flow loop.

Wall temperature is measured by calibrated T-type thermocouples (TC) attached to the outer walls of the tubular test sections and sliding K-type TCs traversed longitudinally and azimuthally inside the bundle rods. 41 TCs have been attached along the outer surface of the 8 mm test section (Figure 2). The CO_2 temperatures at the inlet and the outlet of each test sections are measured by in-flow RTDs. The pressure in the loop is measured using a high-precision pressure transducer. The pressure drop across each heated length is measured with a differential pressure transmitter. The mass flow rate is measured with a Coriolis-type flow meter. All instrument signals are conditioned, monitored and recorded using a dedicated data acquisition and processing system with a Labview software interface.

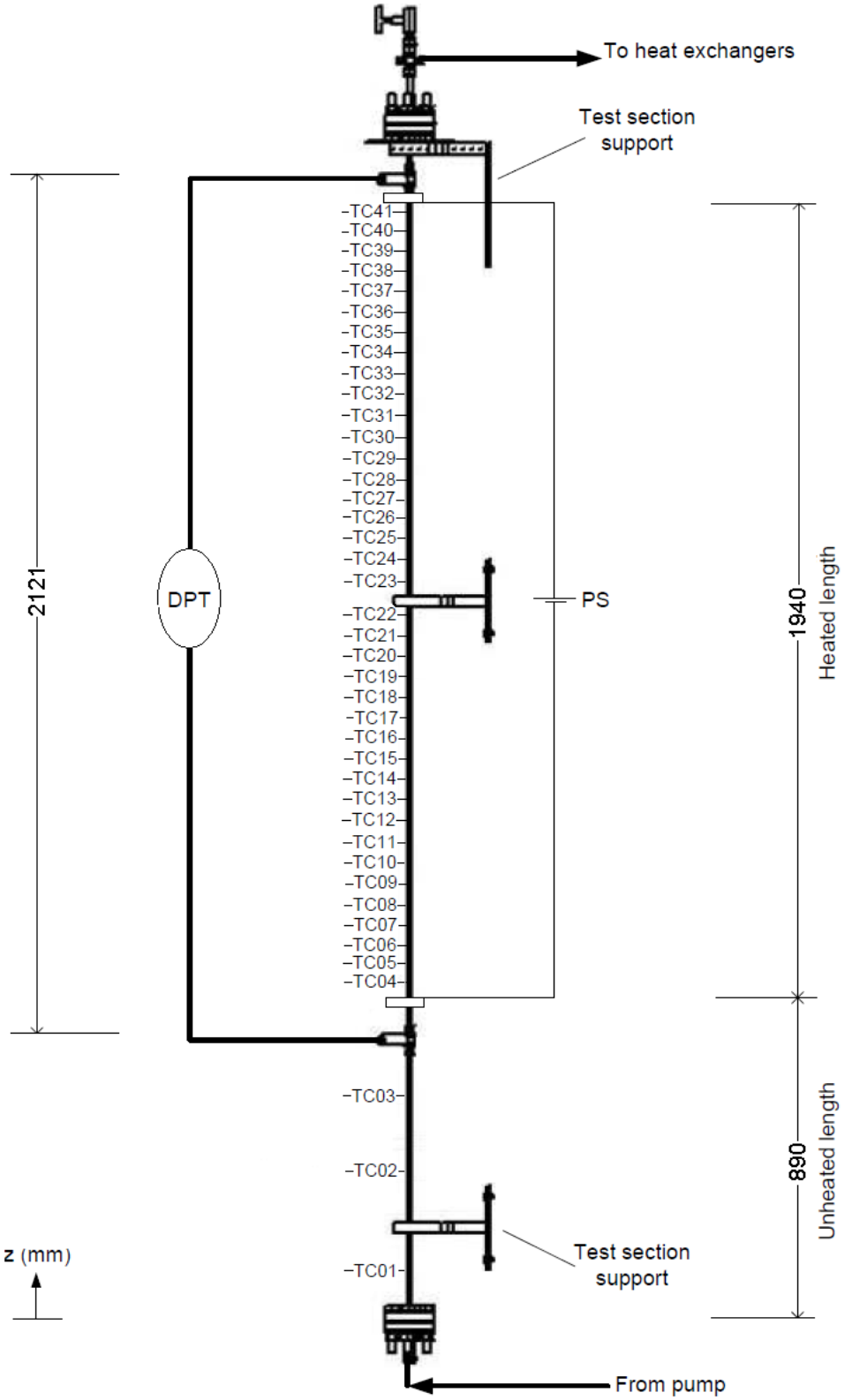

Fig. 2: Schematic diagram of the 8 mm test section showing the locations of thermocouples.

3. Loop commissioning tests

To serve as loop commissioning, measurements were conducted on the 8 mm tube test section under conditions presented in Table 1. Wall temperature variations under some of the measured subcritical, near-critical and supercritical conditions are plotted in Figure 2, 3 and 4, respectively. The results demonstrated that the facility and all instrumentation operate properly.

Table 1 Conditions for commissioning tests

Parameters	Units	Range		
		Subcritical	Near-critical	Supercritical
P	MPa	6.6	7.6	8.8
P/P_c	-	0.89	1.03	1.19
T_{in}	°C	10.5	10.5	10.5
T_{sat}	°C	26.1	–	–
T_{pc}	°C	–	32.3	39.0
G	kg/m² s	400, 800, 1500, 2000	400, 900, 1500	400, 1500
q	kW/m²	20, 50, 120, 140	25-70, 100, 240-280	40, 100, 300

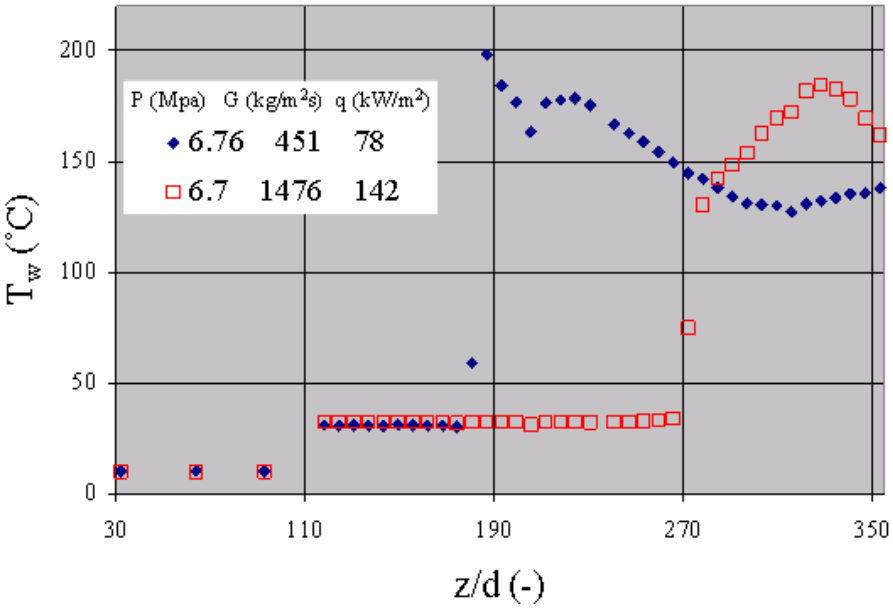

Fig. 3: Wall temperature variations for two sets of subcritical conditions, which show departures from nucleate boiling and film boiling.

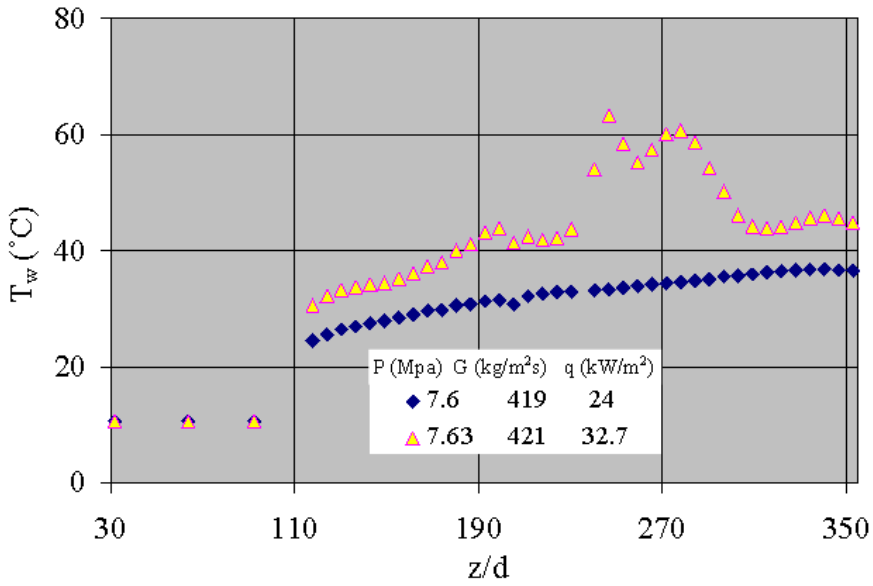

Fig. 4: Wall temperature variations for two sets of near-critical conditions, one of which shows heat transfer deterioration.

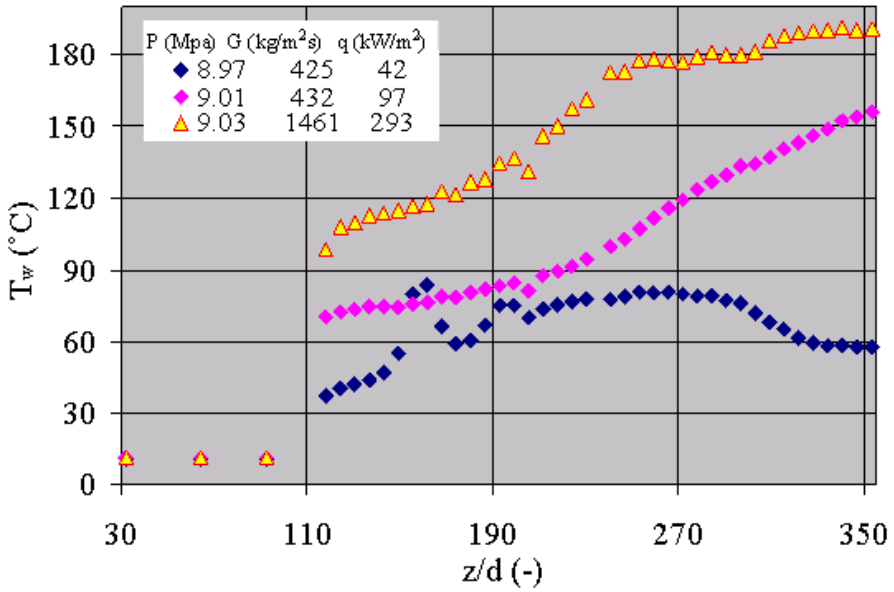

Fig. 5: Wall temperature variations for three sets of supercritical conditions, one of which shows heat transfer deterioration.

Heat balance calculations were performed and demonstrated that the rate of heat losses was very low; the effectiveness of the thermal insulation applied to the test sections was very high and within acceptable uncertainty limits. The measured heat transfer coefficients have been compared with available correlations, including the widely used Dittus-Boelter (D-B) correlation [2] for forced convection in circular tubes at subcritical pressures, the Dougall-Rohsenow form

of the D-B correlation for tests during which film boiling occurred, and the Jackson and Fewster correlation [3] for tests under SC pressures.

4. Ongoing and future work

A few modifications to the loop are being made in efforts to improve loop performance and to address potential problems. A pre-cooling system is being installed to mitigate a predicted difficulty in starting the pumps in warm weather. A pre-heater will be installed to provide elevated inlet temperatures to the test sections and to permit additional control of inlet conditions.

Extensive heat transfer and pressure drop measurements covering broad ranges of conditions, including conditions never considered in previous literature, will be conducted on the 8 and 22 mm tubes. These results will be compared to past measurements in tubes and will complement and expand existing databases. They will also serve as reference for comparisons with upcoming measurements in the rod bundle test section.

Heat transfer and pressure drop measurements in the rod bundle will be conducted over the same ranges of conditions as those planned for the 8 and 22 mm tubes. The axial and circumferential wall temperature variations on the three rods will be measured and used to calculate the heat transfer coefficients. These results will be compared to available measurements in tubes and predictions of empirical correlations. Of particular interest will be the observation of different heat transfer modes occurring in the bundle under various supercritical conditions. The effects of spacers on heat transfer modes will also be examined.

The velocity and temperature fluctuations in the 22 mm ID test section will be measured with hot- and cold-wire probes, respectively. An instrument flange that will house the probes is currently being assembled. This set of measurements is expected to contribute to the understanding of turbulence phenomena in supercritical fluids and to the validation of analytical models and numerical simulations.

5. References

[1] Pioro, I.L. and Duffey, R.B., "Heat Transfer and Hydraulic Resistance at Supercritical Pressures in Power-Engineering Applications", ASME Press, New York, USA, 2007.

[2] F. W. Dittus and L. M. K. Boelter, “Heat transfer in automobile radiators of the tubular type”, University of California, Berkeley, Publications on Engineering, Vol. 2 (13), pp. 443-461, 1930.

[3] I. Pioro, H. F. Khartabil and R. B. Duffey, “Heat transfer to supercritical fluids flowing in channels – empirical correlations (survey)”, Nucl. Eng. Des., Vol. 230, pp. 69-91, 2004.

The 6th International Symposium on Supercritical Water-Cooled Reactors
ISSCWR-6
March 03-07, 2013, Shenzhen, Guangdong, China

ISSCWR6-13XXX

Measurements of heat transfer coefficient, CHF and heat transfer deterioration in flows of CO_2 at near-critical and supercritical pressures

H. Zahlan
University of Ottawa
Department of Mechanical Engineering
161 Louis Pasteur, Ottawa ON K1N 6N5
Tel: 613 562-5800

K. Jiang
University of Ottawa
Department of Mechanical Engineering
161 Louis Pasteur, Ottawa ON K1N 6N5
Tel: 613 562-5800

S. Tavoularis
University of Ottawa
Department of Mechanical Engineering
161 Louis Pasteur, Ottawa ON K1N 6N5
Tel: 613 562-5800

D. Groeneveld
University of Ottawa
Department of Mechanical Engineering
161 Louis Pasteur, Ottawa ON K1N 6N5
Tel: 613 562-5800

Abstract

The University of Ottawa team has recently completed the first phase of an experimental program in their super-critical heat transfer loop (SCUOL) using carbon dioxide as a medium. Thermalhydraulics tests were performed in a directly heated vertical tube having an internal diameter of 8 mm, at high subcritical, near-critical and supercritical (SC) pressures.

The main objective of these tests is to produce heat transfer data at conditions of interest to the current SCWR designs, with emphasis on those conditions for which few data are available in the current database for near-critical and SC pressures. A second objective is to assess the accuracy of current heat transfer prediction methods for these conditions. In addition, the present measurements permit further examination of previously suggested relationships describing the critical heat flux (CHF) and post-dryout heat transfer coefficients at high subcritical pressures and the boundaries of the deteriorated heat transfer regimes for SC pressures.

The experiments include low heat flux cases with single-phase liquid or liquid-like SC fluid along the entire tube length and higher heat flux cases with superheated vapour or vapour-like SC fluid at the downstream end of the tube. Moreover, measurements were made for cases with no dryout or heat transfer deterioration, as well as cases for which the CHF was exceeded and/or heat transfer deterioration did occur.

Typical results are presented as plots of wall temperature and heat transfer coefficient vs. bulk fluid enthalpy. Comparisons of present supercritical heat transfer measurements were in good agreement with those from other investigators for a few cases with comparable test conditions. Comparisons with predictions of correlations for normal heat transfer and for the onset of heat transfer deterioration are also presented.

1. Introduction

Starting in the 1950s, heat transfer in supercritical (SC) water and other fluids was investigated in support of SC fossil-fuelled power plants. This topic has recently received renewed attention because of its relevance to Super Critical Water-cooled Reactors (SCWR), which are among the designs considered by the Generation IV International Forum as innovative nuclear energy systems with increased safety, more compact size, lower cost of energy production and reduced volume of nuclear waste, compared to existing systems. The present research is in support of the Canadian National Program for the development of the SCWR.

Heat transfer in a fluid at near-critical and supercritical pressures has distinct characteristics, which are not present at subcritical pressures. When the fluid pressure and temperature are near their critical values, or when the pressure is supercritical and the temperature is near its pseudocritical value, small changes in temperature cause large changes in the thermophysical properties and the heat transfer may undergo enhancement or deterioration. Of particular importance for the safety of SCWR is the phenomenon of heat transfer deterioration (HTD). A number of tests in upward flow in tubes have identified one or two peaks in wall temperature, whose locations and amplitudes depended on flow conditions. Other tests showed a monotonically increasing wall temperature along the entire test section, without the presence of peaks; these tests were carried out at relatively low mass flux and high heat flux. The literature also contains several attempts to explain these observations. Wall temperature peaks appearing close to the inlet of the heated test section length have been attributed to heat transfer degradation associated with the development of the thermal boundary layer (Pioro and Duffey, 2007) or, alternatively, to buoyancy effects, which result in mixed convection flow (Fewster and Jackson, 2004). The wall temperature drop following a temperature rise has been attributed to further development of buoyancy effects, which result in heat transfer enhancement (Lee, 2006; Jackson, 2011). HTD can also be caused by acceleration of near-wall fluid due to the local decrease in its density (Jackson, 2011); some studies reported that this effect occurs at relatively high mass fluxes (Licht et al., 2008). Under certain conditions, HTD may extend throughout the entire length of the heated test section, without the appearance of hot-spots on the wall (Petukhov and Polyakov, 1988).

Prediction and modelling of the flow and heat transfer at SC pressures remain topics of ongoing research; they require consideration of a large number of parameters that affect the transport of momentum and energy. Experiments in SC water are necessary for the development of SCWR, however, they are difficult and expensive to perform. As a contribution towards an improved understanding of SC heat transfer under wide ranges of flow conditions, we report the results of a series of experiments using carbon dioxide as a surrogate fluid, which, by comparison to corresponding experiments in water, were easier, more safe and less expensive to perform. One objective of the present work was to supplement the experimental database for CO_2 with measurements under conditions for which previous data are scarce or not available. These data will be used to fill some gaps in the experimental database of the trans-critical heat transfer look up table (Zahlan *et al.*, 2012); CO_2 data will be incorporated in the trans-critical LUT database after their transformation into their water equivalent values using appropriate scaling laws. In addition, data obtained at high subcritical pressures will be used to fill some gaps in the experimental database for CHF and film boiling look up tables and boiling heat transfer correlations. Data at near-critical pressures are particularly scarce and the present results will contribute to our understanding of deterioration and enhancement of heat transfer and the testing of the accuracy of existing heat transfer correlations in this pressure regime.

2. Experimental Facility and Procedures

2.1 Super-Critical University of Ottawa Loop (SCUOL)

The Super-Critical University of Ottawa Loop (SCUOL) was designed to operate with carbon dioxide as a coolant at a maximum operating pressure of 10 MPa. The CO_2 was circulated through the loop by means of two gear pumps connected in parallel. Five bellow-type accumulators, using nitrogen as the secondary fluid, were connected to the loop to dampen flow and pressure oscillations and to provide a means for pressure adjustment. Electrical power for the direct heating of the test section was provided by a rectified power supply, rated at a maximum voltage of 60 V DC and a maximum current of 2833 A. The fluid exiting the test section was passed through two heat exchangers connected in series, where it was cooled by a centrally supplied chilled water stream.

Measurements of test section wall temperature were made using T-type thermocouples (Omega SA1XL-T-SRTC), having an uncertainty of 0.5 K and a time constant of 0.15 s. The thermocouples were attached to the exterior wall of the test section using a silicone-based adhesive, which can withstand temperatures up to 260˚C. The bulk fluid temperatures at the inlet and outlet of the test section and other locations of the loop were measured with ultra precise immersion RTD sensors (Omega P-M-1/10-1/8-5-1/2-G-15), having a maximum uncertainty of 0.1˚C within the range between 0 and 100˚C. The test section inlet pressure was measured by a pressure transducer (Omega PX01C1-3KA5T) with an uncertainty of 21 kPa. The pressure drop across the heated length of the test section was measured with a differential pressure transmitter (Omega PX771A-300DI), having an uncertainty of 75 Pa. The pressure drop readings were corrected for the elevation difference between the transmitter and the pressure taps. The CO_2 mass flow rate was measured with a Coriolis flow meter (Micro Motion® ELITE® CFM050M320N0A2E2ZZ), having an uncertainty of 0.05% for liquid flow. The instantaneous voltage drop across the heated length of the test section was measured with a 24-bit digital voltage measurement module (National Instrument NI 9225), having a range of ±300 V and an uncertainty of 0.034 V. The rectified voltage fluctuated at a frequency of 360 Hz and was sampled at a much higher sampling rate. The electrical power supplied to the test section was calculated from the measured time-averaged voltage and the measured electrical resistance of the test section.

2.2 Test section

All measurements presented in this paper were collected using a tube with 8 mm ID and 1 mm wall thickness as a test section. The tube was made of Inconel 600 and was mounted vertically with CO_2 flowing upwards. The tube in the test section had a total length of 3.05 m and a heated length L_h = 1.94 m. The heated part of the tube was preceded by an unheated section with a length of 0.89 m, which ensured that the flow entering the heated section was hydrodynamically fully developed and free of entrance effects. The test section was insulated thermally by two or three layers of fibreglass cloth tape, with a thickness of 0.8 mm and rated by its manufacturer to maintain its tensile strength up to 343˚C; additional insulation was provided by a rubber-foam insulation tube, mounted on top of the fiberglass tape. Figure 1 shows a schematic diagram of the test section with the locations of the thermocouples.

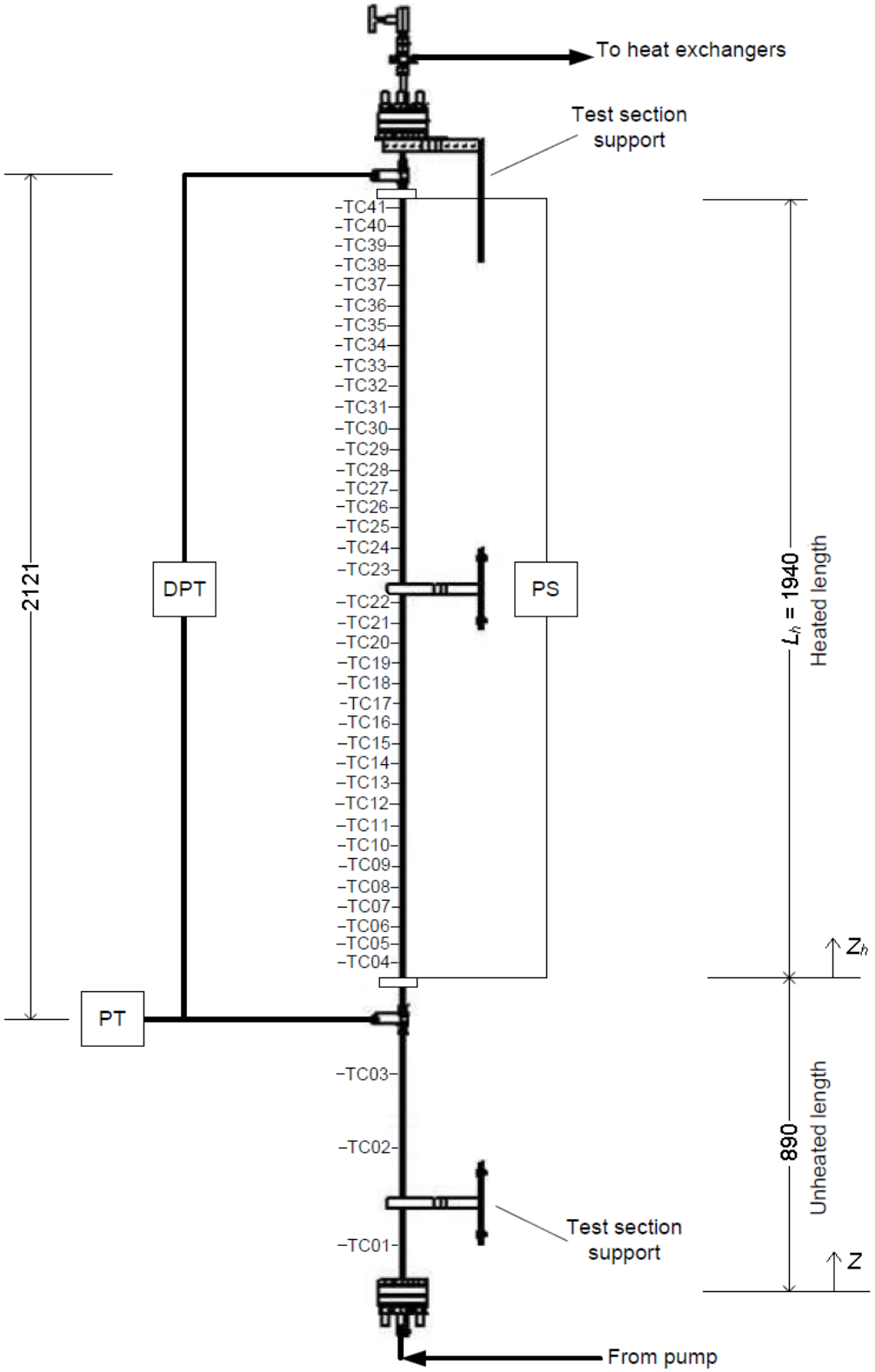

Figure 1: Schematic diagram of the 8 mm test section showing the locations of thermocouples; PS: power supply; PT: pressure transducer; DPT: differential pressure transducer; dimensions in mm.

2.3 Data reduction

The volumetric heat flux in the test section wall was calculated as

$$q^v = \frac{N}{\pi(r_o^2 - r_i^2)L_h} \quad , \tag{1}$$

where N is the measured electrical power supplied to the test section, r_o and r_i are the tube outer and inner radii, respectively, and L_h is the heated length. The inner wall temperature T_w was calculated from the measured outer wall temperature $T_{w,o}$ using the heat diffusion equation with uniform internal energy generation in cylindrical coordinates (Incropera *et al*., 2007), as

$$T_w = T_{w,o} + \frac{2q_{loss}r - q^v r_o^2}{2k}\ln\frac{r_o}{r_i} + (r_o^2 - r_i^2)\frac{q^v}{4k} \quad , \tag{2}$$

where the heat losses q_{loss} to the surroundings were neglected and k is the thermal conductivity of Inconel 600, evaluated at the local $T_{w,o}$.

The wall heat flux through the test section was calculated as

$$q = \frac{N}{\pi d L_h} \quad , \tag{3}$$

assuming no losses to the environment or axial conduction losses. It must be pointed out, however, that the readings of the two thermocouples that were located the closest to either end of the heated test section seemed to have been affected by axial heat conduction towards the adjacent unheated parts of the test section. The result was that these thermocouples read lower temperatures than would have been the case in the absence of conduction; this error was clearly noticeable at high wall temperatures but it was insignificant otherwise.

Then, the bulk fluid specific enthalpy along the heated test section was calculated using the simplified energy equation as

$$H_b = H_{in} + \frac{N}{\dot{m}}\frac{z_h}{L_h} \quad , \tag{4}$$

where H_{in} is the specific enthalpy at the inlet, $\dot{m}$ is the mass flow rate and z_h is the axial distance along the heated section. The corresponding local bulk fluid temperature T_b and the thermophysical properties of carbon dioxide were calculated using NIST software (Lemonn *et al*., 2002). Finally, the local heat transfer coefficient (HTC) was calculated as

$$h = \frac{q}{T_w - T_b} \quad . \tag{5}$$

The difference between the electric power provided to the test section and the power given to the fluid was estimated in real time during each test as

$$\Delta N = N - \dot{m}\,(H_{out} - H_{in}) \quad , \tag{6}$$

where the inlet and outlet fluid specific enthalpies were calculated from linked NIST tables at the measured test section inlet and outlet fluid temperatures. This power imbalance was generally less than 5%*N*. Additional tests were performed under different conditions to ensure that all instrumentation worked properly and that the reported measurements were sufficiently accurate.

The experimental heat transfer coefficient at supercritical pressures is presented in normalized form as h/h_J, where h_J is the value provided by the following correlation for normal heat transfer in flows with variable properties (Jackson, 2009)

$$\mathrm{Nu}_b = 0.021\mathrm{Re}_b^{0.8}\mathrm{Pr}_b^{0.4}\left(\frac{\rho_w}{\rho_b}\right)^{0.3}\left(\frac{\overline{C_p}}{C_{p\,b}}\right)^n \quad . \tag{7}$$

In this expression, $\overline{C_p} = (H_w - H_b)/(T_w - T_b)$ is an average specific heat and the exponent n of the specific heat ratio is given by (T in K)

$$n = 0.4, \text{ for } T_b < T_w < T_{pc} \text{ and } 1.2T_{pc} < T_b < T_w$$

$$n = 0.4 + 0.2(T_w/T_{pc} - 1), \text{ for} T_b < T_{pc} < T_w$$

$$n = 0.4 + 0.2(T_w/T_{pc} - 1)(1 - 5(T_b/T_{pc} - 1)), \text{ for } T_{pc} < T_b < 1.2T_{pc} \quad .$$

A more recent version of this correlation (Jackson *et al.*, 2012) was also considered, however, it was not used because its predictions deviated more from CO_2 data at low heat fluxes than those of Equation (7).

3. Results

3.1 Experimental flow conditions

The reported tests were performed over ranges of flow conditions at the high subcritical and supercritical pressure regions, including the conditions of main interest to SCWR. Table 1 lists the experimental flow conditions and their water equivalent values.

Table 1: Ranges of experimental flow conditions

Parameter	Range			
	Subcritical		Near-critical and supercritical	
	CO_2	Water equivalent*	CO_2	Water equivalent*
P [MPa]	5.91 − 6.87	17.65 − 20.52	7.48 − 8.67	22.28 − 26.04
P/P_c [–]	0.8 − 0.93		1.01 − 1.18	
T_{in} [˚C]	7.5 – 10.34	325 − 331	7.06 – 13.4	323 – 336
T_b/T_c [–]	0.92 − 0.99		0.92 − 1.16	
G [kg/m² s]	490 − 2040	550 − 2290	405 − 2030	400 − 1930
q [kW/m²]	20.5 − 225	213 − 2330	20 − 436	210 − 4950

* Scaling of CO_2 conditions to their water equivalent values followed the method discussed by Zwolinski *et al.* (2011); for scaling purposes, temperatures were normalized by the saturation temperature for subcritical pressures and by the pseudocritical temperature for supercritical pressures.

It is worth reporting that, during some tests, the loop experienced low-frequency (*e.g.*, at 0.05 Hz) oscillations in flow rate, accompanied by oscillations in the recorded temperatures. Similar flow oscillations have been occasionally reported in the literature (Pioro and Duffey, 2007). Further investigation is needed to clarify the causes of this phenomenon. All results reported in the following sections were obtained during steady operation of the loop.

3.2 Comparisons with previous measurements

Commissioning tests of SCUOL were reported recently by Jiang *et al*. (2012). A small number of tests under conditions that were intended to replicate those in a selected number of experiments reported in the literature were conducted in order to serve as additional loop commissioning tests and as evidence of reproducibility of the results in different laboratories. These included one set of results reported by Fewster and Jackson (2004) for a supercritical pressure slightly exceeding the critical value (P/P_c = 1.03) and two sets by Song *et al*. (2008) for a supercritical pressure that is relevant to the SCWR operation (P/P_c = 1.10). As Table 2 shows, the present experimental conditions approximated fairly closely those in the previous tests, but could not match them exactly because of differences in the

designs of the loops, diameters and lengths of the test sections and inlet temperatures. Such differences also introduced differences in the enthalpy ranges over which measurements were reported.

Table 2: Conditions in selected tests from the literature and in present replicate tests

P/P_c	Authors	D [mm]	L_h [mm]	P [MPa]	G [kg/s m^2]	q [kW/ m^2]	T_{in} [ºC]	T_{pc} [ºC]	H_{pc} [kJ/kg]
1.03	Fewster & Jackson (2004)	7.9	1,185	7.58	398	33.6	14.5	32.2	337.7
	Present	8.0	1,940	7.61	402	33.9	13	32.3	337.8
1.10	Song *et al.* (2008) - Case B1	9.0	2,650	8.12	400	30	7.5	35.3	339.3
	Present	8.0	1,940	8.14	405	29.9	13.4	35.4	339.4
	Song *et al.* (2008) - Case B3	9.0	2,650	8.12	1200	50	6.4	35.3	339.3
	Present	8.0	1,940	8.14	1210	50.1	9.0	35.4	339.4

The wall temperatures measured by Fewster and Jackson (2004) showed significant heat transfer deterioration and had a sharp first peak that moved upstream as the inlet temperature increased. Figure 2 demonstrates that our results are in excellent agreement with theirs. As shown in Figure 3, present measurements of wall temperature and heat transfer coefficient are also in fair agreement with corresponding results in the two runs by Song *et al.* (2008). In conclusion, it is evident that heat transfer results in the present loop can be treated with confidence, as they demonstrate good reproducibility with results from the literature.

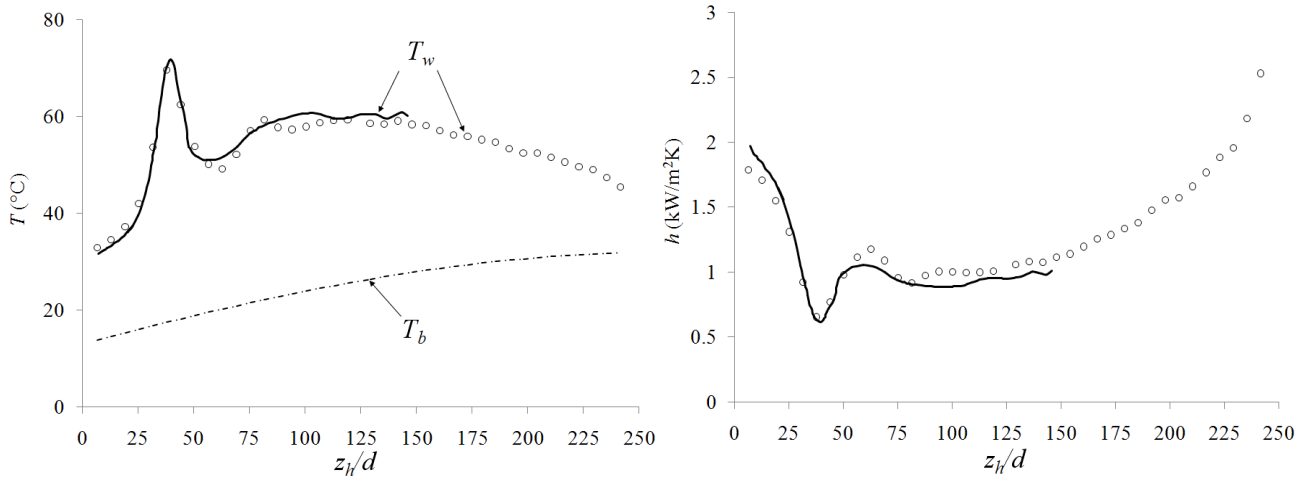

Figure 2: Wall and bulk fluid temperature variations (left) and the corresponding heat transfer coefficients (right) in the present study (circles) and as reported by Fewster and Jackson (2004; solid lines).

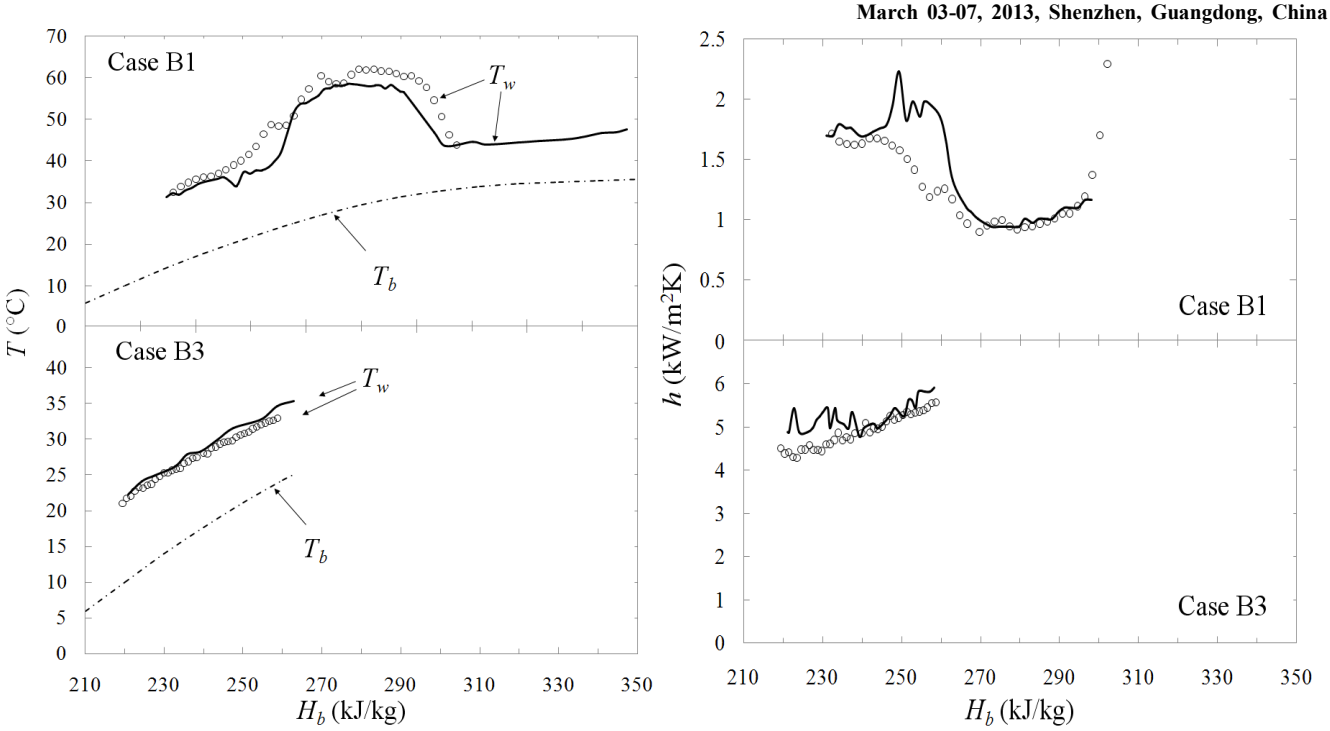

Figure 3: Wall and bulk fluid temperature variations (left) and the corresponding heat transfer coefficients in the present study (circles) and as reported by Song *et al.* (2008; solid lines).

3.3 CHF and film boiling measurements at high subcritical pressures

In this section, we report measurements of critical heat flux (CHF) q_c and film boiling wall temperatures for CO_2 flows at high subcritical pressures. Figure 4 shows two sets of plots at different flow conditions: the LHS plots show the variation of measured wall temperature against thermodynamic quality at different heat fluxes and the RHS plots show the corresponding measured CHF values along with the predicted CHF values of the CHF look-up table (Groeneveld *et al.*, 2005), transformed into CO_2-equivalent values using the scaling laws proposed by Groeneveld *et al.* (1997).

The wall temperature rise at CHF was relatively small compared to those at low subcritical pressures, in agreement with expectations (*e.g.*, Groeneveld *et al.*, 2003). The parametric trends of the film boiling wall temperature agreed with the corresponding trends for water: with increasing heat flux, the CHF location moved upstream (LHS plots) and the CHF decreased with increasing quality (RHS plots). The CHF- LUT overpredicted the measured CHF of CO_2 by 10 – 50%. This is attributed to two possible causes. First, the water-equivalent pressure of the present CO_2 data was near the upper limit of pressure for the CHF-LUT, and, second, the applicability of the used scaling laws between CO_2 and water to the present data remains unknown, because these laws have only been tested against data obtained at much lower pressures ($P/P_c < 0.6$) and not at near-critical pressures.

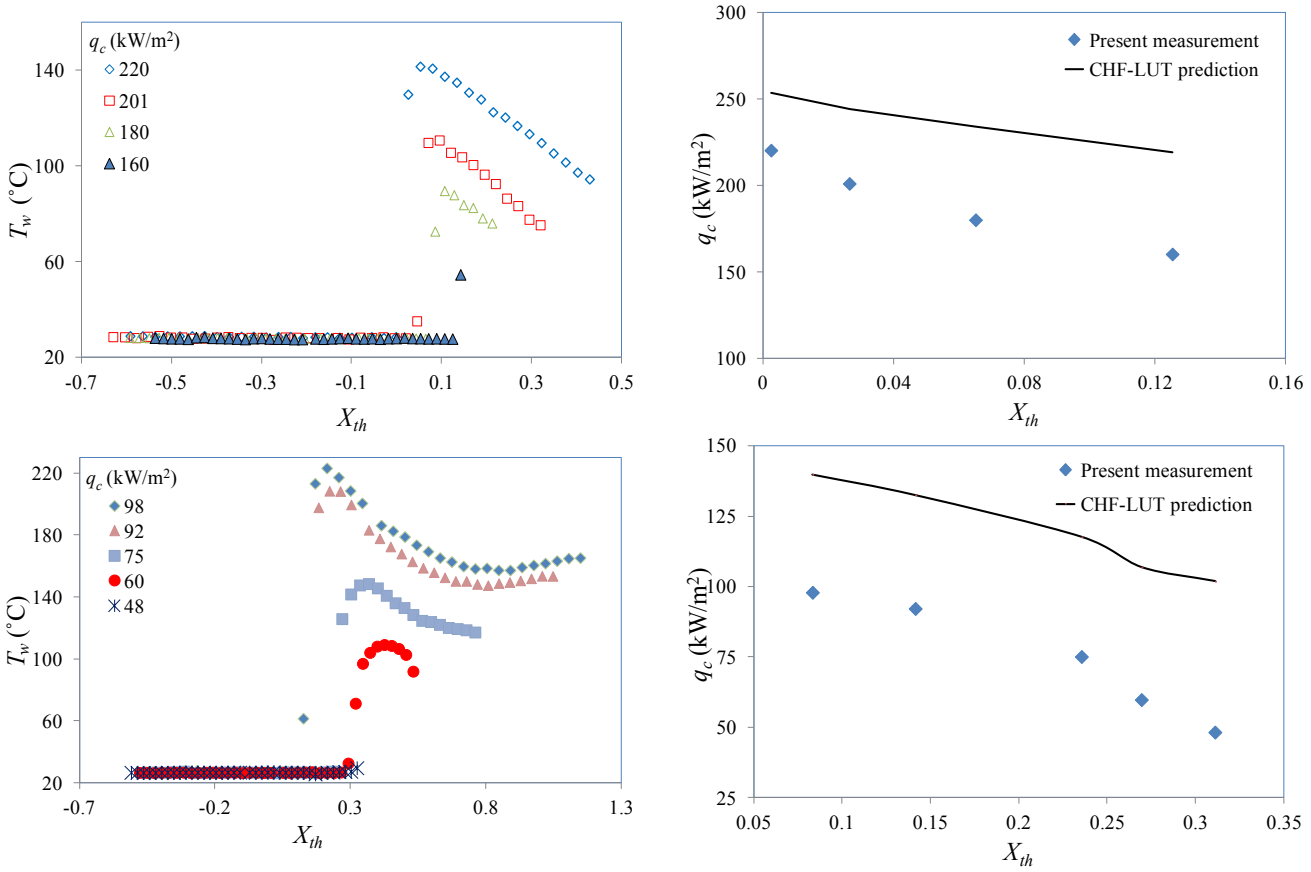

Figure 4: Film boiling wall temperatures at high subcritical pressures (left) and comparison between experimental and predicted CHF (right). Top: $P = 6.68 \pm 0.11$MPa, $G = 1980 \pm 60$ kg/m^{2}s, $T_{in} = 8.4 \pm 0.1$˚C; bottom: $P = 6.54 \pm 0.08$ MPa, $G = 500 \pm 10$ kg/m^{2}s, $T_{in} = 10.3 \pm 0.0$˚C.

3.4 Supercritical heat transfer measurements

Pressure effect: Figure 5 shows the effect of pressure on SCHT. Results at three different pressures, corresponding to $P/P_c = 1.02$, 1.14 and 1.15 and approximately the same mass flux, heat flux and inlet temperature are shown in this figure. In all three cases the wall temperature variations had two peaks, the upstream one of which was significantly higher than the other one. With increasing pressure, both peak temperatures decreased and both peak locations moved downstream. This is consistent with the fact that changes in fluid thermo-physical properties occurring as the temperature crosses the pseudo-critical value become less steep at higher pressures. The normalized heat transfer coefficient h/h_J was significantly less than 1.0 in the upstream half of the heated test section for all three pressures considered, which indicates heat transfer deterioration. The same parameter in roughly the downstream half of the test section slightly exceeded 1.0 which is an indication of mild heat transfer enhancement.

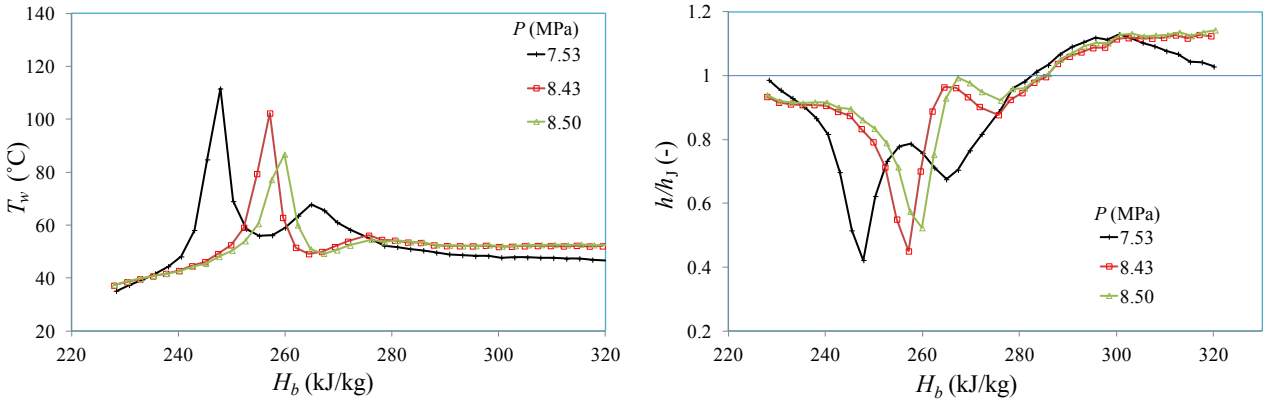

Figure 5: Variations of the wall temperature and the normalized heat transfer coefficient along the heated test section for three different pressures; G = 510 ± 10, kg/m^{2}s, q = 50 ± 0 kW/m^2, T_{in} = 11.7 ± 2.0˚C; for P = 7.53 MPa, T_{pc} = 31.9˚C and H_{pc} = 332 kJ/kg.

Mass flux effect: Figure 6 shows the effect of mass flux on SCHT at P = 8.33 ± 0.18 MPa (P/P_c = 1.13), which corresponds approximately to the operating pressure of the SCWR. In all cases, the wall temperature increased monotonically, except for the test with the lowest mass flux (G = 496 kg/m^{2}s), in which case a mild temperature peak was noticeable near the inlet of the heated length. Normalized heat transfer coefficient variations at the higher mass fluxes show significant enhancement.

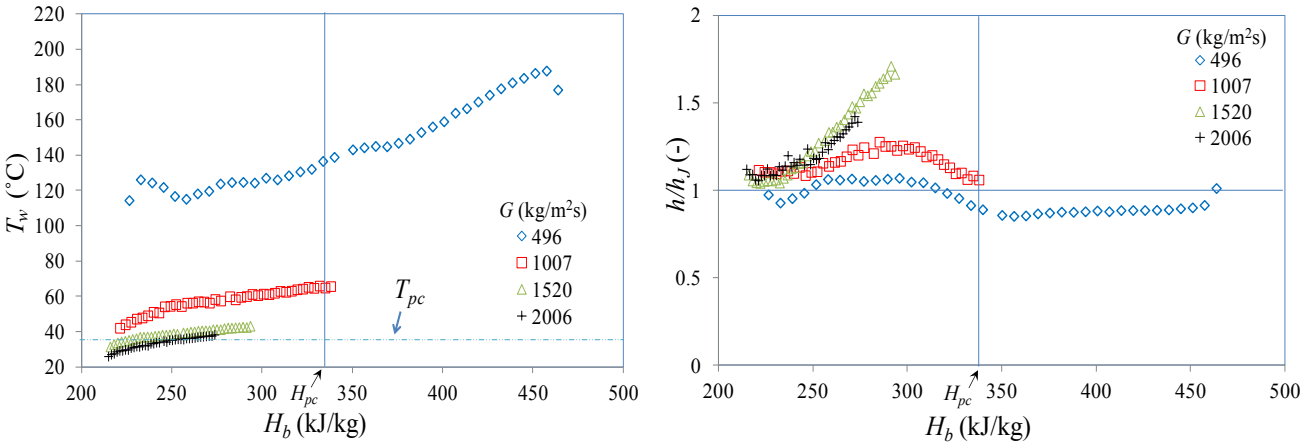

Figure 6: Variations of the wall temperature and the normalized heat transfer coefficient along the heated test section for four different mass fluxes; P = 8.33 ± 0.18 MPa, q = 125 ± 0 kW/m^2, T_{in} = 8.5 ± 0.4˚C.

Heat flux effect: Figures 7 and 8 show the effect of heat flux on SCHT at SC pressures and two different mass fluxes. Figure 7 shows results at a relatively low mass flux (G = 505 kg/m^{2}s) and P/P_c = 1.15. In this case, for $q \leq$ 40 kW/m^2, the wall temperature increased monotonically up to the exit of the heated section, but for $q \geq$ 50 kW/m^2 it presented two peaks, which moved upstream with increasing q; the upstream peak was quite sharp and narrow, whereas the downstream one was much milder and tended to become less noticeable as the heat flux increased. Figure 8 shows results at a pressure (P/P_c = 1.13) and a mass flux (G = 1000 kg/m^{2}s) that were close equivalents to those in the SCWR. Once more, for relatively low heat fluxes ($q \leq$ 125 kW/m^2) the wall temperature in the heated

test section increased monotonically downstream. For higher heat fluxes ($q \geq 175$ kW/m^2), the wall temperature presented double peaks, albeit much milder ones than those in the low-G/high-q cases.

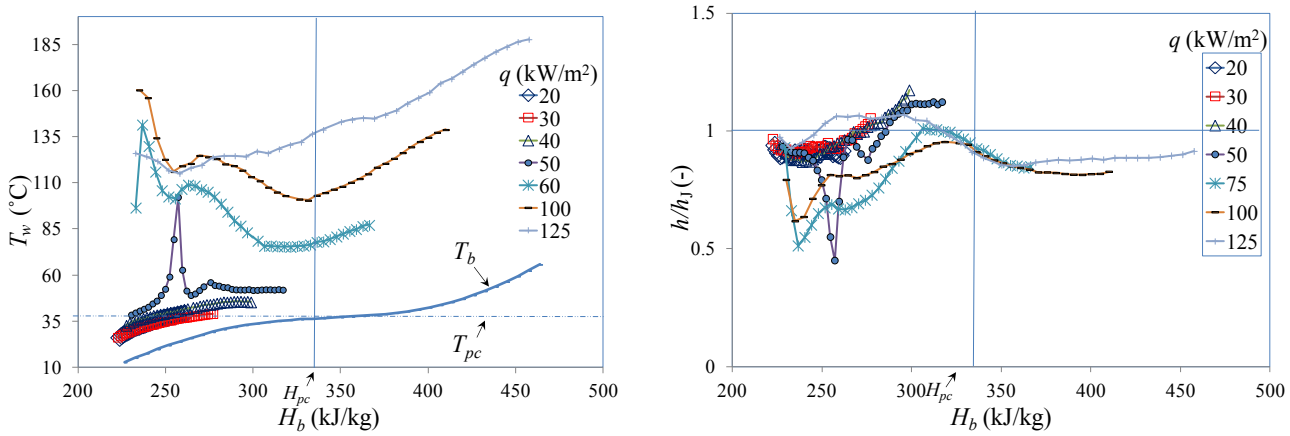

Figure 7: Variations of the wall temperature and the normalized heat transfer coefficient along the heated test section for seven different heat fluxes; P = 8.48 ± 0.16 MPa, G = 505 ± 12 kg/m^{2}s, T_{in} = 12.0 ± 1.4˚C.

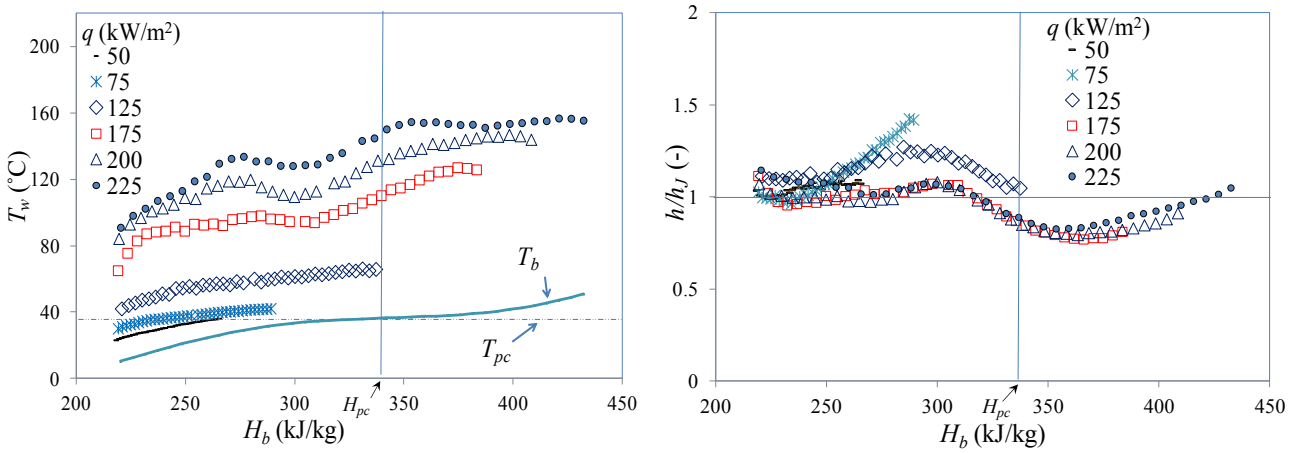

Figure 8: Variations of the wall temperature and the normalized heat transfer coefficient along the heated test section for six different heat fluxes; P = 8.35 ± 0.05 MPa, G = 1000 ± 10 kg/m^{2}s, T_{in} = 8.0 ± 1.2˚C.

3.5 Onset of heat transfer deterioration

Although the presence of heat transfer deterioration in upward flows in heated tubes has been documented by many investigators, there is no consensus in the literature on how to identify the onset of deterioration and several references discuss this phenomenon without clearly defining the procedure of separating their runs into those with and without HTD. Most authors consider heat transfer to be deteriorated when the local heat transfer coefficient drops below the corresponding prediction of an empirical correlation developed for normal heat transfer. This approach introduces uncertainty, because such correlations would be based on results under conditions that may differ from those in the tests being analysed and, besides, all correlations contain sizeable errors. More importantly, this type

of criterion can only bring forward secondary evidence for HTD, because it is not based on direct observation of the characteristics of each particular case. A direct approach should be based on observations of wall temperature and/or heat transfer coefficient variations, but this introduces the difficulty of defining a suitable threshold for temperature rise or heat transfer coefficient drop. Additional complications may arise by possible peculiarities that may be specific to individual sets of results. For example, the absence of a visible temperature rise along a test section is not necessarily evidence for the absence of HTD, because it may be possible for the fluid in the entire test section to be under HTD conditions. Moreover, a flow that shows no signs of HTD may have deteriorated, if the heated section were longer or if the inlet temperature were higher. Licht *et al.* (2008) classified their results using two different thresholds of temperature rise: those cases that had large localized wall temperature spikes were considered to have HTD with high confidence, whereas those cases that had only small localized temperature increases were considered to have possible HTD; thus, Licht *et al.* (2008) classified heat transfer in each of their experimental runs in one of three categories: a normal, an uncertain or a deteriorated category.

Simple criteria for the prediction of heat transfer deterioration at SC pressures have been based on the observation that, for a given mass flux, the onset of heat transfer deterioration occurs when the heat flux exceeds some value q_{onset}. For example, a criterion for HTD of CO_2 flows was proposed by Kim *et al.* (2005) as

$$q_{onset} = 2\times10^{-4} G^2 \quad . \tag{8}$$

Bae *et al.* (2010) reported that this criterion applied fairly well to their SCHT data in tubes with diameters 4.40 and 6.32 mm. These authors appeared to have considered heat transfer as deteriorated when $h/h_B \leq 1$, where

$$h_B = 0.021\frac{k_b}{d}\mathrm{Re}_b^{0.8}\mathrm{Pr}_b^{0.5}\left(\frac{\rho_w}{\rho_b}\right)^{0.3}\left(\frac{\overline{C_p}}{C_{pb}}\right)^n \quad . \tag{9}$$

In order to test the applicability of equation (8) to our results, we have followed the same procedure as Bae *et al.* (2010) to identify the onset of HTD in the present data. Figure 9 shows that, for the present test section with an 8 mm tube ID, the Kim *et al.* (2005) criterion significantly overpredicted q_{onset}. For rough purposes, we fitted a power law to our limited number of data points and found it to be

$$q_{onset} = 3\times10^{-4} G^{1.8} \quad . \tag{10}$$

Although it is known that, for the same pressure and mass flux, heat transfer is more likely to deteriorate in larger tubes than smaller ones, the difference between the predictions of q_{onset} by Equations (8) and (10) is too large to be attributed to diameter differences alone. It is noted that other investigators have also suggested power-law relationships between q_{onset} and G, in which the exponent was 1 or 1.2 (Bae *et al.,* 2010). All these expressions make significantly different predictions of q_{onset}. It seems clear that simple q_{onset}-G relationships cannot describe HTD under all possible conditions, because they cannot account for differences in the values of other parameters that affect HTD.

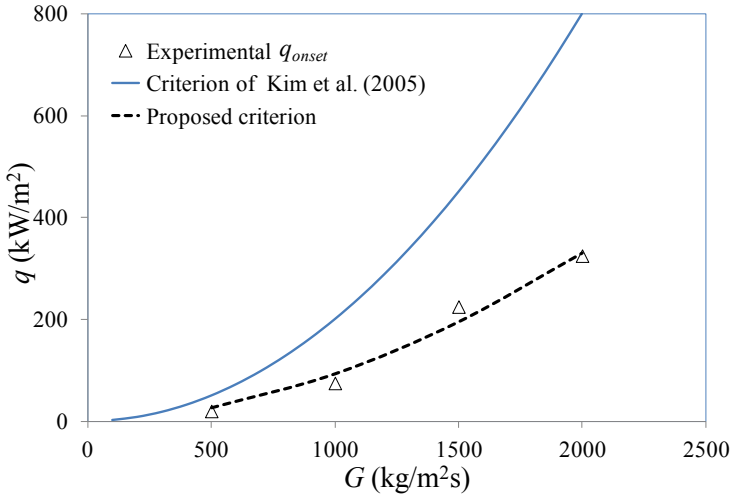

Figure 9: Onset of heat transfer deterioration plotted *vs*. mass flux; P = 8.46 ± 0.15 MPa, T_{in} = 9.0 ± 2.8˚C.

Phenomenological criteria for the onset of HTD, based on the effects of buoyancy and acceleration, have also been proposed. Although several authors have tested these criteria with a fair amount of success, there seems to be no universal agreement on the values of empirical coefficients appearing in them.

The buoyancy deterioration criterion (Jackson, 2011) specifies that buoyancy effects would cause HTD if the buoyancy parameter Bo_b^* were

$$Bo_b^* = \frac{\mathrm{Gr}_b^*}{\mathrm{Re}_b^{3.425}\mathrm{Pr}_b^{0.8}} > 4\times10^{-7}\left(\frac{\overline{\mathrm{Pr}}}{\mathrm{Pr}_b}\right)^{0.4} \quad . \tag{11}$$

We have tested this criterion against the present data (152 data points) and found it to be valid, although the coefficient 3.3×10^{-7} seems to be more appropriate to our data than the value in Equation (11). It is well known that, as buoyancy effects become stronger, or equivalently as Bo_b^* exceeds a certain value, heat transfer would be enhanced rather than deteriorated, even in upward flows. This phenomenon could not be observed in the present results, because none of the present tests was in this regime.

Finally, the acceleration deterioration criterion (Jackson *et al.*, 2011) specifies that acceleration effects would be negligible if the acceleration parameter Ac_b^* were

$$Ac_b^* = \frac{Q_\mathrm{b}^*}{\mathrm{Re}_b^{1.625}\mathrm{Pr}_b} < 2\times10^{-6} \quad . \tag{12}$$

Tests of this criterion against our data (152 points) showed that HTD occurred when Ac_b^* exceeded 3.5×10^{-7}.

4. Conclusions

Presently obtained measurements of wall temperature variations and CHF values in upwards flows of CO_2 at high subcritical pressures are qualitatively similar to previous results obtained in water at lower subcritical pressures. The present CHF results are 10-50% lower than predictions of water-based CHF look up tables at equivalent conditions. The present data can used for improving fluid-to-fluid scaling methods at high subcritical pressures and supplementing the water database for conditions for which water data are not available.

The present supercritical heat transfer data are in good agreement with data of previous authors at comparable experimental conditions, thus demonstrating the reproducibility of such measurements. Representative comparisons of the supercritical heat transfer measurements in CO_2 have illustrated the effects of pressure, mass flux and heat flux values on the variations of the wall temperature and the heat transfer coefficient under conditions relevant to the operation of the SCWR.

Several criteria predicting the onset of deteriorated heat transfer were tested against the present results and adjustments of the corresponding empirical coefficients were made to improve fit.

Acknowledgment

The financial support of NSERC, NRCan and AECL and technical assistance by AECL are gratefully acknowledged.

Nomenclature

Symbols

C_p	coefficient of specific heat at constant pressure	(J/kgK)
$\overline{C_p}$	average coefficient of specific heat	(J/kgK)
d	tube inner diameter	(m)
d_h	hydraulic diameter	(m)
G	mass flux	(kg/m^2 s^1)
g	gravitational acceleration	(m/s^2)
H	specific enthalpy	(J/kg)
H_f	specific enthalpy of saturated liquid	(J/kg)
H_{fg}	vapourisation latent specific heat	(J/kg)
h	heat transfer coefficient	(W/m^{2}K)
k	thermal conductivity	(W/mK)
L_h	heated length	(m)
$\dot{m}$	mass flow rate	(kg/s)
N	electrical power	(W)

P	pressure	(Pa)
q	heat flux	(W/m^2)
q^v	volumetric heat flux	(W/m^3)
r	radius	(m)
T	temperature	(K)
Z	axial location	(m)

Greek letters

β	volumetric thermal expansion coefficient	(1/K)
μ	viscosity	(Pa s)
v	kinematic viscosity	(m^2/s)
ρ	density	(kg/m^3)

Subscripts

b	bulk
c	critical
i	inner
in	inlet
o	outer
out	outlet
pc	pseudo-critical
w	wall

Dimensionless numbers

Bo_b^*	buoyancy parameter	$(\mathrm{Gr}_b^* / \mathrm{Re}_b^{3.425}\mathrm{Pr}_b^{0.8})$
Gr^*	modified Grashof number	$(g\beta q d_h^{\,4} / k\nu^2)$
Nu	Nusselt number	$(h\, d_h/k)$
Pr	Prandtl number	$(\mu C_p/k)$
$\overline{\mathrm{Pr}}$	averaged or modified Prandtl number	$((H_w-H_b)\mu_b/(k_b(T_w-T_b)))$
$\mathcal{Q}_b^*$	thermal loading/expansion group	$(\beta_b q_w d/k_b)$

Re	Reynolds number	$(G\,d\,\mu^{-1})$
X_{th}	thermodynamic quality	$(H_b - H_f / H_{fg})$

Acronyms

CHF	critical heat flux
HTD	heat transfer deterioration
SC	supercritical
SCUOL	supercritical University of Ottawa loop
SCWR	supercritical water-cooled reactor

5. References

Bae, Y.Y., H.Y. Kim and D. J. Kang, "Forced and mixed convection heat transfer to supercritical CO_2 vertically flowing in a uniformly-heated circular tube, Exp. Thermal Fluid Sci. Vol. 34, pp. 1295-1308, 2010.

Fewster, J. and J.D. Jackson, "Experiments on supercritical pressure convective heat transfer having relevance to SPWR", Proc. ICAPP'04, Paper 4342, Pittsburgh, PA, USA, June 13−17, 2004.

Groeneveld, D.C., J.E. Shan, A.Z. Vasic, A. Durmayaz, J. Yang, S.C. Cheng and A. Tanase, "The 2005 CHF Look-up Table", NURETH-11, Avignon, France, October 2-6, 2005.

Groeneveld, D.C., S. Doerffer, R.M. Tain, N. Hammouda and S.C. Cheng, "Fluid to fluid modeling of the critical heat flux and post dry out heat transfer", Proc. of Experimental Heat Transfer. Fluid Mechanics and Thermodynamics, Brussels, Vol. 2, pp. 859-866, June 2-6, 1997.

Incropera, F.P, D.P. DeWitt, T.L. Bergman and A.S. Lavine, *Fundamentals of Heat and Mass Transfer*, 6th ed., John Wiley and Sons, 2007.

Jackson, J.D., "Validation of an extended heat transfer equation for fluids at supercritical pressure", Proc. 4th Int. Symp. Supercritical Water-Cooled Reactors (ISSCWR-4), Heidelberg, Germany, Paper No. 24, March 8-11, 2009.

Jackson, J.D., "A model of developing mixed convection heat transfer in vertical tubes to fluids at supercritical pressure", Proc. 5th Int. Sym. Supercritical Water-Cooled Reactors (ISSCWR-5), Vancouver, British Columbia, Canada, March 13–16, 2011.

Jackson, J.D., M. Anderson, X. Cheng, H. Zahlan, Y.Y. Bae and K. Yamada, "Review of progress on the development of new empirical correlation equations under the framework of the IAEA Coordinated Research Programme on heat transfer in SCWR's", Proc. ICAPP'12, Paper 12268, Chicago, USA, June 24–28, 2012.

Jackson, J.D., P.X. Jiang, B. Liu and C.R. Zhao, "Interpreting and categorising experimental data on forced and mixed convection heat transfer to supercritical pressure fluids using physically-based models", P103, Proc. 5th Int. Sym. SCWR (ISSCWR-5), Vancouver, British Columbia, Canada, March 13–16, 2011.

Jiang, K., H. Zahlan, S. Tavoularis and D.C. Groeneveld, "Commissioning tests of the University of Ottawa Supercritical CO_2 Facility," 3rd Annual Conference of the Canadian Nuclear Society, Saskatoon, Saskatchewan, June 10 – 13, 2012.

Kim, J.K., H.K. Jeon, J.Y. Yoo and J. S. Lee, "Experimental study on heat transfer characteristics of turbulent supercritical flow in vertical circular/non-circular tubes," NURETH-11, Avignon, France, 2005.

Lee, J., *The Flow Structure under Mixed Convection in a Uniformly Heated Vertical Pipe*, M.Sc. thesis, Department of Nuclear Science and Engineering, Massachusetts Institute of Technology, 2006.

Lemmon, E.W., M.O. McLinden and D.G. Friend, *Thermophysical Properties of Fluid Systems*, NIST Standard Reference Database Number 69, NIST Reference Fluid Thermodynamic and Transport Properties Database: Version 7.0, 2002.

Licht, J., M. Anderson and M. Corradini, "Heat transfer to water at supercritical pressures in a circular and square annular flow geometry", Int. J. Heat Fluid Flow, Vol. 29, pp. 156 –166, 2008.

Petukhov, B.S. and A.F. Polyakov, *Heat Transfer in Turbulent Mixed Convection* (edited by B.E. Launder), Hemisphere Publishing Corporation, 1988.

Pioro, I. L. and R.B. Duffey, *Heat Transfer and Hydraulic Resistance at Supercritical Pressures in Power-Engineering Applications*, ASME Press, New York, 2007.

Song, J.H., H.Y. Kim, H Kim and Y.Y. Bae, "Heat transfer characteristics of a supercritical fluid flow in a vertical pipe", J. Supercritical Fluids, Vol. 44, pp. 164–171, 2008.

Zahlan, H., D.C. Groeneveld and S. Tavoularis, "A look-up table for trans-critical heat transfer in water-cooled tubes", 3rd China-Canada Joint Workshop on Supercritical-Water-Cooled Reactors, CCSC-2012, Xi'an, China, April 18-20, 2012.

Zwolinski, S., M. Anderson, M. Corradini and J. Licht, "Evaluation of fluid-to-fluid scaling method for water and carbon dioxide at supercritical pressure, Proc. 5th Int. Sym. Supercritical Water-Cooled Reactors (ISSCWR-5), Vancouver, Canada, 2011.